A CURRENT SOURCE

FOR

ELECTRICAL IMPEDANCE TOMOGRAPHY

A CURRENT SOURCE

FOR

ELECTRICAL IMPEDANCE TOMOGRAPHY

BY

DOST MUHAMMAD KHAN, B.Sc., M.Sc.

A Thesis

Submitted to the School of Graduate Studies

in Partial Fulfilment of the Requirements

for the Degree

Master of Science

McMaster University

MASTER OF SCIENCE (2010)
(Medical Physics)

McMaster University
Hamilton, Ontario

TITLE: **A Current Source for Electrical Impedance Tomography**

AUTHOR: **Dost Muhammad Khan B.Sc., M.Sc. (McMaster University)**

SUPERVISOR: **Dr. Gerald R. Moran**

NUMBER OF PAGES: **xviii, 170**

To My Family

Abstract

The first prototype version of the current source for electrical impedance tomography was studied. Based upon its performance, a second version of the current source was built, including various improvements designed to address the issues of this first version.

The frequency range was extended from 1kHz to 125kHz up to 1kHz to 1 MHz, and additionally the new design allow the production of either sine, triangular or square waves.

The DC offset from the DDS output voltage signal was removed and the voltage signal was amplified to ±10V (peak to peak) from ±325mV (peak to peak) in two stages. A fixed gain of 5 was implemented in the first stage and a variable gain (from 0 to 6) was implemented in the second stage to provide more control of the injected current.

The single-ended voltage signal from the variable gain stage was translated into double-ended signals by implementing two unity gain buffer operational amplifiers, one inverting and the other non-inverting. This double-ended voltage signal then was applied to the voltage control current source.

Three voltage control current source circuits; current pump, improved Howland and Bi-polar were implemented on a PCB and a wire board.

The following five quality indicators were used to assess the performance of both versions of the current source: (1) The stability, (2) the balance of the current injection, (3) the output impedance, (4) the variation in the output current due to changes in the impedance at a fixed frequency and (5) the variation in the output current due to changes in frequency at a fixed load.

All three circuits in the second version were stable; however, the first version was not stable. Only in the second version - the improved Howland voltage control current source was the current injection balanced over the full range of frequencies.

The output impedances of the second version current source circuits were 25KΩ (bi-polar), 256KΩ (Howland) and 7KΩ (current pump) at 100 KHz as compared to the first version 8KΩ at 62.5 KHz. The output impedance for the second version Howland circuit was much higher than the other circuits.

The maximum variations in the output current were 6.35% (bi-polar), 22.44% (current pump) and 0.77% (Howland) due to variations in the load (150Ω - 2150Ω) at a fixed frequency (100 KHz). This is in comparison to the first version, which was 10.55% due changes in load (480Ω -1180Ω) at a fixed frequency (62.5 KHz). Clearly the improved Howland circuit demonstrates the lowest current variation as a function of the load.

The maximum variations of the output current due to changes in frequency (1kHz to 300kHz) was about 37% (bi-polar), 55% (Howland) and 89.83% (current pump) at a fixed maximum load 2150Ω for this second version of the McMaster EIT current source. This compares to the first version of the current source which was about 8.47% due changes in frequency range from 1 kHz to 62.5 kHz at maximum load of 1180Ω. In this case the bipolar current source demonstrated the lowest variation in output current with frequency.

However based upon all of the test results, the improved Howland current source version II outperforms the other circuits and the first version.

Acknowledgements

This thesis is the result of my MS project work and support of many people. I am very pleased to have the opportunity to express my gratitude to all those. I would like to thank to my research supervisor, Dr. Gerald Moran, for his guidance, kindness, patience, encouragement and financial support, which has been tremendous support for me. Many hours of face-to-face discussions, video conferences calls and very critical comments related to the project, kept me on the right track.

I like very much, Dr. Gerald Moran idea about weekly club presentation, where everyone had a chance to express his or her critical views about research projects and selected research papers. It was a very good opportunity to discuss and learn through the critical question raised by Dr. Gerald Moran and others.

I would also like to thank my examination committee members Dr. Soo Byun and Dr. Colin Syemour for their helpful suggestions.

I would like to thank, to all our lab members Cassie Zhang, Farukh Saeed, Ian Edward and Sana Jivraj and my especial thanks to Kyle Wilson, for his extended help and supporting remarks.

I would like to extend my thanks to Kenrick Chin and Tyler Ackland (Department of Electrical & Computer Engineering) for providing me the electrical components and measuring equipments.

I am also thankful to the staff at Medical Physics Vera Iarossi, Nancy Brand and Wendy Malarek and especially Fiona Alhang who always helped me out with the administrative issues.

My family always provided encouragement and a belief in my abilities and that has enabled me to pursue my studies. Their sacrifice and hard work is the reason for all my achievements and my never-ending appreciation for them.

Table of contents

Abstract iv

Acknowledgements vii

1.0 Introduction 1

1.1 Cancer biology 2

1.2 Cancer cells vs normal cells 3

1.3 Breast morphology 4

1.4 Cancer statistics 7

1.5.0 Cancer detection modalities 8

1.5.1 X-ray mammography 9

1.5.2 Ultrasound 11

1.5.3 Magnetic resonance imaging (MRI) 12

1.5.4 Positron emission tomography (PET) 14

1.5.5 Molecular imaging (MI) 16

1.6 Electrical properties of cells and tissues 18

1.7 Cells electrical model 20

2.0 Electrical impedance tomography (EIT) detection techniques 25

2.1 Electric current and electric field patters in fluids 26

2.2.0 Electric current injection and electric potential measurement strategies 28

2.2.1 Adjacent method 30

2.2.2 Opposite method 32

2.2.3 Cross method 33

2.3.0 Electrical impedance imaging 36

2.3.1 Image reconstruction process 37

2.3.2 Forward problem 40

2.3.4 Inverse problem 42

3.0 Signal generator 46

3.1 Signal generator using RC network 47

3.2 Signal generator using lookup table 49

3.3 Signal generator using field programmable gate array (FPGA) 50

3.3.1 Field programmable gate array (FPGA) 50

3.3.2 FPGA based signal generator 53

3.4 Direct digital synthesis (DDS) 53

3.5 Signal generator literature review 55

3.6. Signal generator of the McMaster EIT system 57

3.6.1 Signal generator version I of the McMaster EIT system 57

3.6.2 Signal generator version II of the McMaster EIT system 59

4. Current sources 69

4.0.1 Current source 71

4.0.2 Current sink 72

4.0.3 Current mirror 72

4.1 Current source parameters 74

4.2 Voltage control current sources 77

4.2.1 Floating load current source 78

4.2.2 Transformer coupled current source 79

4.2.3 Current mirror sources 80

4.2.3.1 Widlar current mirror 81

4.2.3.2 Wilson current mirror 82

4.2.3.3 Wyatt cascade peaking current source 84

4.2.3.4 Current mirror using operational amplifiers 86

4.2.3.5 Current source using current pump 92

4.2.3.6 Howland current source 93

4.3 Literature review 98

5.0 McMaster EIT system voltage control current sources (VCCS) 103

5.1 McMaster EIT system VCCS version I 103

5.2 McMaster EIT system VCCS version II 107

5.2.1 Current pump voltage control current source (VCCS) 108

5.2.2 Improved Howland voltage control current source (VCCS) 110

5.2.3 Bi-polar voltage control current source (VCCS) 114

6 Testing methods and experimental results 117

6.1 Test circuit and experimental setup 118

6.2.0 Experimental methods 120

6.2.1 Stability test 121

6.2.2 Balance current injection test 121

6.2.3 Output impedance test 122

6.2.4 Current vs load variations 123

6.2.5 Current vs frequency variations 124

6.3 Experimental results of the McMaster EIT system current source version I 125

6.4.0 Experimental results of the McMaster EIT system current source version II 128

6.4.1 Current pump VCCS results 129

6.4.2 Improved Howland VCCS results 131

6.4.3 Bi-polar VCCS results 133

6.5 Discussion 135

7.0 Conclusion and future goals 140

Appendix A 151

Appendix B 154

Appendix C 157

Appendix D 160

Bibliography 162

List of Figures

1.1 Basic morphological units of the breast 4

1.2 Morphological units of breast (a) normal and ductal (b) lobules carcinoma 5

1.3 Mammography screening equipment 9

1.4 Ultrasound screening equipment 11

1.5 MRI screening equipment 12

1.6 Positron emission tomography (PET) screening equipment 14

1.7 Tissue and Fricke equivalent electrical model of cell 20

1.8 Cole-Cole plot of the tissue electrical model 21

2.1 Current and electric field lines in fluid 26

2.2 Distortion of the field lines in the presence of an insulator 27

2.3 Distortion of the field lines in the presence of a conductor 27

2.4 A ring of electrodes for EIT 28

2.5 Adjacent method for current injection and voltage measurements 30

2.6 Opposite method for current injection and voltage measurements 32

2.7 Cross method for current injection and voltage measurements 34

2.8 A 3D mesh representation of a cylindrical volume 41

3.1 Signal generator circuit using RC network 48

3.2 Block diagram of a signal generator using lookup table 49

3.3 Block diagram of a waveform generator using FPGA 50

3.4 A direct digital synthesizer implemented in FPGA 56

3.5 Signal generator implemented in FPGA using DDS and DDS 57

3.6 McMaster EIT system version II signal generator block diagram 62

3.7 Amplitude vs frequency with and without filter 64

3.8 Circuit diagram for (a) DC shift and (b) variable voltage gain stage 66

3.9 Single ended to double ended conversion 67

4.1 Current (a) source (b) sink using bipolar junction transistors 72

4.2 Basic bipolar junction current mirrors 73

4.3 Current source circuit model 74

4.4 Inverting op amps configuration with load in the feedback path 78

4.5 Transformer coupled current source 79

4.6 Current mirror (a) symbol (b) block diagram 80

4.7 Wildar's current source 82

4.8 Wilson current mirrors 83

4.9 The Wyatt cascade peaking current source 85

4.10 Current mirror using operational amplifier 87

4.11 Current flow path for positive input voltage 88

4.12 Current flow path for negative input voltage 88

4.13 Current pump circuit 92

4.14 Howland current source; (a) basic (b) improved 95

5.1 Block diagram of the McMaster EIT system current source version I 104

5.2 McMaster EIT system current source version II 105

5.3 Current pump circuits diagram for floating load 109

5.4 Improved Howland current source circuit for single voltage input 111

5.5 Improved Howland current source circuit for differential voltage 112

5.6 Bi-polar differential current pump circuit diagram 115

6.1 Test circuit to measure various performance parameters of the current source 118

6.2 Current vs variable load at fixed frequencies 126

6.3 Current vs variable load at fixed frequencies (50kHz and 62.5kHz) 127

6.4 Current vs frequencies at fixed load 128

6.5 Current as a function of load at various fixed frequencies 129

6.6 Current as a function of frequencies at a fixed maximum load 130

6.7 Current as a function of load at a fixed frequency 131

6.8 Current as a function of frequencies at a maximum load 132

6.9 Current as a function of load at a fixed frequencies 133

6.10 Current as a function of frequency at a fixed maximum load 134

A.1 Current pump circuit 151

B.1 Improved Howland current source circuit 154

D.1 Output impedance, current variations measurements circuit 160

List of Tables

1.1 Estimated new cases and deaths for cancer by sex 7

4.1 Comparison of output impedance for current mirror and modified 99

6.1 Summary of current source performance parameters 136

C.1 DIP switch position for waveform shape selection 157

C.2 DIP switch position for frequency selection 157

Chapter 1

Introduction

The motivation for this thesis is the improvement of our McMaster Electric Impedance Tomography (EIT) prototype. The most fundamental, and the most crucial, step in this development is the redesign of the current driver for this system. However to put this technology in perspective, this chapter will first introduce the utility of EIT in the detection of breast cancer, and discuss other competing modalities.

1.1 Cancer biology

Cancer is an abnormal growth of cells caused by multiple changes in gene expression leading to an unbalance regulation of cell proliferation and cell death (cell replication and cell death). This ultimately develops into a population of cells that can invade surrounding tissues and spread to other parts of the body by way of the blood or lymphatic vessels or membranous surfaces to distant sites, causing significant increased risk of disease and, if untreated may cause death of the host. The abnormal growth of the cell population is called a tumor, which can be divided into two categories; benign or malignant.

Benign tumors are usually encapsulated and expand locally meaning they do not invade the surrounding tissue. Even though benign tumors do not spread through regional lymph nodes, their location and size can cause severe problems for example; pinching a nerve or blood supplying vessel that might be vital for an organ or tissue. Other than their abnormal growth, benign tumors closely resemble normal tissue as compared to malignant tumors.

Malignant tumors are not localized they can invade surrounding tissues. They can also spread through regional lymph nodes to infiltrate and damage distant organs in the body. The location of the tumor will determine its effect on the vital function of the tissue or organ and the tumor name reflects the effected organ or tissue such as brain, lung, colon, prostatic, breast cancer etc. For additional information about cancer biology, see text "Cancer Biology" 4^{th} edition by Raymond W. Ruddon. (Ruddon, 2007)

1.2 Cancer cells vs normal cells

Studies of the microscopic appearance of cells enable the differentiation of cancer cells from normal cells. Some of the findings are summarized (Ruddon, 2007).

1. The structure (morphology) of cancer cells is different from the normal cells when both, normal and cancer cells are taken from the same tissue.
2. Cancer cells differ in size and shape from normal cells.
3. Within the cancer population, the number of cell divisions (mitosis) is greater as compared to normal cell population. The number of divisions in the normal cell population is about 1 per 1000 cells and it is about 20 division per 1000 cells in cancer cell population.
4. The nucleus of a cancer cell is larger than the nucleus in the normal cell and the ratio of the nucleus to cell substance is higher as compared to normal cells. Some time there are multiple nuclei present in the cancer cell.

Using these differentiating features such as structure, size, population growth and ratio of nucleus to cell substance the cancerous and non-cancerous region can be detected. In electrical impedance tomography, the structural differences are used to identify cancerous from normal tissue. In the next section of the thesis, an overview of morphology of the breast cancer is presented.

1.3 Breast morphology

Tumours in breast are believed to arise from terminal ductal and lobular units and consist of two common morphological types: ductal and lobular neoplasia and rarer morphological types include tubuloductal, comedo, medullayr and mucinous (Kari Hemminki, 2002).

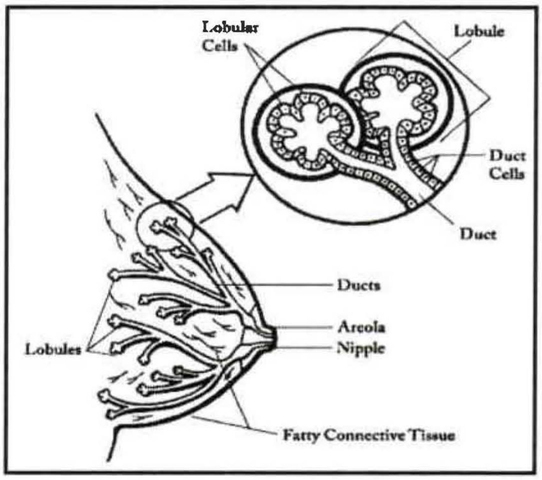

Figure 1.1 Basic morphological units of the breast

Basic morphological units of the breast are shown in Figures 1.1, 1.2 (a) and 1.2 (b). These figures also shows the inner sections and non-structured and invasiveness of the tumor.

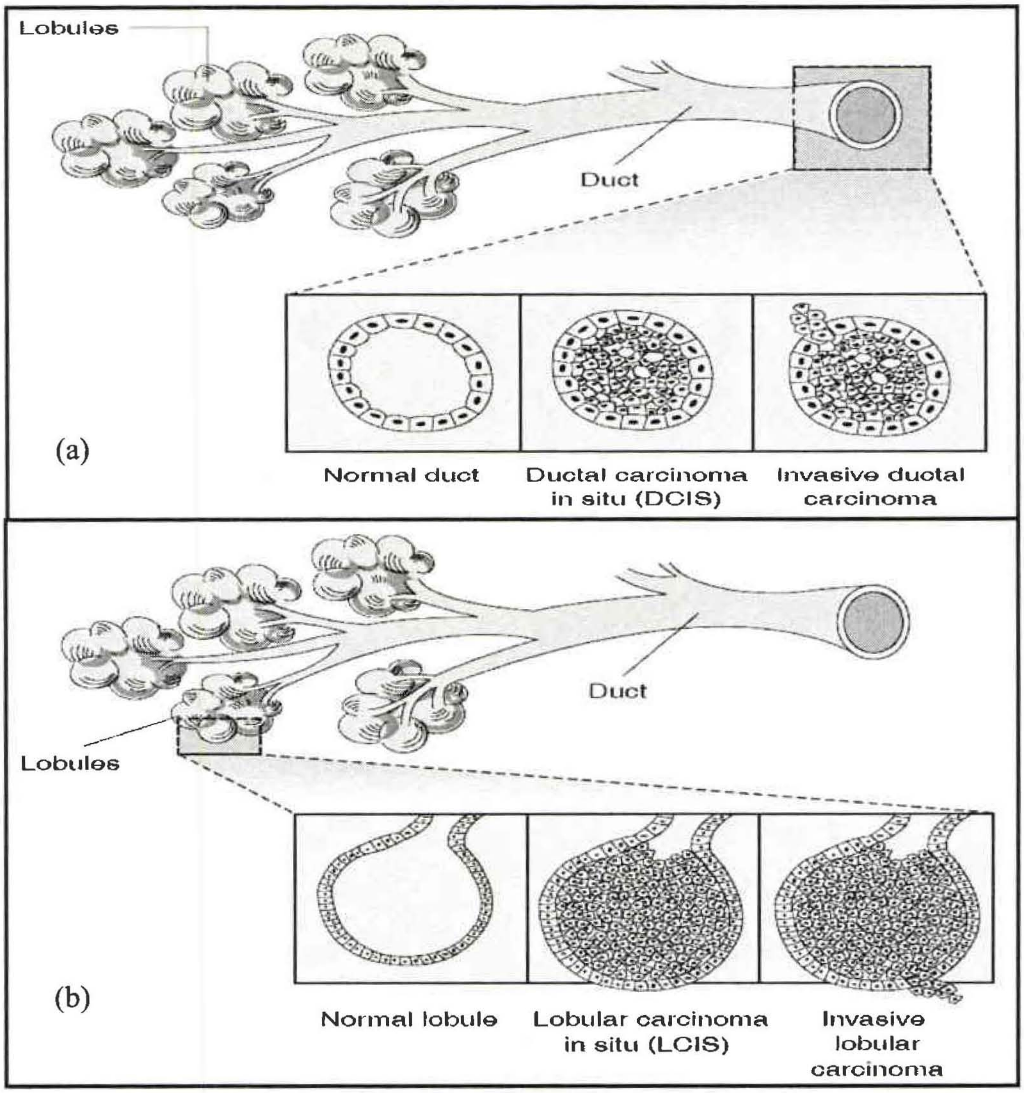

Figure 1.2 Morphological units of the breast (a) normal and ductal (b) lobules carcinoma

The terminal duct lobular unit is composed of smaller branches of lactiferous ducts (ducts leads from the lobules of the mammary gland to the tip of the nipple), the extra-lobular terminal duct and the lobule. The lobule is composed of the intra-lobular duct and small channels (ductules). The ducts and the lobules are the sites where most breast abnormalities arise, both benign and malignant. The size of the ducts is approximately 1 to 2 mm in diameter (Ruddon, 2007). In the next section of this thesis, the Canadian cancer estimates for 2009 will be presented.

1.4 Cancer statistics

Table 1.1 shows the estimated number of new cases and deaths for all types of cancers by sex for the year 2009.

	New Cases 2009 Estimates			Deaths 2009 Estimates		
	Total*	M	F	Total*	M	F
All Cancers	**171,000**	**89,300**	**81,700**	**75,300**	**39,600**	**35,700**
Prostate	25,500	25,500	–	4,400	4,400	–
Lung†	23,400	12,800	10,700	20,500	11,200	9,400
Breast	22,900	180	22,700	5,400	50	5,400
Colorectal	22,000	12,100	9,900	9,100	4,900	4,200
Non-Hodgkin Lymphoma	7,200	3,900	3,300	3,200	1,750	1,450
Bladder†	6,900	5,100	1,750	1,850	1,300	550
Melanoma	5,000	2,700	2,300	940	580	360
Thyroid	4,700	990	3,700	190	70	120
Leukemia†	4,700	2,700	1,950	2,500	1,450	1,050
Kidney†	4,600	2,800	1,800	1,600	1,000	610
Body of Uterus	4,400	–	4,400	800	–	800
Pancreas	3,900	1,900	2,000	3,900	1,850	2,000
Oral	3,400	2,200	1,150	1,150	770	390
Stomach	2,900	1,850	1,050	1,850	1,150	720
Brain	2,600	1,450	1,150	1,750	1,000	750
Ovary	2,500	–	2,500	1,750	–	1,750
Multiple Myeloma†	2,200	1,250	980	1,400	750	640
Liver†	1,700	1,300	410	700	540	160
Esophagus	1,600	1,200	420	1,800	1,350	440
Cervix	1,300	–	1,300	380	–	380
Larynx	1,150	940	220	510	410	95
Testis	900	900	–	30	30	–
All Other Cancers	14,500	7,000	7,600	9,400	5,000	4,500
Non-melanoma skin	75,100	41,100	34,000	270	160	100

Table 1.1 Estimated new cases and deaths for cancer by sex (Cancer Society, 2009)

As per Canadian cancer statistics 2009 report, the mortality estimate due to lung cancer is higher for males and females for the year 2009. The leading cause of cancer death for man is prostate cancer where as for women it is breast cancer. The study also suggests that approximately 470 Canadians will be diagnosed each day with some form of cancer. For further information related to the statistic about cancer can be found in the Canadian cancer statistic report (Cancer Society, 2009) .

Because the rapid growth and invasive nature of cancer cells, early detection will significantly improve the chance of survival. A subset of cancer detection modalities will be described in the following section.

1.5 Cancer detection modalities

Using the differentiating features between cancer cell population (tumor) and normal cell population, the breast cancer (tumor) in women can be detected. There are different breast cancer detecting modalities such as X-ray mammography, Ultrasound, MRI and PET etc. A brief overview of these modalities with reference to breast cancer is presented in the following section of the thesis.

1.5.1 X-ray mammography

In X-ray mammography, the breast is irradiated. As the radiation passes through the breast in a straight line, attenuation differences in this radiation due to the normal and tumor (denser) tissue is detected. A Radiologist interprets these differences as tumor or normal tissue. A normal mammogram does not guarantee that a woman is free of breast cancer because some tumors are not detected by mammography.

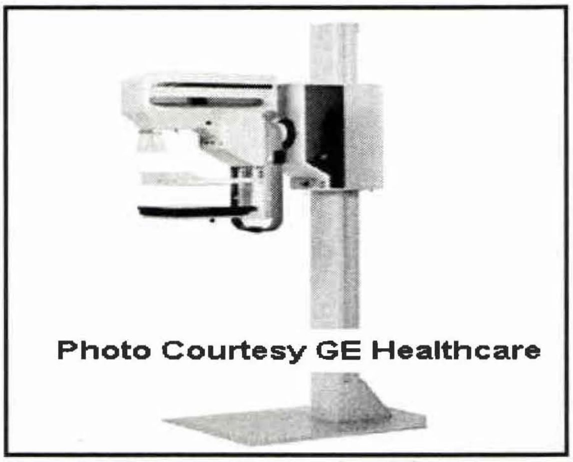

Figure 1.3 Mammography screening equipment

Mammograms are difficult to interpret for women with dense breast tissue, which is especially common in young women. Women's with dense breast tissue interferes with the identification of tumors, leading to a higher rate of false negative and false positive (Jane Wang, 2007)

The false negative rate goes higher for smaller lesion size, denser breast, and deep retro-glandular location. Undetected calcification results in false negative as well. The rates of false negative for mammographic detection for breast cancers range from 4.3% to 34.2% (Jane Wang T. T.-F., 2000).

A screening study was performed over 10 years (Joann G., 1998). This study suggests that the chances of a false-positive result, depending on the lesion and a women's risk, about 49.1% after 10 mammogram. This study also estimated the cost; for every $100 spent for screening, an additional $33 was spent to evaluate the false positive results. This implies that a higher cost to overcome the false positive results and more subsequent mammogram to rectify the false positive results in breast cancer detection.

Mammography is an efficient proven tool and a gold standard for diagnosing breast cancer in women over 50 years of age. However, for 40 to 50 year old women, it is more controversial due to more denser /glandular breast in younger women.

The Sydney breast imaging accuracy study (Houssami, 2003) found that the sensitivity of mammogram is remain constant in women 45 years and young and increase in women older than 45 years and further increase in women 51-55 years. They found that the sensitivity is 75.8% for 50 and older women and the specificity is approximately 88.0%. Another study by Kerige (Mieke Kriege,

2004) in Netherlands for women's breast cancer (age of 25 to 70 years) the detected sensitivity of mammography was less than 50% and the specificity was 95.0%.

Thus, there is a need for an additional adjunct examination method for breast cancer, which should be, low-cost, comfortable, and non-invasive, which does not depend upon the density of the breast tissue. Although our lab is proposing that EIT may be developed to serve as an adjunct to mammography, some other techniques that are currently used in screening will also be presented.

1.5.2 Ultrasound

In Ultrasound, the acoustic properties of tissue are used to differentiate the normal tissue (fluid filled) from tumor (solid filled) tissue.

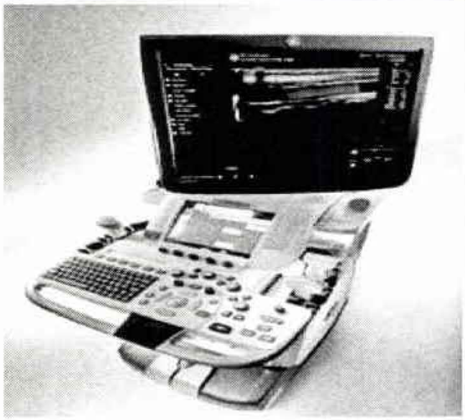

Photo Courtesy GE Healthcare

Figure 1.4 Ultrasound screening equipment

The interpretation criteria are variable, and breast ultrasound does not consistently detect micro-calcifications (Elmore G.Joann, 2005). The sensitivity of ultrasound declines in detecting nonpalpable tumor such as micro-calcifications. (Tomo Osaka, 2007). The overall accuracy of ultrasound depends on expertise of the physician conducting the procedure and interpreting the image. Breast ultrasound has been considered a useful tool in dense breasts and characterizing an abnormality detected in mammograms (Pavel Crystal, 2003).

1.5.3 Magnetic resonance imaging (MRI)

As oppose to one parameter i.e., the liner X-ray attenuation coefficient in X-ray CT. MRI provides three (radiation free) parameters for contrast mechanisms i.e., free water density, longitudinal relaxation time T1, and transverse relaxation time, *T2*. (Chris Guy, 2005).

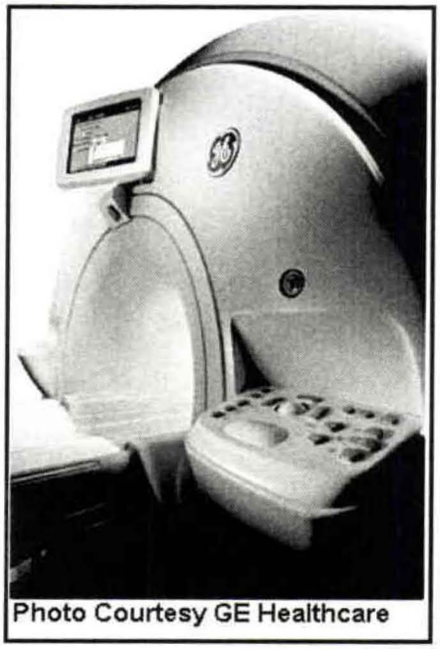

Figure 1.5 MRI screening equipment

MRI uses powerful magnets and radio waves to create detailed images of the interior of the body under investigation. It can be done with or without contrast. Contrast agent (Gadolinium) is a type of dye that is injected intravenously either right before, or during MRI procedure.

Certain abnormalities (tumors), will absorb the dye and show up very clearly on the MRI with contrast.

MRI spectroscopy can be used to differentiate tumor from normal tissue. The variation in the resonance frequencies of different compounds are used to differentiate the normal and tumor tissue. The presence of Choline-containing compound in tumor can be detected by using MRI (Baek1, 2008 September 1). MRI brings the advantage of high resolutions of 3D imaging to breast cancer stage and it is based on the size and degree of tumour spread. The disadvantages of MRI are it cannot always accurately distinguish between cancer and benign breast condition, it cannot detect micro-calcifications and interpretation results in a high rate of false-positive detection, imperfect specificity and cost of the unit is an important factor. (Liberman, 2004)

A study by Kerige (Mieke Kriege, 2004) in Netherlands for women's breast cancer (age of 25 to 70 years) the detected sensitivity of MRI was 79.5% and the specificity was 89.8%.

1.5.4 Positron emission tomography (PET)

The cancer cells grow at much faster rate, consuming more sugars (glucose) as compared to normal cells and this higher consumption of glucose is detected in positron emission tomography.

A small amount of radioactive tracer (Fluorine 18F) in combination with glucose (fluoro-de-oxy-glucose FDG) is injected into the body the radioactive tracer emits signals (positrons).

As the radioisotope undergoes positron (an antiparticle of the electron with opposite charge) emission or positive β decay, it emits a positron. Mean range of these β particles is only 0.5 mm and a maximum range of 2.4 mm in water before annihilation (Burian, 2007), when positron encounters an electron.

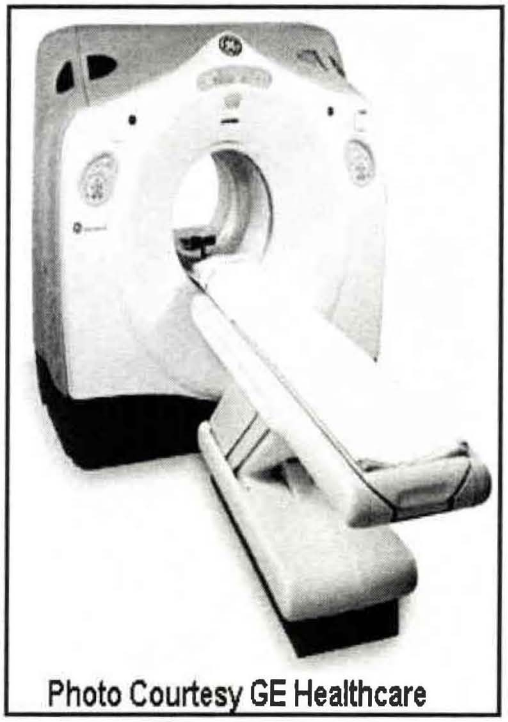

Figure 1.6 Positron emission tomography (PET) screening equipment

The encounter annihilates them both, producing a pair of annihilation photons (gamma) moving in opposite directions 180 degree apart. These are detected when they reach a scintillation detector in the scanning device, creating a burst of light, which is detected by photomultiplier tubes (PMT) or silicon avalanche photodiodes (SAPD). The technique depends on simultaneous or coincident detection of the pair of photons moving in approximately opposite direction. Photons that do not arrive in temporal "pairs" i.e. within a timing-window of few nanoseconds are ignored.

The most significant fraction of electron-positron decays result in two 511 keV gamma photons being emitted at almost 180 degrees to each other; hence it is possible to localize their source along a straight line of coincidence. As the radioactive tracer travel, and the signals get stronger near the tumor since the tumor will consume more glucose as compared to other tissue.

The major disadvantages of the techniques are the images are of substantially lower resolution than MRI and CT and higher cost (Griffeth, 2005). A good source of information on positron emission tomography can be found in text "Positron Emission Tomography Basic Sciences" by Dale L Bailey (Dale L Bailey, 2005).

1.5.5 Molecular imaging (MI)

History of medical imaging started with bone (X-ray) then organ moved to tissue (CT), went to chemical compounds (MRI, PET), and now there is a further push is to image at molecular level (MRI, PET, SPECT) in vivo. The motivation behind this push to image at the molecular level and it came from, that the diseases can be defined as "abnormal processes as well as the abnormalities in molecular concentrations of different biological markers, the signalling molecules and receptors" (Vallabhajosula, 2009).

The important advancement in the imaging instrumentation is the development of combined modalities. Multimodality image guided diagnosis means acquisition and interpretations of combined image in order to diagnose the diseases before they spreads. One of the multimodality is PET/CT, is considered to be a road map for the future diagnostic imaging in oncology studies, due to its low cost as compared to MRI. In multimodality, PET provides the functional details and the structure details added by CT, for exactly localization of the molecular abnormalities (Vallabhajosula, 2009).

For additional information about Molecular Imaging, see the texts "Molecular Imaging in Oncology" edited by Martin G. Pomper published by

Informa Healthcare USA, Inc 2008. "Molecular and Cellular MR Imaging" Edited by Michel M. J. Modo Jeff W. M. Bulte CRC Press Taylor & Francis Group FL 2007 and another good source of information "Molecular Imaging for Integrated Medical Therapy and Drug Development" By N. Tamaki, Y. Kuge (Eds.) published by Springer 2010 Japan.

All imaging methods under investigation i.e., mammography, ultrasound, MRI and PET, MRI offered by far the highest sensitivity. The lowest sensitivity was achieved by mammography / ultrasound.

The sensitivity of mammography in women at increased risk of breast cancer, including BRCA gene mutation carriers, is substantially lower, in the range of 33%–56% (C.T.M. Brekelmans, 2001; IK Komenaka, 2004). This is due to multiple factors, such as the younger age at screening for these women, increased breast radio-density, as well as pathologic and imaging characteristics of breast cancers in this population.

Recent studies indicate that breast magnetic resonance imaging (MRI) is highly sensitive and can detect breast cancers not seen on mammography, particularly in women at increased risk (F Sardanelli, 2007; CK Kuhl, 2005; M Kriege, 2004)

Further information related to these detection modalities can be found in text, "An Introduction to The Principles of Medical Imaging" by Chris Guy published by Imperial College Press London (Chris Guy, 2005) and another good text Medical Imaging Physics by Hendee W.R. published by Wiley –liss (William R. Hendee, 2002).

EIT is an alternate imaging modality that has shown promise as an adjunct imaging modality to improve the sensitivity of X-ray mammography (Tzu-Jen Kao, 2006). It is not currently approved clinically however it used at the research stage. To understand its application in the human body, one must first look at the electrical properties of tissues.

1.6 Electrical properties of cells and tissues

The conduction of electricity and dielectric behaviour in the human body is due to the presence of cells and the dielectric properties of tissue. The cell is the basic building block of the human body. The living cell is surrounded by a plasma membrane providing protection, firmness, allow different ions to enter or leave through channels and communication between cells, through gap junctions. A tissue is formed by cells performing a similar function and an organ is a structure containing several tissue types working together to carry out specific functions. In a tissue, the space between cells contains a conductive medium, the conductivity of which depends on the particular tissue, due to this reason (conductivity) the dielectric properties of body tissue are highly variable from one tissue to another. (Jossinet, 2008).

Frick and Morse reported differences in the value of electrical capacitance between malignant breast tumors and normal tissue in the year 1926 (Y. Zou, 2003). Small impedance variations are observed in normal breast and these variations can be used to differentiate various types of breast tissues. Zou and Jossinet reported that the malignant breast tumors have significantly increased capacitance and impedance than the normal tissues (Y. Zou, 2003) (J, 1998). These differences are due to the changes (1) in cellular water content, amount of extracellular fluid i.e., the surrounding of a tumor contain less water as compared to normal tissue. (2) Packing density i.e., higher number of cells are packed in tumor as compared to normal tissue. (3) Destruction of tight junctions, cell membranes and a changed orientation of malignant cells due to abnormal growth in tumor as compared to normal tissues (Malich, 2007).

1.7 Cell electrical model

The electrical properties of living tissues may be modelled as a group of electronic components (FRICKE, 1926). One of the simplest combinations uses three components. The intra-cellular space, and the membrane are modelled as a resistor $\boldsymbol{R_s}$ and a capacitor $\boldsymbol{C_s}$. respectively and the extracellular space is modelled as resistor $\boldsymbol{R_p}$ as shown in the left side along with tissue on the right side of the Figure 1.7.

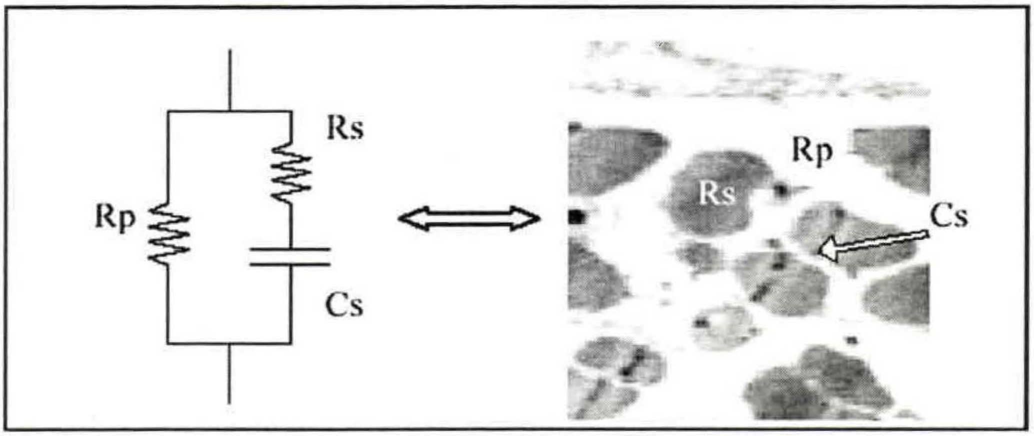

Figure 1.7 Tissue and Fricke equivalent electrical model of cell (RS and RP are the resistances of the intracellular and extra-cellular and CS is the membrane capacitance conductive medium)

The cell membrane contains lipids act as a capacitor since it separates intracellular and extra-cellular charges. The intracellular and extracellular spaces contain salt ions and are conductive. At lower frequencies all the current will flow though the RP since the reactance of the capacitor is high at zero frequency I.E., at DC (zero frequency) no current flows though the intracellular space since, the capacitor acts as an open circuit and the total impedance (resistance + reactance) is due to the extracellular space. However, as the frequency increases the current can pass through the capacitance of the cell membrane and through the intracellular resistance. The relationship between resistance and reactance can be represented by Cole-Cole plot. The Cole-Cole plot in Figure 1.8 shows the relationship between extracellular resistance and reactance for low to high frequency (right to left). The total impedance of the tissue decreases as the frequency is increases.

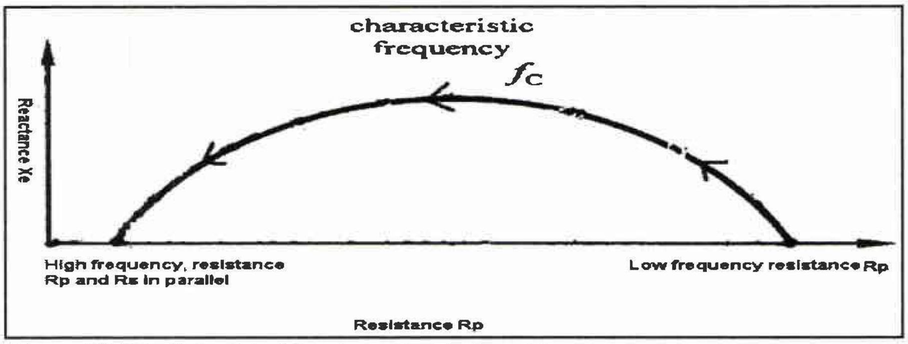

Figure 1.8 Cole-Cole plot of the above electrical model.

The Cole equation characterizes tissue impedance at multiple frequencies is given by.

$$Z^* = Z_\infty + \frac{Z_0 - Z_\infty}{1 + (f/f_0)^\beta}$$

Where $\boldsymbol{Z}^{*}$ is the complex impedance of the tissue at frequency $\boldsymbol{f}$; $\boldsymbol{Z_0}$ and $\boldsymbol{Z_\infty}$ are the limiting values of the impedance at low and high frequencies respectively; $\boldsymbol{f_0}$ is the characteristic frequency and $\boldsymbol{\beta}$ is an index ($0<\boldsymbol{\beta}<1$) representing the spread of relaxation times of the tissue (Cole, 1940).

Breast cancer can be detected by using these differentiating features (electrical properties) of normal and cancer tissue and electrical impedance tomography is the modality that promises to differentiate these electrical properties of normal and cancerous tissue.

As a potential imaging modality, EIT offers several advantages over existing medical imaging techniques such as X-ray Mammography (film-screen or digital) and Magnetic Resonance Imaging (MRI). The positive attributes of EIT are its ability to produce images non-invasively, its relatively inexpensive instrumentation requirements, physical ease of operation and portability. The technique has potential in medical and industrial application.

For medical applications, EIT is being considered as a screening or a diagnostic tool such as; imaging of the thorax, brain function, breast cancer, gastrointestinal tract etc (Holder, 2005).

In industry, EIT has been used to image fluid (oil or gas) flows in pipelines, crack detection in pipelines, bubble column dynamics, density flow meter, nuclear waste site characterization etc. (Holder, 2005)

Designing and developing a constant current source for EIT is motivated by the great potential of EIT to be used in clinical environments as a diagnostic and monitoring modality. However, EIT suffers from a low spatial resolution, and is susceptible to noise and electrode errors. The spatial resolution of EIT is relatively poor in comparison to other modalities, such as, magnetic resonance imaging (MRI) and computed X-ray Tomography (CT). In comparison however, EIT is a technique that does not use ionizing radiation, it is safe and non-invasive, inexpensive, and portable.

An outline of the thesis contents is listed here: In chapter 2, the electrical impedance tomography detection technique including electric field patters in fluids due to electric current, various electric current injection techniques and image reconstruction process will be described.

The EIT system can be divided into two sections i.e., hardware and software. The hardware section can be subdivided into electric current injection and electric potential measurement. Electric current injection can further be subdivided into signal generator and electric potential to current conversion (the current source). Since the objective of this study is to improve the first version of the McMaster EIT system current source. The following chapters will describe the signal generator and current sources.

In chapter 3, the various signal generator techniques, first prototype version of the McMaster EIT signal generator its limitation, solution to those limitation and implementation in the second version of the McMaster EIT signal generator will be described. In chapter 4, the various techniques to implement electrical current source and their advantages and disadvantages will be described. In chapter 5, the first version of the McMaster EIT current source, detected limitations and solution as implemented in the second version of the McMaster EIT current source are described. In chapter 6, the experimental methods and results related to the both versions of the McMaster EIT current sources are described. In chapter 7, conclusion and future goals are described.

In the next chapter of this thesis, EIT detection and image reconstruction techniques will be describe.

Chapter 2

Electrical impedance tomography detection technique

In electric circuit, electric currents usually flow through in copper wires; on the other hand, electric current in fluids tend to spread out in all directions. If the flow of electric current in the circuit resembles water flow in pipes, then current in a fluid, is like air motion in the atmosphere, spread out in three dimensions. In a wire, electric potential depends upon many factors including the circuit components, frequency, and circuit design, however it is unchanged along a conducting path. In a fluid, or conducting object, there is an additional complication that the electric potential can be distributed in space.

The three dimensional electric potential distribution is often called the electric field. An electric field is a region where electric forces can be felt by charged objects, and the direction of the electric field is the one in which positive charges would move. In case of a fluid, a positive ion moves in the direction of the field and a negative ions moves in the opposite direction.

2.1 Electric current and electric field patterns in fluids

The Figure 2.1 shows the circular shape electric currents and electric fields lines orthogonal to the electric current.

When electric current is applied to a fluid, circular electric current patterns are generated within the fluid. Due to the fluid conductivity; equal potential orthogonal electric fields lines are created, i.e., each orthogonal line represents an equal potential however, the electric potential of each electric field line is different from the other.

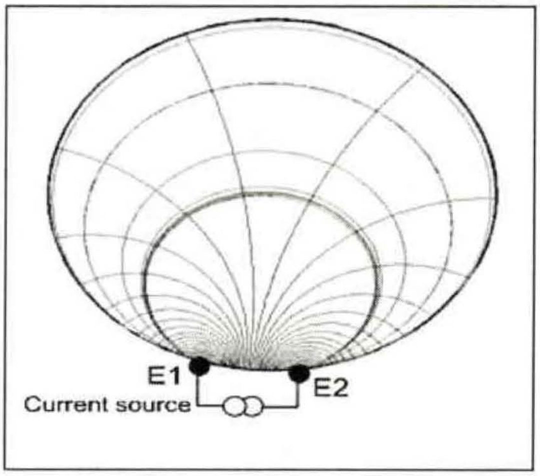

Figure 2.1 Current and Electric field lines in fluid [Rob Morrison]

If an insulator is introduced within the fluid, the electric field distribution will change as shown in the following Figures 2.2.

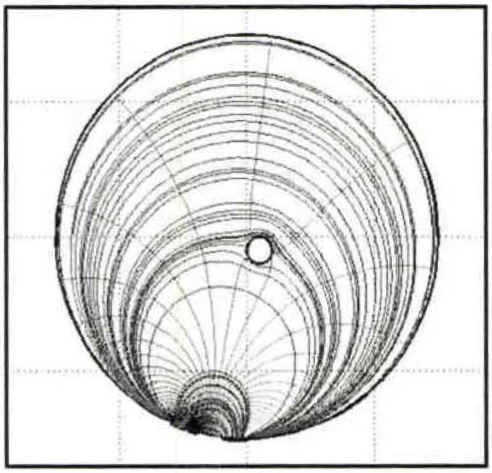

Figure 2.2 Distortion of the field lines in the presence of an insulator

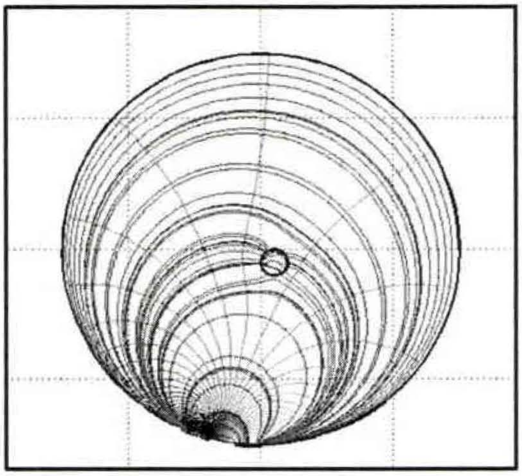

Figure 2.3 Distortion of the field lines in the presence of a conductor

Similarly, the presence of a more conductive object in the fluid, the electric field lines will change as shown in the Figure 2.3.

The above figures (2.2 and 2.3) show the distortion in the electric field lines in the presence of an insulator and a conductor. This distortion could be used in EIT to differentiate a less conductive (normal tissue) region from a more conductive (malignant tissue) one.

To measure the conductivity contrast of an object (fluid) an array of electrodes is attached to the periphery of the object. A known magnitude of electric current is applied to two or more electrodes and electric potential is measured at the remaining electrodes. A ring of electrodes is attached to the boundary of the cylindrical volume as shown in Figure 2.4.

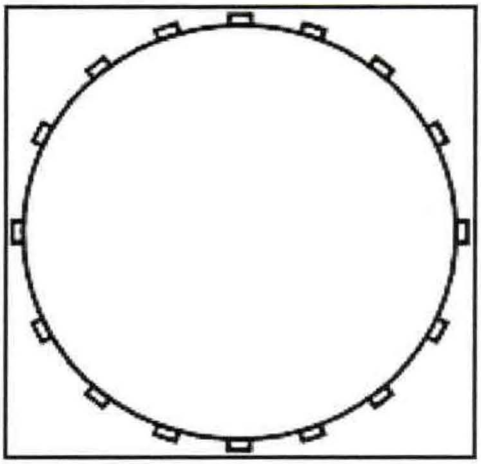

Figure 1.4 A ring of electrodes for EIT

2.2 Electric current injection and electric potential measurement strategies

In EIT there are number of strategies for electric current/potential injection and electric potential/current measurements at the boundary of an object. Some of these strategies apply electric potential and measure electric current while other apply electric current and measure electric potentials and may use the same or different electrodes for these two purposes. Many EIT systems inject the electric current into the object and measure the resulting electric potential, as this method is less sensitive to the degrading effects of contact impedance (Isaacson, 1986).

An array of electrodes in the form of a ring is attached to the boundary of the object under observation as shown in Figure 2.4. A differential electric current source is used to inject current into a pair of electrodes and resulting electric potential differences are measured on the remaining electrodes. Subsequently, the electric current is applied to another pair of electrodes and the process of potential measurement repeats. The way in which the electric current pair is switched and the potential measurements are collected varies. Some of the most common configurations used in EIT (medical application) will be described in the following section of the thesis.

2.2.1 Adjacent method

Brown and Segar (Brown, 1987) suggested a method in which the EIT system sequentially apply electrical currents to the body using a pair of adjacent electrodes. While current is applied to the body, electric potential between the adjacent remaining electrodes are measured. The procedure repeats, until electric current is applied on all electrodes and all resulting electric potentials are measured. Figure 2.5 shows the application of this method for a cylindrical volume with 16 equally spaced electrodes on a single plane of the cylindrical volume.

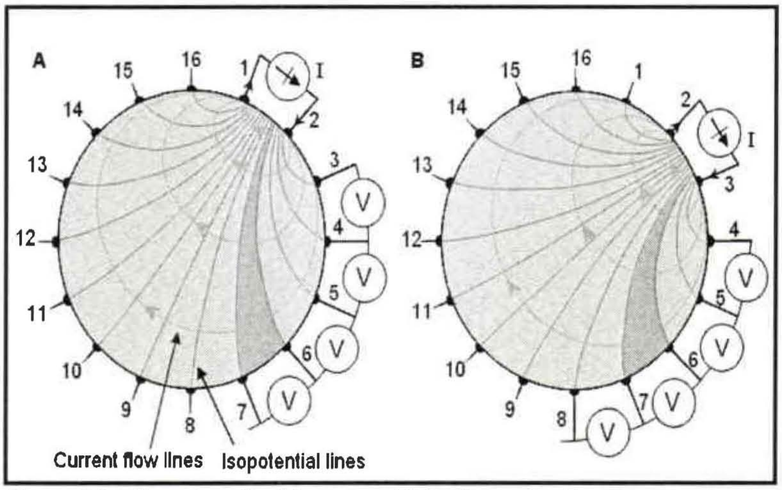

Figure 2.5 Adjacent method for current injection and voltage measurements

The electric current is first applied through electrodes 1 and 2 and the potential is measured using electrodes pairs 3-4, 4-5, 5-6,..., 15-16. The first four out of 13 independent measurements are shown in Figure 2.5(A). The next sets of 13 electric potential measurements are obtained by applying electric current through electrodes 2 and 3 as shown in Figure 2.5(B) etc.

For an N electrode system, N x (N-3) electric potential measurements are obtained. Due to reciprocity i.e., those measurements in which the electric current electrodes and electric potential electrodes are interchanged will produce identical measurements results. For example, the electric potential on the electrodes 3-4 while electrodes 1-2 are used for electric current injection will be equal to the electric potential on electrodes 1-2 while electrodes 3-4 are used for current injection. Thus, the number of independent electric potential measurements can be reduced to N x (N-3) / 2.

In the adjacent method, the electric current is driven mostly through the outer region of the object, so this method is very sensitive to conductivity contrasts near the boundary and almost insensitive to the central contrast of the object, making the ill-posedness of the inverse problem even worse (Malmivuo, 1995).

2.2.2 Opposite method

An alternative is the opposite method introduced by Hua (Hua P, 1987) as shown in Figure 2.6, again for a cylindrical object (single plane of cylinder). With opposite method, electric current is injected through two diagonally opposite electrodes (eg. electrode 16 and 8). The reference electric potential is measured from the electrode that is adjacent to the electric current injecting electrode, as shown in Figure 2.6 (A).

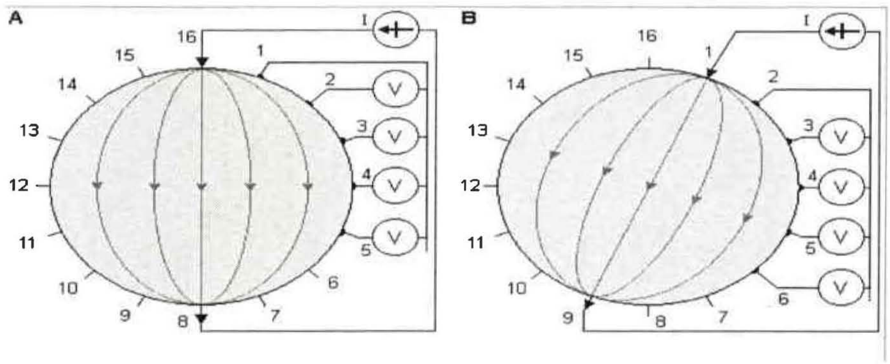

Figure 2.6 Opposite method for current injection and voltage measurements

The electric potential is measured from all other electrodes except from the electric current injection electrodes; out of 13 measurements, the first four are show in Figure 2.6 (A). The next sets of 13 electric potential measurements are obtained by selecting electrodes 1 and 9 as electric current applying electrodes as shown in Figure 2.6 (B).

For N number of electrode system N x (N-3) electric potential measurements are obtained and due to reciprocity, the number of independent electric potential measurements can be reduced to N x (N-3) / 2. The electric current distribution in this method is more uniform in the middle as compared to adjacent method and, therefore, has a good sensitivity in the middle however, it is less sensitive to conductivity variations at the boundary as compared to adjacent method (Malmivuo, 1995).

2.2.3 Cross method

A more uniform electric current distribution is obtained when electric current is applied between a pair of electrodes which are farther separated from each other. Because of this, Hua and Webster (Hua P, 1987) suggested cross method.

This method is similar to the opposite method in terms of electric potential measurements however, the electric current is not applied in opposite pairs of electrode.

In the cross method, first one chooses two adjacent electrodes one for electric current application and another for reference electric potential electrode 16 and 1 respectively as shown in the Figure 2.7 (A).

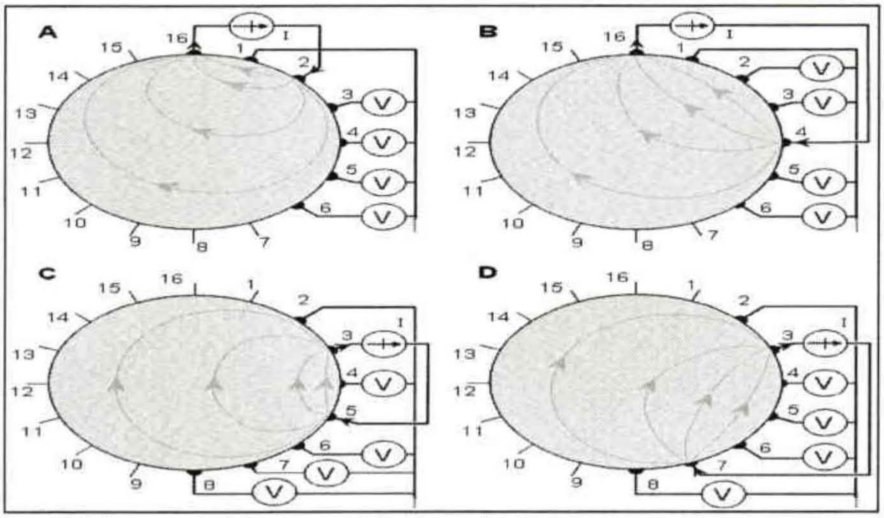

Figure 2.7 Cross method for current injection and voltage measurements

The electric current is applied through electrode 16 and 2 and the electric potential is measured for all remaining 13 electrodes with electrode 1 as the reference. The first four electric potential measurements are shown in Figure 2.7 (A). The electric current is then applied through electrode 16 and 4, and the electric potential is measured for all remaining 13 electrodes keeping electrode 1 as the reference as shown in Figure 2.7 (B). This procedure is repeated keeping electrode 16 fixed and moving to every second electric current application electrode i.e., 6, 8, 10,...14. Thus, by this method, in total 7 x 13 = 91 measurements are acquired by keeping electrode 16 fixed for electric current application and electrode 1 fixed for electric potential reference.

The measurement sequence is repeated again using electrodes 3 and 2 as electric current application and electric potential reference respectively as shown in Figure 2.7 (C). Applying electric current first to electrode 5 and measuring the electric potential for all other 13 electrode with electrode 2 as an electric potential reference. The procedure is repeated again by applying electric current to electrode 7 as shown in Figure 2.7 (D) on the previous page. Applying electric current through electrodes 9, 11, 13, ...1 and measuring the electric potential for all remaining 13 electrodes with electrode 2 being electric potential reference, making 91 measurements. From these 182 measurements, only 104 are independent.

The Cross method does not have as good sensitivity in the periphery as the Adjacent method, but has better sensitivity over the entire region (Malmivuo, 1995).

Each of the above-described method has a sensitivity advantage over the other. The Adjacent method is the least sensitive in the center as compared to

Opposite and Cross methods. The sensitivity values of Opposite and Cross methods do not vary largely (P Kauppinen, 2006).

If the location of the expected impedance change is approximately known, then the most sensitive method in that region may be use to get best results. Another sensitivity feature pointed out by Isaacson is that the low (spatial) frequency electric currents produce electric potential that are the most sensitive to changes in conductivity far from the boundary (in the middle) and high frequency electric currents produce electric potential most sensitive to changes near the boundary (Isaacson, 1986).

2.3.0 Electrical impedance imaging

The impedance (conductivity, permittivity) can be imaged to differentiate the contrast in the impedance of the object. One technique is the absolute or static imaging that attempts to quantify the actual (absolute) value of the impedance inside the object. It requires an accurate calculation of the estimated electric potential for known impedance distributions and it assumes for the technique that the properties of the object do not change during the measurement procedure. A small change in the contact impedances, the electrode sizes, the electrode locations and the object boundary shape can cause significant problems in static image reconstruction (V Kolehmainen, 1997).

Another technique is the dynamic (time difference, multi-frequency) or difference imaging, which reconstructs changes in the impedance of the object. In this technique, the object impedance is measured twice (at different frequencies or times) and the difference between these two impedance distributions is reconstructed as an image, which enhances the difference and reduces the error and geometrical uncertainties.

2.3.1 Image reconstruction process

Image reconstruction in EIT is the process of converting the electrical potential measurements and corresponding injected electric currents into images. The reconstruction process makes use of the relationship between electric potential, electric current, and resistance (impedance).

The EIT image reconstruction is a non-linear, ill posed and an inverse problem. The conductivity of the object is not homogenous (non-linear), since the electric current in the object (fluid) is three-dimensional and it does not follow a straight path as electric current in a wire or high-energy radiation.

A problem is called well posed, if the solution must exists (existence), has a unique solution (uniqueness) and if the solution continuously depends on the data (stability), i.e., solution must not be unstable if there are small changes in the data. If any one of these three conditions (existence, uniqueness, stability) is violated then the problem is called ill posed. Therefore, the EIT image reconstruction is categorized as an ill-posed problem (Holder, 2005).

EIT is an inverse problem since from the boundary injected electric current and measured electric potentials the conductivity of the object is estimated ***(J=σ E).*** Where $\boldsymbol{E}$ is the electrical field, $\boldsymbol{J}$ is the electric current density and $\boldsymbol{\sigma}$ is the conductivity.

Since the conductivity inside the object volume is non-linear, discretization is used to linearize the non-linear conductivity, conductivity is treated as liner within these discrete regions, and further-more to overcome the ill-posed problem regularization is implemented.

There are many proposed methods for solving the inverse nonlinear problem of EIT. These methods fall into two broad categories i.e., non-iterative and iterative methods. The non-iterative (single-step) methods are based on linear approximations. The basic assumption of these methods is that the conductivity distribution is approximately homogeneous. Examples of these linear approximation methods include the Barber-Brown back-projection (D. C. Barber, 1983; Avis, 1995) and sensitivity matrix (R. Gadd, 1992; P. Morucci, 1994) methods. Single-step methods produce an image by using the mathematical operation once (Boone, 1997). The sensitivity matrix uses a theorem derived by Geselowitz (Geselowitz, 1971).

The above mention linear non-iterative methods are very attractive due to their mathematical simplicity and computational speed, but they pay no attention to the non-linearity of the EIT. Furthermore, there are number of undesirable features such as, the recovered images of a centrally-placed object appears physically larger than that of a peripheral one of equivalent size, and underestimation of overall difference in the resistivity is normally greatest for centrally-placed objects (Boone, 1997).

Iterative methods are used to (try to) solve the 'static' reconstruction problem, i.e., find the actual conductivity in the body rather than a change in conductivity such as Wexler double constraint algorithm (Wexler A. , 1988). These methods generally solve a series of linear problems via solution of the Laplace equation ($\boldsymbol{\nabla} \cdot \boldsymbol{\sigma} \boldsymbol{\nabla} \boldsymbol{\varphi} = \boldsymbol{0}$) in an attempt to solve the full nonlinear problem. Most of these methods acknowledge the non-linearity and ill posedness of EIT and still attempt to treat it without linearization, unlike non-iterative methods

Construction of an image in EIT has two parts i.e., the forward solution and the implementation of the forward solution to solve the inverse problem. Solution of the forward problem allows the calculation of electric potential at any point on the surface of an object under investigation, using a given (assume) approximate conductivity distribution and boundary electrical current density. The calculation of the conductivity distribution is the inverse problem, which often requires multiple iterations of the forward problem, in order to optimize a specific criterion of fit between measured and calculated values.

2.3.2 Forward problem

The objective of the forward problem is to estimate the electric potential distribution within and at the surface object volume. An accurate model is used to estimate the electric potential distribution of the physical system. The physical model should include the circumference geometry, structure, electrodes and practical boundary conditions, such as electrode location, shape and contact impedance.

Several electrode models has been developed for use in EIT such as; Complete Model (Cheng K S, 1989), Shunt Model (Holder, 2005), Gap Model (Cheng K S, 1989), Continuum Model (Cheng K S, 1989) etc.

In order to solve the forward part of the problem one of the above physical model is usually implemented in finite element method (FEM, the FEM approximate the variations in a process) (Holder, 2005). In FEM the geometry of the object volume is divided into finite number of discrete elements (tetrahedral or hexahedra) and the unknown functions can be approximated by linear or higher order polynomials.

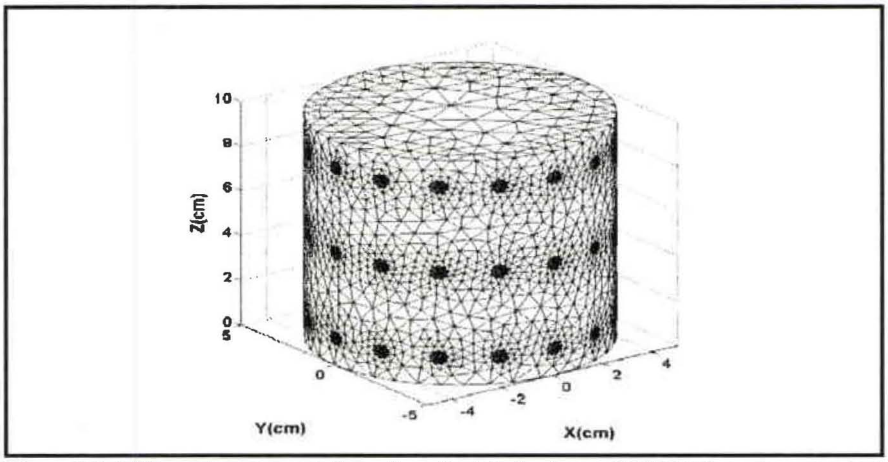

Figure 2.8 A 3D mesh representation of a cylindrical volume (NETGEN mesh generator)

The 3D mesh is constructed using NETGN (NETGN is an open source, automatic 3d tetrahedral mesh generator) as shown in Figure 2.8 on the next page, each element in the mesh consists of nodes and faces.

2.3.3 Inverse problem

The electrical field $\boldsymbol{E}$ in terms of the electrical potential $\varphi(x, y)$ can be expressed as $E = -\nabla\varphi(x, y)$ and general form of Ohm's law for a point within a volume conductor can be expressed as $J(x, y) = \sigma(x, y)\, E(x, y)$, where J is the electric current density, σ is the conductivity. If the electric current source is absent within the volume conductor ($\nabla \cdot J = 0$) then by combining above two equation one gets

$$\nabla \cdot (\sigma(x, y)\, \nabla\varphi(x, y)) = 0 \quad (2.1)$$

Conductivity distribution image can be reconstructed by solving equation 2.1 for conductivity $\sigma(x, y)$. The simple (linear) conductivity distribution can be solved analytically however, analytical solutions are unable to solve for arbitrary (non-linear) distributions. Many EIT systems solve (2.1) for conductivity by dividing the region of interest into a finite number of elements in which the conductivity may be specified simply (liner). A relationship is obtained between the electric potential measurements made on the boundary and the conductivities of such regions.

If there are N such regions, then N simultaneous equations can be made to define the dependence of the conductivity values on the boundary measurements. This may be expressed as:

$$\boldsymbol{V} = \boldsymbol{T} \cdot \boldsymbol{\sigma} \quad (2.2)$$

Where $\boldsymbol{\sigma}$ is a vector of conductivity values, $\boldsymbol{V}$ is the vector of electric potential measurements and $\boldsymbol{T}$ is the transformation relating $\boldsymbol{V}$ to $\boldsymbol{\sigma}$. If $\boldsymbol{T}$ and $\boldsymbol{\sigma}$ are the known then it is easy to solve the above equation and is known as the forward problem discussed in the previous section. EIT seeks the solution of the relationship: $\boldsymbol{\sigma} = \boldsymbol{T}^{1} \cdot \boldsymbol{V}$ *(2.3)*

Hence, values of $\boldsymbol{V}$ measured at the boundary are formed into a vector and applied to (2.3) to obtain $\boldsymbol{\sigma}$ and this is known as the inverse problem. However, simple inversion of $\boldsymbol{T}$ is not possible because $\boldsymbol{T}$ is a non-linear transformation and cannot be inverted by standard matrix methods. One solution is to assume that, for small variations from the uniform case, $\boldsymbol{T}$ may be approximated as linear and may then be inverted. The inversion of $\boldsymbol{T}$ is however error-prone.

To solve the inverse problem the conductivity of the object volume is linearized and regularized. For linearization, most commonly used methods are probabilistic approaches, back-projection (Natterer, 1982), Newton-Raphson and variant of Newton-Raphson methods (Holder, 2005). For regularization techniques such as singular value decomposition (SVD), truncated singular value decomposition (TSVD), total variation (TV) (Holder, 2005), Tikhonov regularization (Phillips, 1962; N. Tikhonov, 1963) and others are used. Detailed theory and examples of liner ill posed problems can be found in text (Richard Aster, 2005; Bertero M, 1998; Bertero M, 1998; Heinz W. Engl, 2000; Higham, 1996; Tarantola, 2004; Vogel, 2002)

To reconstruct, the impedance images from measured data, a Matlab developed package called the EIDORS (Electrical Impedance and Diffuse Optical Reconstruction Software) project is available; a review of the software package is presented by Andy Adler (Andy Adler, 2006). The objective of EIDORS project is to develop free software that can deal with the non-linear and ill-posed problem from boundary measurements. Such software facilitates research and development in EIT field by providing a reference implementation against which new developments can be compared and by providing a functioning software base from which new ideas may be built and tested.

The EIT system can be divided into two sections i.e., hardware and software. The hardware section can be subdivided into electric current injection and electric potential measurement. Electric current injection can further be subdivided into signal generator and electric potential to current conversion (the current source). In the next two chapters of this thesis the signal generator and subsequently the current source, using various techniques will be described.

Chapter 3

Signal generators

A device (circuit) which generates signal (voltage or current) is called a signal generator. The signal generator is used as a stimulus for electronic measurements, for instance in EIT the current signal is use to stimulate the subject and the response is measured as the boundary voltage. The signal may be a true bipolar AC signal (with peaks oscillating above and below a ground reference point) or it may vary over a range of DC offset voltages, either positive or negative. It may be a sine wave or other analog function, a digital pulse, a binary pattern or a purely arbitrary wave shape.

There are many techniques to generate signals, however only a small set of them will be explained in this chapter. For additional information about signal generator, some good references are "Analysis and design of quadrature oscillators" by Oliveira, Luis B. RF (Oliveira, 2008) and "Microwave Transistor Oscillator Design" By Grebennikov, Andrei (Grebennikov, 2007)

This chapter also covers the first version of the McMaster EIT signal generator and its limitations. To address the limitations in the first version, a second version of the McMaster EIT signal generator was build and this will be described as well.

3.1 Signal generator using RC network

A signal generator can be constructed simply using a combination of resistors (R), capacitors (C) and a device (an operational amplifier or transistor). A signal generator is shown in Figure 3.1 which includes an operational amplifier and three RC networks. In this signal generator circuit, multiple resistor/capacitor (RC) networks are connected in parallel to each other and the last network is connected to the device.

The operation of the RC network is simple: assume that when power is first applied, the operational amplifier output goes into saturation positive V+. Since the output is fed back to the input of the RC network, the first capacitor begins charging up toward V+ with time constant *RC*. When it reaches half the supply voltage, the operational amplifier switches into negative saturation (device acts as a Schmitt trigger), and the first capacitor begins discharging toward V- with the same time constant. The cycle repeats indefinitely and it is independent of supply voltage. Each RC network will translate the signal 60 degrees out of phase with respect to the input signal (John C West, 1951).

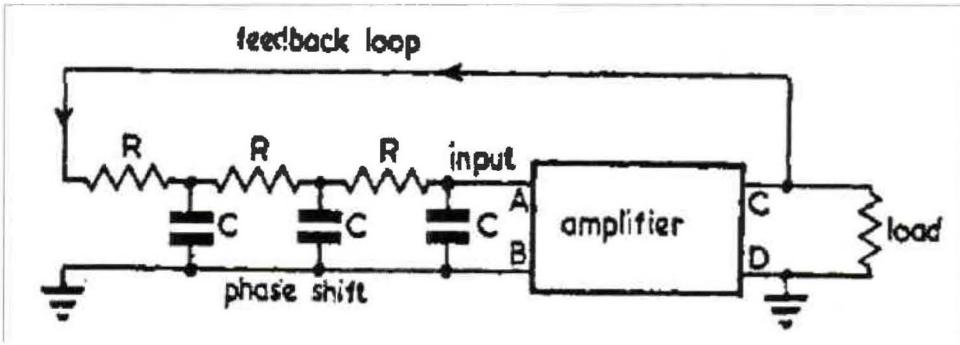

Figure 3.1 Signal generator circuit diagram using RC network.

The frequency of oscillation depends on the value of time constant (RC). Frequency of the above circuit is given by $f = \frac{1}{2\pi RC\sqrt{6}}$. Where f is the output frequency in Hz, R is the resistance in Ohms, C is the capacitance in Farads. The phase angle is given by $\varphi = \tan^{-1}\frac{R}{X_c}$ where $X_c = \frac{1}{2\pi f C}$. The performance of this type of signal generator will degrade over time and temperature.

3.2 Signal generator using lookup table

Another commonly used technique for a signal generator as shown in the following Figure 3.2.

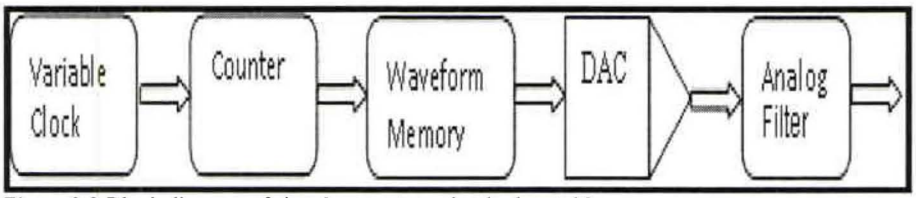

Figure 3.2 Block diagram of signal generator using lookup table

A variable clock is used to control the time between two consecutive voltage amplitudes (specified in a look-up table) of a cycle of the waveform, thus allowing the control of the frequency of the waveform. Discrete successive amplitude values of signals are stored in consecutive memory locations (the look-up table). A counter provides the address of the locations where the next amplitude value is stored in memory. The digital to analog converter (DAC), converts the digital values into corresponding voltages. An analog filter smooth's out the discrete voltage values to remove unwanted frequencies and approximates a continuous signal.

This type of arrangement provides the flexibility to produce any type of waveform i.e., sine, triangular, sum of two or more sine wave or any desired waveform. However, it has some disadvantages such as: the propagation delay time and the settling time. Plus, in order to change the shape, phase and/or number of amplitudes, the entire waveform memory must be reprogrammed each time.

3.3 Signal generator using field programmable gate array (FPGA)

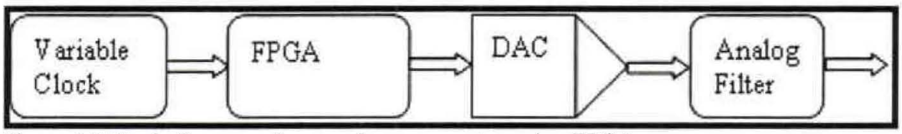

Figure 3.3 Block diagram of a waveform generator using FPGA

Another technique is to combine the counter and waveform memory in a field programmable gate array (FPGA) as shown in Figure 3.3.

3.3.1 Field programmable gate array (FPGA)

Before the invention of the programmable logic gate array, the board level circuits were built using standard components or chips. If discrete chips were used in a high-speed communications system, the main bottleneck came from the data transmission from one chip to another. To overcome the communication bottleneck, application specific chips were designed and built by the manufacturer in custom integrated circuits however, the circuit designer was unable to change or modify the function of the application specific chip (electronic device) at the design time.

In contrast to the application specific electronic devices, there are other types of devices which allow the circuit designers to define (program) the function of the electronic device rather than the device manufacturer. This type of electronic device is called a field programmable gate array (FPGA). This user programmability gives the circuit designer access to the complex integrated designs without requiring manufacturer collaboration for application specific integrated circuits. This results in savings in terms of the design time and lowers the cost for components.

The FPGA is an integrated circuit that contains over 10,000 identical standard logic components (www.xilinx.com). In FPGA terminology, these components are called logic cells.

The architecture of a logic cell varies between different device families. Generally, each logic cell combines inputs and one or two outputs as specified by the user program. The user program also specifies the individual cell Boolean operation or function that acts on these logical inputs to produce the desired output. These individual cells are interconnected by a matrix of wires and selectively programmable open/close switches.

A user's circuit design is implemented by specifying a simple logic function for each cell. The information or outcome of one cell is routed through the interconnecting wire matrix by selectively opening or closing the switches to another cell or out of the FPGA. The interconnected arrays of logic cells form a matrix of basic building blocks for logic circuits. Complex designs can be implemented by combining these basic building blocks to create the desired circuit operation.

To translate the user's schematic diagrams (circuits) a textual hardware description language (THDL) or software is used. Software packages come with libraries of more complex optimized functions and those functions can be implemented as macros which simplify the design process by providing common optimized circuits. Depending on the particular device type, the program can be "burned" permanently as in Programmable Read Only Memory (PROM), or semi permanently (as in Erasable PROM or EPROM) or it can be loaded from an external memory each time the device powers up (boot sector loading source code).

3.3.2 FPGA signal generation

This FPGA logic structure can be utilized synchronously to generate any arbitrary waveform. The advantage of using a FPGA is to overcome the propagation time delay of the counter and programmable memory. It is much faster than the previous technique and any functional shape such as sine, triangular, sum of two or more sine, etc, can be generated. However, there is still an issue with the digital to analog converter settling time, thus for higher frequencies a faster DAC is required. For a more comprehensive review of signal generation, and how to use an FPGA for signal generation, see the text FPGA-based Implementation of Signal Processing Systems by Roger Woods (Woods, 2008).

3.4 Direct digital synthesis (DDS)

Direct digital synthesis (DDS) is a new signal generation technology. About a decade ago, this technique was a novelty used in a very limited number of applications. Since then there has been an enormous evolution in the digital technology resulting in increased speed, lower power consumption, lower cost, improved digital signal processing (DSP), and more precise data conversion devices. The DDS is becoming increasingly popular and its performance is improving constantly. The signal in the DDS devices is generated, manipulated digitally from "the ground up," and converted into an analog signal, using a digital to analog converter (DAC). The DDS is a computing machine where analog waveform signals can be generated using a representation of numbers generated digitally.

There are many compelling reasons to generate signals using a DDS since; reducibility, repeatability, reliability and very high accuracy and precision can be obtained in the digital regime.

By programming the DDS, adaptive channel bandwidths, modulation formats and frequency hopping are easily achieved. This has opened up the possibility of software control waveforms generation that can be used in various systems.

In this thesis, a DDS system was used for signal generation, for all of the reasons outlined above. The specifics of the methodology will be outlined below, however to put this section into the context of current work in the field, a brief literature survey of the similar usage of signal generation will be presented. Note that as this topic is broad in scope, this review will be limited to relevant applications in medical physics, with a particular interest in EIT. For comprehensive details about DDS see text "Digital Frequency Synthesis Demystified" by Bar-Giora Goldberg. (Goldberg, Digital Frequency Synthesis Demystified, 1999)

3.5 Signal generator literature review

Tong In Oh and David Holder (Oh1, 2007) for their signal generator used a FPGA and a 16bit digital to analog converter. Their system was able to generate frequencies in the range of 10 Hz to 500 kHz of either a single sinusoidal waveform or a sum of multiple frequencies. Their study shows that there is no advantage in using sum of multiple frequency waveforms higher than 10 kHz instead of single frequency. They also used a FPGA to synchronize the injection and measurement events.

For the second version of the McMaster EIT signal generator the FPGA technique was not implemented to avoid the digital to analog converter settling time issue and requirement of reprogramming the FPGA for every new frequency waveform generation. The sum of multiple frequency waveform signal generation is avoided as well.

Ning Liu (Liu, 2003) implemented a direct digital synthesizer within a FPGA with a complex modulator to generate a sinusoidal waveform with controllable amplitude, phase and frequency as shown in Figure 3.4. Their system was able to generate discrete frequencies of a sinusoidal waveform in the range of 300Hz to 1MHz through a 16bit DAC. Their system showed the effects of timing-jitter, high frequency digital noise, truncation errors, and other sources of noise.

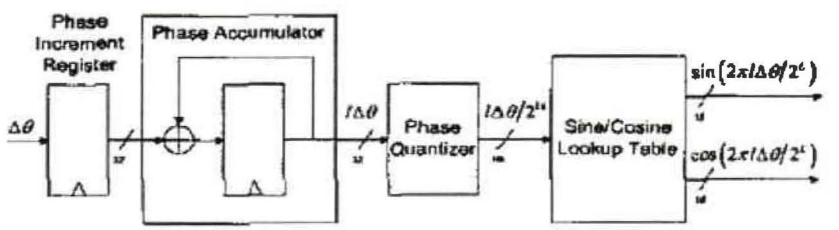

Figure 3.4 a direct Digital synthesizer implemented in FPGA (Liu, 2003)

For our second version of the McMaster EIT signal generator, a standalone DDS was used instead of implementing a DDS within a FPGA to minimize the above mentioned sources of error and be able to enhance the frequency resolution.

Ryan Halter (Halter, 2004) implemented a signal generator in a FPGA as well. For the FPGA clock input, they use the output of the DDS and a DSP was used to control / program the output of the DDS. Their signal generator system block diagram is shown in Figure 3.5.

Figure 3.5 Signal generator implemented in FPGA using DDS and DSP

The FPGA can output frequencies in the range of 10 kHz to 10 MHz. In their design, they used a 14 bit DAC. This was a good design, since the FPGA output frequency was controlled through a DDS clock and the DDS output clock can be manipulated by software. The issues (reprogramming for new frequencies, DAC settling time) related to the FPGA and DAC are still exists and therefore this technique was not implemented in the second version of the McMaster EIT system signal generator.

3.6 Signal generator of McMaster EIT system

In this section, the two versions of McMaster EIT system signal generator of will be described.

3.6.1 Signal generator version I of McMaster EIT system

The first version of the McMaster EIT system signal generator was designed using a DSP and a 16bit DAC. The clock for the DSP was provided through an 80 MHz oscillator. The signal patterns for the waveform were programmed into the DSP, allowing for the generation of any arbitrary waveform. A Seventh-order Taylor series expansion was selected for the data set for waveform signal approximation, due to its accuracy over other simulation methods (Jegatheesan, 2008).

The DSP was interfaced to the PC through a serial communication port. On the PC, a Graphical User Interface was written in LabView (National Instrument) to control the signal generation of frequency and amplitude through the DSP. The signal generator was able to produce signal waveforms in the preselected frequency range from 100 Hz to 125 KHz.

Two limitations and an issue were identified in the first version of the McMaster EIT signal generator. The restrictions were that the maximum frequency was limited to 125 KHz and only preselected frequencies could be generated. The issue was that the digital to analog converter (DAC) inputs were updated less than the DAC settling time i.e., the inputs of the DAC were updated ever 2μsec however, the settling time was 2.5 -13μsec.

Jossinet showed in his study that there are significant differences between the phase angle of carcinoma and normal tissue at the frequencies at 125KHz, 150KHz, 250KHz, 500KHz and 1MHz (Jacques Jossinet, 1999).

To use this variation in the frequency with McMaster EIT system it was decided to increase the maximum frequency up to 1MHz and instead of generating only preselected frequencies, the frequencies can be increase or decrease is steps of 1Hz. To meet these requirements and DAC settling time issue the second version of McMaster EIT signal generator was initiated.

3.6.2 Signal generator version II of McMaster EIT system

The major EIT research groups have designed their signal generation using a DSP based look-up table or field programmable gate array (FPGA) for high bandwidth frequency synthesizers. However, for this second version of the McMaster EIT system, a direct digital synthesizer (DDS) was selected since it provides many significant advantages over the FPGA approach, such as, the fast settling time, its sub-hertz frequency resolution, its continuous-phase switching response and its low phase noise. These features are easily obtainable in a DDS as compared to a FPGA based design.

Although the principles of DDS have been known for many years, the DDS did not play a dominant role in wideband frequency generation until more recently. Earlier DDSs were limited to produce narrow bands of closely spaced frequencies, due to limitations of digital logic and DAC technologies. Recent advances in integrated circuit technologies have brought a remarkable progress in this area (Eva Murphy, 2004).

For this prototype, a DDS (AD9833) was selected. This DDS is a low power (20mW at 3V) waveform signal (sine, triangular, square) generator. The output phase and frequency are programmable through software and there is no need for external components except an oscillator. A 25 MHz oscillator was interfaced as the input clock to the DDS. A frequency resolution of 0.1 Hz can be achieved by programming the 28 bit registers. The DDS can be controlled via a 3-wire serial peripheral interface (SPI) interface, which can operate at clock rates up to 40MHz. (Analog Devices AD9833)

In this design, the DDS was controlled through an ATmega162 microcontroller. The ATmega162 is a low-power CMOS 8-bit microcontroller based on the reduced instruction set computers (RISC) architecture manufactured by ATMEL. Through RISC architecture a powerful instruction is executed in a single clock cycle that gives a throughput approaching 1 million instructions per second (MIPS) per MHz clock frequency.

Other reasons for this microcontroller selection were due to its internal programmable clock, in-system programmable (ISP) flash with read-while write capabilities, on-chip debugging support, RAM and programming via JTAG interface.

For the second version of the McMaster EIT system, there was no need for improved communication between the microcontroller and the DDS, as the microcontroller only communicates with the DDS to change the shape or frequency output.

No external oscillator (clock) was interfaced to the microcontroller. The internal programmable clock of the microcontroller was programmed to produce the timing sequence since, for lower frequency applications, the internal programmable clock is sufficient and this microcontroller application is a low frequency application.

The on-chip ISP flash allows the program memory to be reprogrammed in-system through an SPI interface, by a conventional non-volatile memory programmer, or by an on-chip Boot program running on the AVR core. The boot program can use the JTAG interface to download the application program into the application flash memory. Software in the boot flash section will continue to run while the application flash section is updated providing true read-while-write operation (ATMEL 162). This capability of the microcontroller was utilised to program and test the application program at various stages. In this design, the on-chip debugging support helped to identify and correct the programming bugs and reduce the programming time significantly.

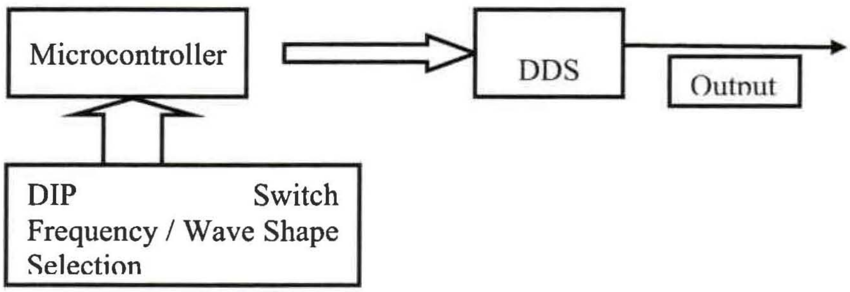

Figure 3.6 McMaster EIT system version II signal generator block diagram

Port C of the microcontroller was implemented as the human interface through the 8 bit dual in-line package (DIP) switches. Through these 8 DIP switches the frequency and wave shape can be selected. The lower six bits select the frequency and the upper two bits select the wave shape i.e., sine wave, triangular wave or square wave (see appendix C for frequency and shape selection details). The selected frequency, wave shape and other DDS control information is sent through the serial peripheral interface (SPI) to the DDS from the microcontroller. The block diagram of the microcontroller and DDS circuit is shown in Figure 3.6.

The microcontroller software was written in assembly language. The program was divided into subroutines for better management, readability and debugging. Assembly subroutines were tested separately, after verifying the functionality of each subroutine the whole program (collectively all subroutines) was tested again and this confirmed the correct functionality. The final test was conducted using the dipswitches, the microcontroller and the DDS. Using dipswitches the shape and frequency of the signal was selected. This information (from dipswitches) was translated into control commands by the microcontroller and sent to the DDS. The DDS output shape and frequency were observed with a digital oscilloscope and this confirmed that the system was working according to specifications.

Initially it was decided that the output signal from the DDS would be fed through a low pass filter to remove any unwanted frequencies however, observations with and without the filter revealed that the unfiltered waveform did not have a significant noise contribution within the desired measurement precision. The amplitudes at various frequencies with and without the filter are very similar as shown in Figure 3.7.

The output waveform from the DDS was uni-polar, positive and about 650mV (peak-to-peak) at 1 KHz, It increases slightly with frequency, and as the frequency increases above about 200 KHz, its magnitude decreases.

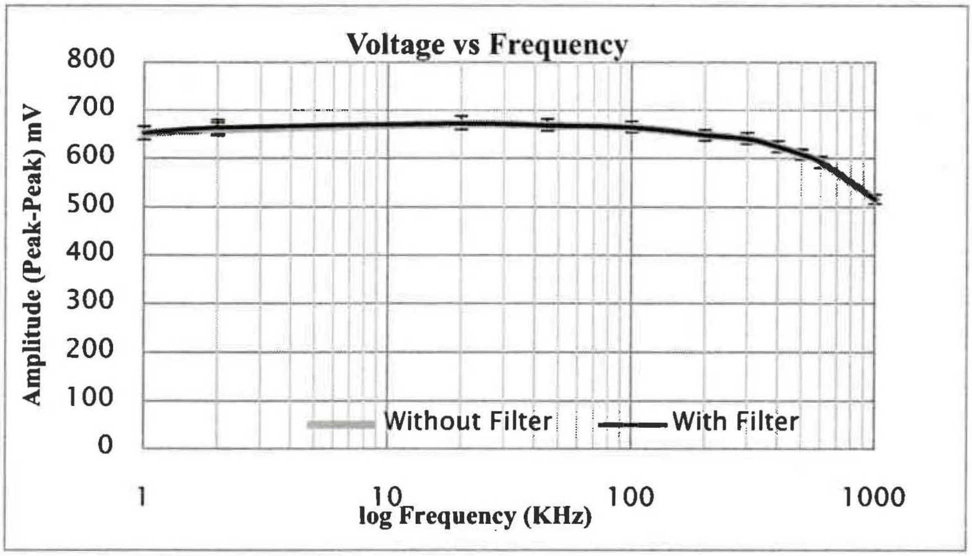

Figure 3.7 Amplitude vs Frequency with and without filter

There were two issues with the output amplitude of the DDS with reference to use in an EIT system, namely DC offset and fixed amplitude.

The output frequency was oscillating above zero volts (DC offset) and output amplitude was fixed (650mV below 200 KHz).

To overcome these two issues, two stages using operational amplifiers were implemented. The first stage corrects the DC offset making the waveform oscillate above and below a ground (0 V) reference point, not just above ground, so the ground reference is same for the entire equipment. The second stage acts as an amplifier to regulate the output gain by means of a variable potentiometer. This stage was implemented to increase or decrease the fixed voltage to control the injected current magnitude as required by EIT system.

The DDS voltage signal was converted into a bi-polar signal of ±325mV (peak-to-peak) after adjusting the DC shift. It was estimated that a voltage signal of ±10V (peak to peak) is required as input to the voltage control current source. To translate the ±325mV (peak-to-peak) voltage signal into a ±10V (peak-to-peak) voltage signal a gain of about 30 was required. The gain of 30 for an operational amplifier could be achieved if the frequency is low; however, for higher frequencies the slew rate becomes a problem. The slew rate is the maximum rate of change of voltage at the operational amplifier output. The output of an ideal operational amplifier can change as quickly as the input voltage (waveform signal) however, a real operational amplifier has a practical limit to this rate of change and therefore the gain of the operational amplifier is frequency dependent. To avoid this slew rate issue of the operational amplifiers, the gain of 30 was divided into two steps using two operational amplifiers instead of one.

A gain of 5 was introduced at the first stage using the same operational amplifier where the signal DC offset was removed (uni-polar to bi-polar voltage signal) and the remaining gain was achieved through a second operational amplifier. This combination of splitting the gain in two stages gave very stable results, not only the desired gain was achieved at higher frequency the higher signal to noise ratio was achieved as well. Stage one (DC offset + gain) and stage two (gain) of the circuit were tested and verified for said gain where the output voltage swings up to ±10V (peak-to-peak).

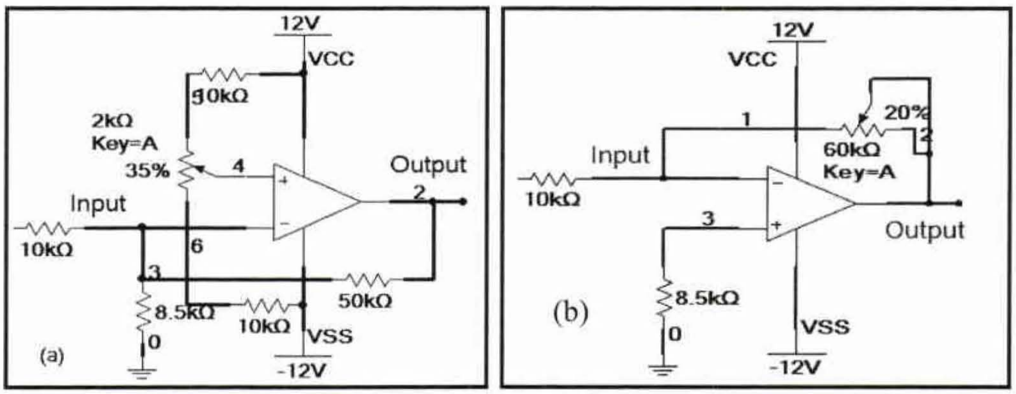

Figure 3.8 Circuit diagram for (a) DC shift and (b) variable voltage gain stage

The fixed gain + DC offset and variable gain circuitry is shown in Figure 3.8 (a) and (b) respectively. Another requirement for the McMaster EIT signal generator was to have differential signals as opposed to a single-ended signal.

Differential signals use two complementary paths carrying copies of the same signal in equal and opposite polarity (relative to ground). As the signal's cycle proceeds one path becomes more positive, the other becomes more negative to the same degree. For example, if the signal's value at some instant in time was +10V on one of the paths, then the value on the other path would be exactly –10V at that instant in time, assuming the two signals were perfectly in phase.

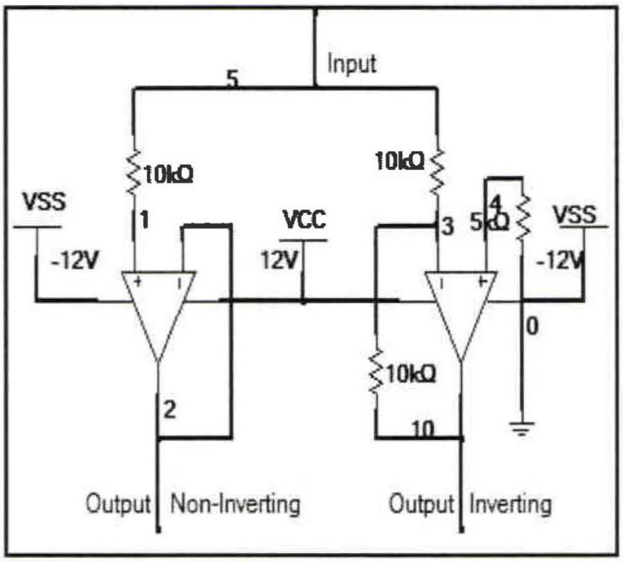

Figure 3.9 Single ended to double ended conversion

The differential architecture is good for floating loads, better for rejecting cross talk and noise rejection where as the single-ended injection is more common for a grounded load configuration.

To convert the single ended signal into differential signals two unity gain inverting and non-inverting operational amplifiers were employed. The amplitude and phase differences for the inverting and non-inverting operational amplifiers were calibrated to a unity gain and a 180 degrees phase difference.

The differential amplitude and phase was also tested and verified for its accuracy i.e., the differential signals were an exact replica of the input signal 180 degrees out of phase with each others. The circuit diagram for inverting and non-inverting operational amplifier is shown in Figure 3.9.

The second version of McMaster EIT signal generator can produce any programmed differential voltage output frequency from 1Hz to 1MHz a with frequency resolution of 1Hz and the signal shape can be sine wave, triangular wave or square wave.

In the next chapter of this thesis, the stimulating probe i.e., electric current and various techniques to convert electric potential into electric current along with performance related parameters will be described.

Chapter 4

Current source

Object impedance can be measured accurately by injecting an accurate constant magnitude of electric current through the object and measuring accurately the electric potential at the surface. There are two main devices (circuits) involved in this procedure i.e., electric current application (current source) and electric potential measurements.

The current source is very critical in this type of measuring system, it must inject a constant magnitude of electric current otherwise any change in the electric current will be interpreted as a change in impedance.

The goal of this study is to construct a constant current source, which can be use to image, the conductivity distribution at multiple frequencies. In the following sections, the current sources and various performance related parameters will be described.

Current sources are part of the basic electronic building blocks that are used extensively in the architecture of analog ICs, as well as in measuring the response of a circuit by injecting current. In both cases, current sources are created by combining resistors, diodes and bipolar junction transistors (BJTs) or field effect transistors (FETs). They can also be created at the circuit board level using discrete, matched pairs of transistor arrays, or by combining operational amplifiers with precision voltage references.

Although most forms of instrumentation today use either voltage or current references, the voltage sources are more widespread than current. The circuits are frequently designed to use a voltage reference together with precision resistors, so that a stable reference voltage is converted into a precise current. The current source applications range from biasing, stabilizing the reference and for a stimulus response measurement.

Current sources are not novel. They predated the integrated circuit by at least a couple of decades. Before their implementation in integrated circuits, they were used in vacuum tube–based circuits (triodes and pentodes). In 1960s both NPN and PNP silicon transistors became available and in the late 60s the analog designers were able to build current sources that connected to either a positive or a negative supply. Then, when the silicon bipolar integrated circuit (IC) became a practical reality, the current source became an integral part of the internal architecture for the purposes of biasing and stability.

Simple current injection devices can be divided into following three categories;

4.0.1 Current source

A current source (usually comprising P-type BJT or FET device) connects between the positive supply voltage (+V) and the load as shown in Figure 4.1(a) on the next page.

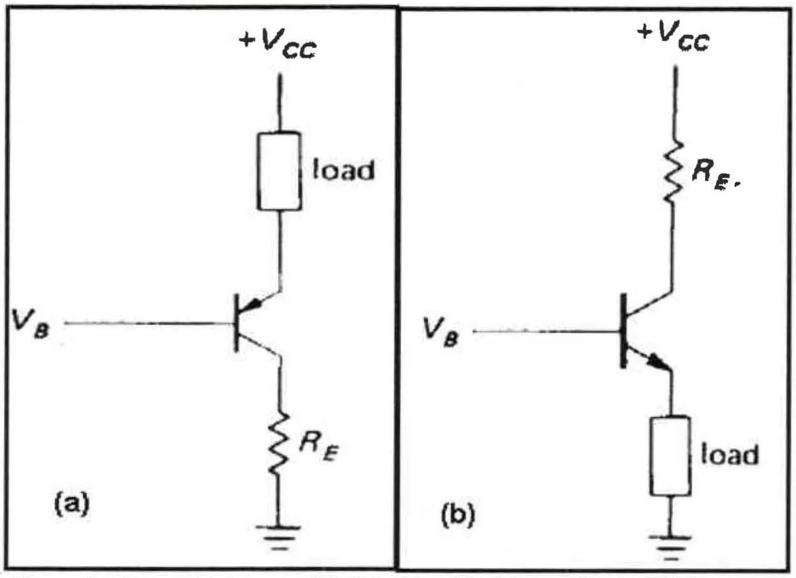

Figure 4.1 Current (a) source (b) sink using bipolar junction transistor

4.0.1 Current sink

The current sink (usually comprising N-type BJT or FET devices) connects between the load and a negative supply voltage (-V) or ground (0V) potential as shown in Figure 4.1(b).

4.0.2 Current mirror

A current mirror can connect to either supply and usually provides multiple current sources/sinks that either mirror (1-1 match) or are arranged in preset current ratios. The circuit shown in Figure 4.2 is a basic PNP current source circuit. In this circuit the base to emitter biasing (V_{BE1}=V_{BE2}) is same for both transistors and by programming the I_{REF} current through resistor R the I_{C2} current is controlled (mirror). A monolithic dual transistor is ideal for this type of function. The Current I_{C2} is controlled (mirror) by I_{REF} (V_{CC1}/R).

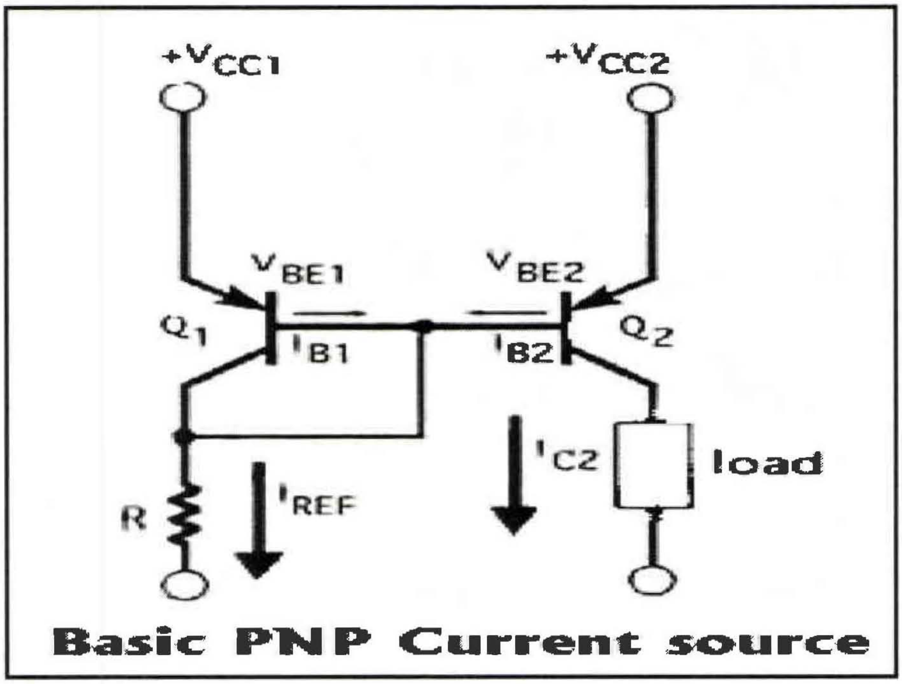

Figure 4.2 Basic bipolar junction current mirrors

4.1 Current source parameters

For impedance measuring systems, the output of the signal generator is a voltage waveform, which must be converted into a current waveform and furthermore the magnitude of the converted current must be unaffected by the variation in the impedance. If the current magnitude remains constant under variable impedance then by measuring the voltage drop across the impedance and using the value of current magnitude the value of impedance can be accurately calculated. Typically, the function of voltage to current conversion performed by voltage controlled current source (VCCS). An important parameter of a current source is its output impedance Z_O which appears in parallel to the load Z_L. As noted by Alexander, a high precision current source requires that the output impedance be very high compared to the load (Alexander S Ross, 2003). The circuit model for the current source is shown in Figure 4.3.

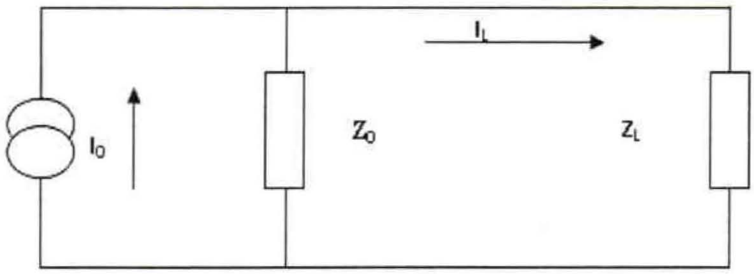

Figure 4.3 Current Source circuit model

For an ideal current source the output impedance Z_O will be infinite, which means the current I_L will remain constant with variation in load impedance Z_L. For real (non-ideal) current sources finite output impedances causes a discrepancy to exist between the current that is soured (I_O) and the current injected into the load (I_L).

To minimize this error, Z_O must be sufficiently large. From Figure 4.3, an equation for injected current (I_L) can be derived.

$$I_L = \frac{Z_O}{Z_O + Z_L} I_O \quad (1)$$

The minimum desired value of output impedance Z_O for which the load current I_L changes within the limits of predetermined error (say 0.1%) over the possible range of load impedances can be calculated as follows.

Equation 1 can be written for max Z_{Lmax} and min Z_{Lmin} load impedance which yields two different load currents I_{Lmax} and I_{Lmin}

$$I_{Lmax} = \frac{Z_O}{Z_O + Z_{Lmax}} I_O \quad (2)$$

$$I_{Lmin} = \frac{Z_O}{Z_O + Z_{Lmin}} I_O \quad (3)$$

Combining these two (2 & 3) equations and solving for Z_O gives us

$$Z_O = \frac{I_{Lmax}\ x\ Z_{Lmax} - I_{Lmin}\ x Z_{Lmin}}{I_{Lmin} - I_{Lmax}} \quad (4)$$

Using equation 4 we can calculate the minimum value of Z_O which will meet the accuracy requirements of the injected current with load variation. For example to the measure variation in the impedance from Z_{Lmin} =0 to $Z_{Lmax} = 2k$ and for the accuracy limit of 0.1% (10bits of ADC) $I_{Lmax} = I_{Lmin} + 0.1\%$, substituting these values in equation 4 give us the required output impedance $Z_O = 2M\Omega$ of current source.

Besides the output impedance, there are additional requirements for EIT current source such as; stability, voltage compliance: A current source can provide a constant current to the load only over some finite range of load voltage (non infinite load) and to do otherwise would be equivalent to providing infinite power ($\boldsymbol{P = RI^2}$), drive current capability (Alexander S Ross, 2003). The balanced current injection: The current source must inject and sink equal quantity of current, temporal stability: The current source can provide constant current over time and temperature and be able to handle loads that include the capacitive components over the working frequency range. Another important parameter for current source is the signal to noise ratio (SNR). Noise is an unwanted signal that is superimposed on the signal of interest. If the noise is higher than the signal of interest then they may become indistinguishable i.e., when the signal-to noise ratio (SNR) is low; the noise has severe consequences on the system response.

There are different techniques to implement the voltage controlled current source VCCS for impedance measuring systems. The simplest version of a current source is to add a resistor in series with a voltage source and choose a very large value of resistor compared to the load impedance (Baker, 1973). The disadvantage of this design is the necessity to use a high voltage source with a high value resistor in order to achieve accurate voltage to current conversion.

4.2 Voltage control current sources (VCCS)

A subset of the possible techniques for designing voltage control current sources will be reviewed in this chapter of the thesis, however a good source of knowledge can be found in the text "Current sources & Voltage References" by Linden T. Harrison (Harrison, 2005) .

4.2.1 Floating load current source

A simple version of a VCCS is an inverting operational amplifier with the load in the feedback path, as shown in Figure 4.4.

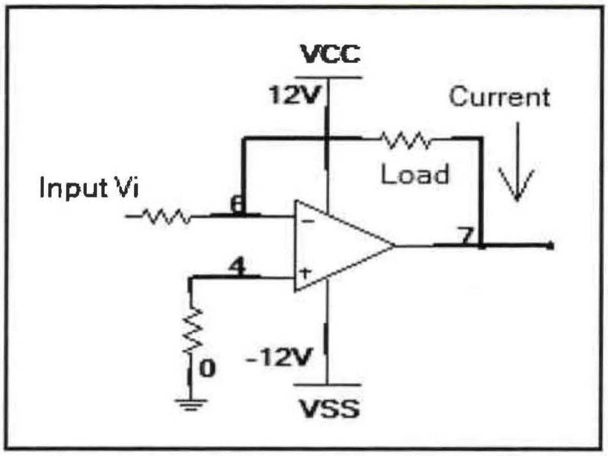

Figure 4.4 Inverting op amps configuration with load in feedback path

The output impedance is given by $Z_O = (1 + A)R_i$. Where A is the open loop gain of the operational amplifier and is a function of the frequency. The value of R_i is limited by the input voltage V_i and the required output current I_L. The gain is limited, and the output impedance $Z_O$decreases at higher frequencies.

The disadvantage of this circuit is that the load must be floating, so it cannot be connected to the reference ground in a multiple current source system (Webster, 1990). The contact impedance of the two current electrodes delivers a high common mode voltage to the input of the voltage measurements part of the system, so it can be difficult to achieve sufficient accuracy and the common mode rejection ratio (CMMR) of the instrumentation amplifier, at unity differential gain must be high enough at the operating frequency (Lidgey(a), 1990).

4.2.2 Transformer coupled current source

To avoid the high common mode voltage with the above design, a transformer coupled current source can be used as shown in Figure 4.5.

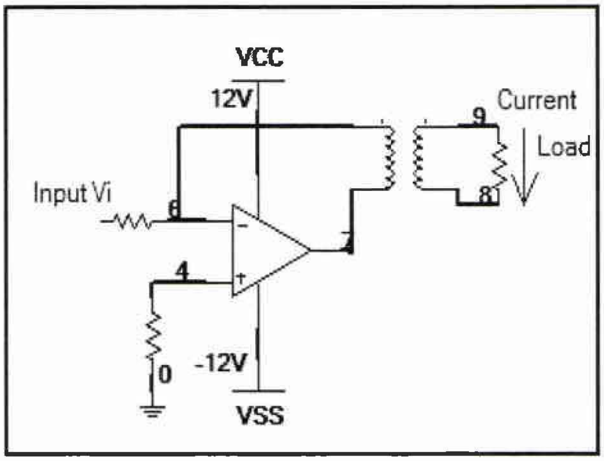

Figure 4.5 Transformer coupled current source

The disadvantage of this circuit is that it cannot provide high output impedance over a wide range of frequencies, because of the properties of the transformer, resulting from the stray capacitance and the limited trans-inductivity of the transformer. The operational amplifier's current source design suffers from performance degradation caused by phase shift at high frequencies as well (Newell, 1988) however, this circuit provides a good DC isolation of the load from the operational amplifier (Skidmore, 1987).

4.2.3 Current mirror source

A current mirror is an element with at least three terminals (i.e., Input, Output and power supply) as shown in Figure 4.6. The common terminal is connected to a power supply, and the input current source is connected to the input terminal. Ideally, the output current is equal to the input current multiplied by a desired current gain. If the gain is unity, the input current is reflected to the output, leading to the name current mirror.

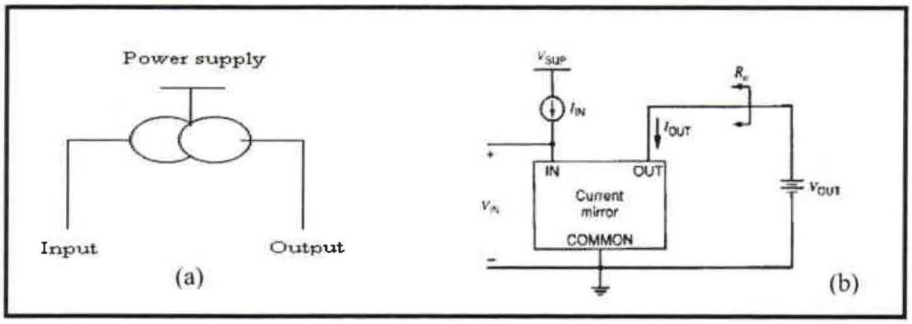

Figure 4.6 Current mirror (a) symbol (b) block diagram

Under ideal conditions, the current-mirror gain is independent of the input frequency, and the output current is independent of the voltage between the output and common terminals. The voltage between the input and common terminals is ideally zero because this condition allows the entire supply voltage to appear across the input current source, simplifying its transistor-level design. Sometimes more than one input and/or output terminals are used.

In practice, real transistor-level current mirrors suffer many deviations from this ideal behaviour. For example, the gain of a real current mirror is never independent of the input gain, output resistance and frequency (Harrison, 2005).

The problem with simple current mirror is that the output current varies (±20%) with the changes in the output voltage compliance range. An improved current mirror designed by Widlar (WIDLAR, 1965) is described in the next section.

4.2.3.1 Widlar current mirror

The simple current mirror is modified by a resistor R_2 inserted (as shown in Figure 4.7) at the emitter of Q_2, so that the transistors Q_1 and Q_2 operate with unequal base-emitter voltages.

The output current is less dependent on the input current and the power supply voltage than the simple current mirror.

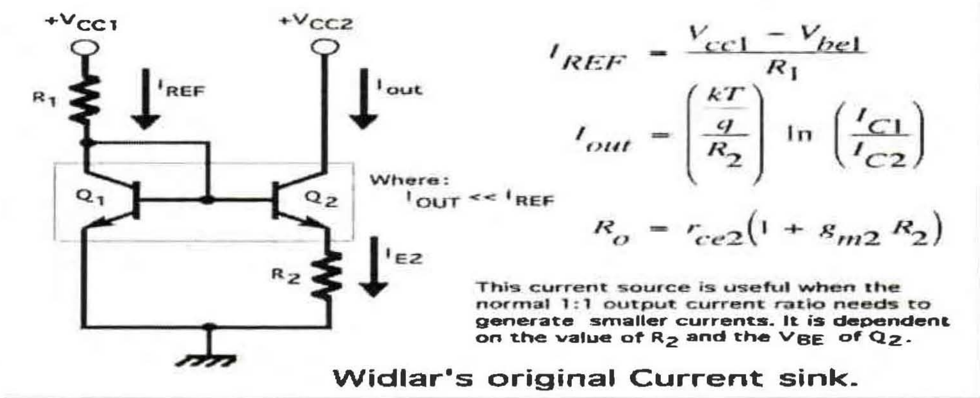

$$I_{REF} = \frac{V_{cc1} - V_{be1}}{R_1}$$

$$I_{out} = \left(\frac{\frac{kT}{q}}{R_2}\right) \ln\left(\frac{I_{C1}}{I_{C2}}\right)$$

$$R_o = r_{ce2}(1 + g_{m2} R_2)$$

Figure 4.7 Wildar's current source (Harrison, 2005).

However, the accuracy of the current gain A is affected by the uneven distribution of the base currents, since both the base currents are supplied from controlling the input. This accuracy issue was improved by Wilson (WILSON, 1968), as described in the next section.

4.2.3.2 Wilson current mirror

The accuracy of the base current was improved by the addition of a third transistor. This design is known as Wilson current mirror and is shown in Figure 4.8.

The Q_1 and Q_2 are in the usual simple mirror configuration, Q_3 is added to the design and Q_3 now keeps the Q_1's collector fixed at two diode drops (np-pn) below V_{CC}. This overcomes the early effect in Q_1, whose collector is now the programming terminal with Q_2 now sourcing the output current. Q_3 does not affect the balance of the currents, since its base current is negligible; its only function is to pin Q_1's collector.

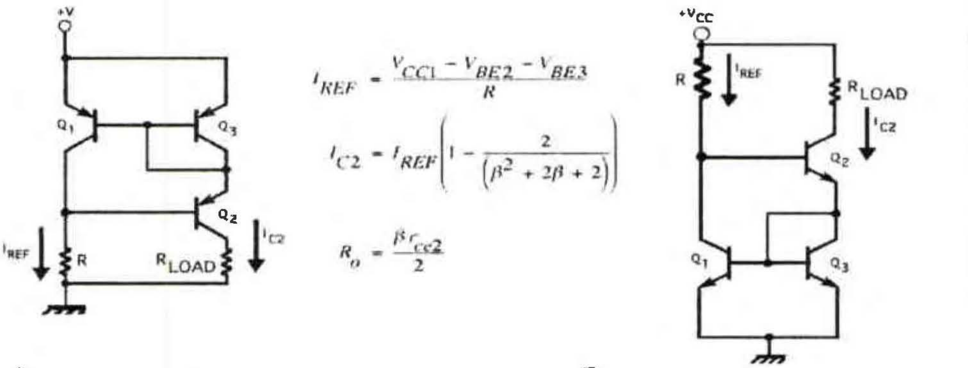

A. The basic Wilson PNP current mirror.

B. The basic Wilson NPN current mirror.

Figure 4.8 Wilson current mirrors (Harrison, 2005)

The result is that both current determining transistors (Q_1 and Q_2) have fixed collector-emitter drops; the Q_3 is simply passing the output current through to a variable voltage load. The distribution of the base currents is more even with this circuit and a feedback effect within the current mirror results in raised output impedance in comparison with the Widlar current mirror design. However, the gain A is now affected by the differences in the collector to emitter voltage of the lower two transistors.

The Q_1 and Q_2 are in the usual simple mirror configuration, Q_3 is added to the design and Q_3 now keeps the Q_1's collector fixed at two diode drops (np-pn) below V_{CC}. This overcomes the early effect in Q_1, whose collector is now the programming terminal with Q_2 now sourcing the output current. Q_3 does not affect the balance of the currents, since its base current is negligible; its only function is to pin Q_1's collector. The result is that both current determining transistors (Q_1 and Q_2) have fixed collector-emitter drops; the Q_3 is simply passing the output current through to a variable voltage load. The distribution of the base currents is more even with this circuit and a feedback effect within the current mirror results in raised output impedance in comparison with the Widlar current mirror design. However, the gain A is now affected by the differences in the collector to emitter voltage of the lower two transistors.

4.2.3.3 Wyatt cascade peaking current

For still greater precision, a fourth transistor may be added. This design, the modified Wilson current mirror as shown in Figure 4.9 is known as the Wyatt current source (Harrison, 2005).

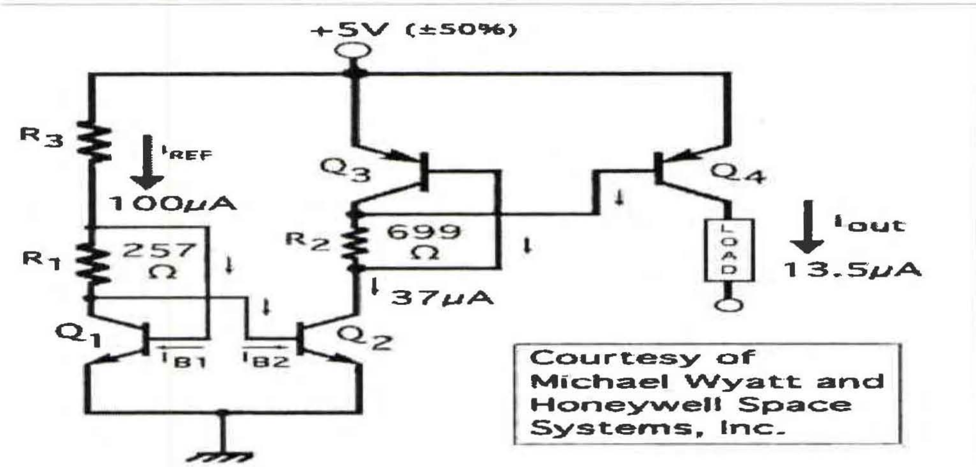

Figure 4.9 The Wyatt Cascade Peaking Current Source.

It has a negligible differences in V_{CE} between the lower two transistors and, therefore gain A is close to unity within 1%. This design reduces the input current to a lower level, and combines high accuracy with a constant output, and temperature compensation.

One of the most important deviations from ideality is the variation of the current mirror output current with changes in voltage at the output terminal. The small-signal output resistance R of the current mirror characterizes the deviation effect. The current mirrors described in the previous section are uni-polar circuits and hence may only sink or source current. However EIT requires AC signals (bipolar). Bipolar current sources are described in the following section.

4.2.3.4 Current mirror using operational amplifiers

Another design of VCCS with a high output impedance is based upon operational amplifiers supply current sensing i.e., current mirror technique (Lidgey(a), 1990) (Denyer, 1994).

The current mirror circuit is shown in Figure 4.10. The operational amplifier power supply terminals are connected to the power supplies ($+V_{CC}$, $-V_{EE}$) via current mirrors, here C_{M1} is a current mirror which connects the operational amplifiers positive supply to $+V_{CC}$ via the low input impedance current mirror. C_{M2} is a current mirror, which connects the operational amplifiers negative supply to $-V_{EE}$ via the low input impedance current mirror. The resistor Z_L, which is the load of the operational amplifier, R_i is the current determining/sense resistor. The operational amplifier is connected as a unity gain buffer with the supply voltage connections providing the input current control to the current mirrors. The inverting and non-inverting inputs have a very high impedance (typically >1MΩ) and hence the current from the output of the operational amplifier must closely match the difference between the positive and negative supply currents if no other connections are used.

Each current mirror (***C_{M1}*** & ***C_{M2}***) will have a gain of close to unity and hence if the current mirror outputs are summed by connecting them to the same node, then the net output current will be equal the difference between the supply currents.

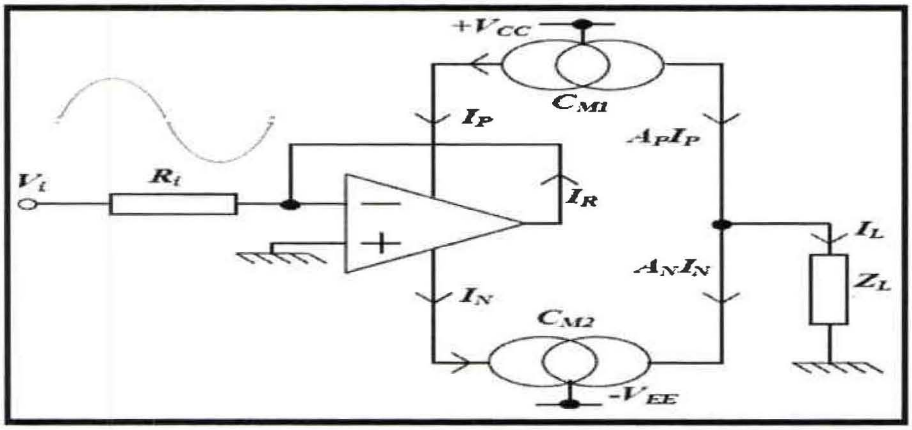

Figure 4.10 Current mirror using operational amplifier

It is equal to $I_R = V_i / R_i$, which is the input current and hence the output current will closely matched to the input current. Since the operational amplifier is in a voltage follower configuration and it supplies a current I_L to the resistor Z_L.

Thus the output current $I_L$is determined by the input voltage V_i (ohm's law $I_L = V_i / Z_L$). The current provided by the output stage of the operational amplifier has to be drawn from its power supplies. It is equal to I_L and it is dependent upon the input voltage and independent of the load Z_L.

The load current for a full cycle of the voltage signal can be analyzed using the circuit shown in figure 4.10.

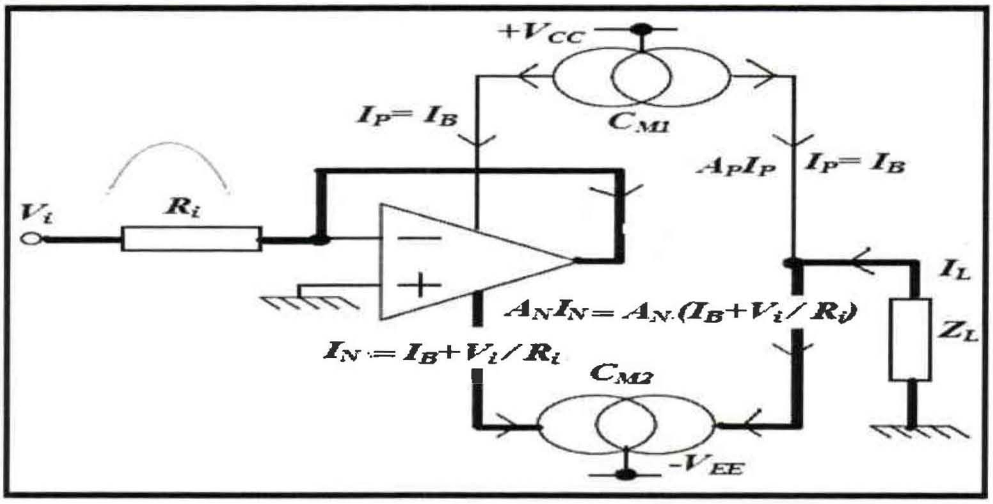

Figure 4.11 Current flow paths for positive input voltage

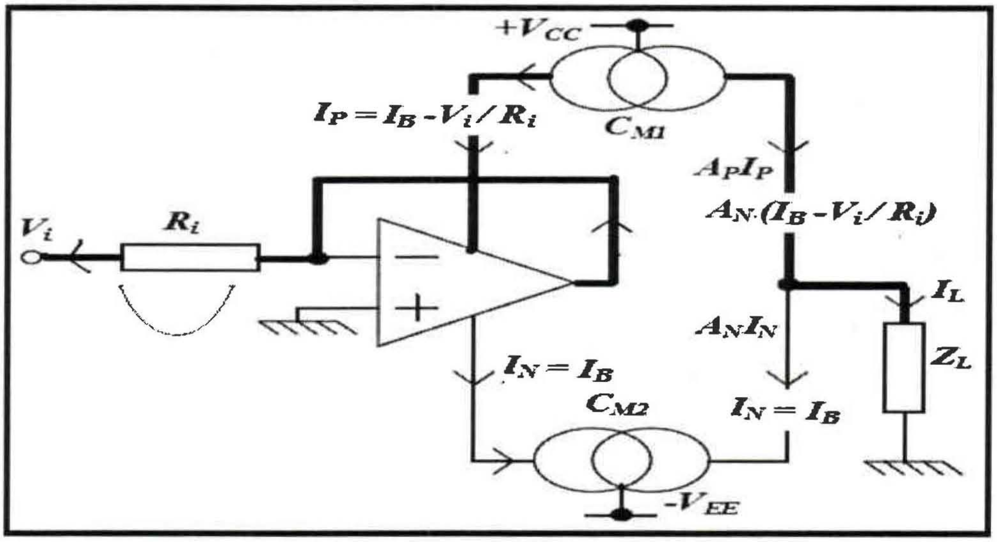

Figure 4.12 Current flow paths for positive input voltage

The current path (indicated by arrows) for the positive half cycle is show in the Figure 4.11 and the current path (indicated by arrows) for the negative half cycle is show in the Figure 4.12.

Let I_B be the quiescent bias current (This is the non-signal power supply current that the operational amplifier will consume within a specified power supply voltage operating range) taken from both supplies and I_P be the positive supply current and I_N be the negative supply current and I_R the (Instantaneous) output current. The current gain for the current mirror is given by; A_P current gain for positive current mirror, A_N current gain for negative current mirror. The current drawn from the positive supply during positive input half cycles $I_P=I_B$ and during negative input half cycles $I_P= I_R +I_B$. The current drawn from the negative supply during positive input half cycles $I_N= -I_R -I_B$ and during negative input half cycles $I_N= -I_B$.

The load current with reference to a complete cycle of the input voltage; for the positive half-cycle the current sink by the lower current mirror C_{M2} and for the negative half-cycle the current is sourced by the upper current mirror C_{M1}.

For the positive half cycles

$I_N = I_B + I_R$ and $I_R = V_i / R_i$ since the input impedance of the operational amplifier is very high therefore the operational amplifier input current is neglected.

$I_N = I_B + V_i / R_i$ and $I_P = I_B$

Therefore the load current $I_L = - A_N I_N + A_P I_P$

$I_L = - A_N (I_B + V_i / R_i) + A_P I_B \rightarrow I_L = (A_P - A_N) I_B - A_N (V_i / R_i)$

Similarly, for negative half cycles

$I_P = I_B - V_i / R_i$ and $I_N = I_B$

Therefore the load current $I_L = - A_N I_B + A_P I_P$

$I_L = - A_N I_B + A_P (I_B - V_i / R_i) \rightarrow I_L = (A_P - A_N) I_B - A_P (V_i / R_i)$

The term $(A_P - A_N) I_B$ is present in both cycles and represent a DC offset current at the output.

If the current gains A_P and A_N differ in value then distortion may be present in the output waveform, hence it is important that the positive and negative current mirrors are well matched, if distortion is to be minimized.

For a stable operation the above circuit has a limitation, it requires a DC path at the output for the bias current term $(A_P - A_N)\, I_B$. In the case of EIT it is necessary to ensure that no DC current flows in the load and hence the output of the circuit must be AC coupled through a DC blocking capacitor. However, if the node connecting the current mirror outputs is to be within the operating region, then the DC currents flowing through each current mirror output must be very close. If the upper current mirror has an output impedance of Z_P and a bias current of I_{PB} and the lower current mirror has Z_N and I_{NB} for the same parameters then the voltage at the connecting node is given by:

$$V_O = (I_{PB} - I_{NB}) \times ((Z_P \times Z_N) / (Z_P + Z_N))$$

The current mirrors can be matched, to within approximately 1% and hence, for a quiescent output current such as $5mA$, $I_P - I_N = 50\mu A$. Therefore, the output stages must be well matched for higher precision.

The advantages of this type of current source circuit are high stability, high output impedance and wide-band operation. The disadvantage of this type of circuit arises from non-idealities of the current mirrors and the operational amplifiers.

4.2.3.5 Current source using current pump

Another implementation of a VCCS is known as a current pump, as shown in the circuit diagram in Figure 4.13. This circuit regulates the load current by feeding back to the input, a voltage signal, which is proportional to the differential voltage across a current sense resistor in series with the load. For the circuit to have high output impedance, it is important that both inputs of amplifiers OA_1 and OA_2 have high impedance. The output of the operational amplifiers OA_1 is V_{O1} and OA_2 is V_{O2} is shown in the Figure 4.13.

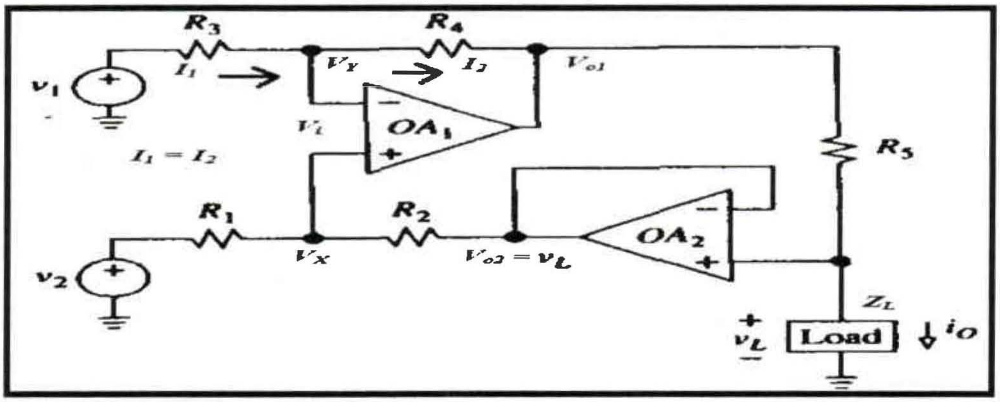

Figure 4.13 Current pump circuit

The output current I_O is given by: (see appendix A for derivation):

$$I_O = A_2 V_2 - A_1 V_1 - \frac{1}{R_O} V_L$$

Where $A_1 = \frac{R_4}{R_5 R_3}$, $A_2 = \frac{1}{R_5} \frac{\left(1+\frac{R_4}{R_3}\right)}{\left(1+\frac{R_1}{R_2}\right)}$, $\frac{1}{R_O} = \frac{1}{\left(1+\frac{R_2}{R_1}\right) R_5} \left(\frac{R_2}{R_1} - \frac{R_4}{R_3}\right)$

V_L is the voltage across the load, and V_1,$V_2$are the input applied voltages.

To make $R_O \rightarrow \infty$ the ratios $\frac{R_2}{R_1}$ and $\frac{R_4}{R_3}$ must be equal that is $\frac{R_2}{R_1} = \frac{R_4}{R_3}$

Therefore, $A_1 = A_2 = \frac{R_2}{R_5 R_1}$; $I_O = AV_i - \frac{1}{R_O} V_L$ where $V_i = V_2 - V_1$

To have very high output impedance the ratios of the resistors must be matched and the gains of the amplifiers must be equal in the operating frequency and the operational voltage range. Since the output of the circuit is the voltage difference, the input differential signal must be equal in magnitude and 180 degree out of phase and the CMRR must be high over the entire frequency range.

4.2.3.6 Howland current source

Another implementation of a VCCS is known as the Howland current source, and is depicted in Figure 4.14. Prof. Bradford Howland of MIT in 1962 invented this circuit and first published in the January 1964 in Lightning Empiricist (Howland, 1964).

The negative and positive inputs of an operational amplifier can be used to make a high impedance current source using a conventional operational amplifier. This basic circuit can supply both positive (current source) and negative (current sink) output currents into various loads. The theory of the circuit is very simple however; the practical problems involved are neither simple nor obvious.

The output impedance of the circuit shown in Figure 4.14(a) on the previous page is infinite provided the ratio of the resistors $\frac{R_4}{R_3} = \frac{R_2}{R_1}$. Which impose a condition, i.e., that the ratios of the resistors values must be matched precisely.

That can be achieved by using 0.01% tolerance resistors and trimming (instead of fixed value resistor a potentiometer i.e., variable resistor is used and the value is adjusted) one of the resistors until the desired precision is achieved. However, the output impedance degrades as the frequency increases when reactive effects increase.

The output impedance degrades as well due to the reduction in the gain of the operational amplifier as the frequency is increased (Franco, 2002).

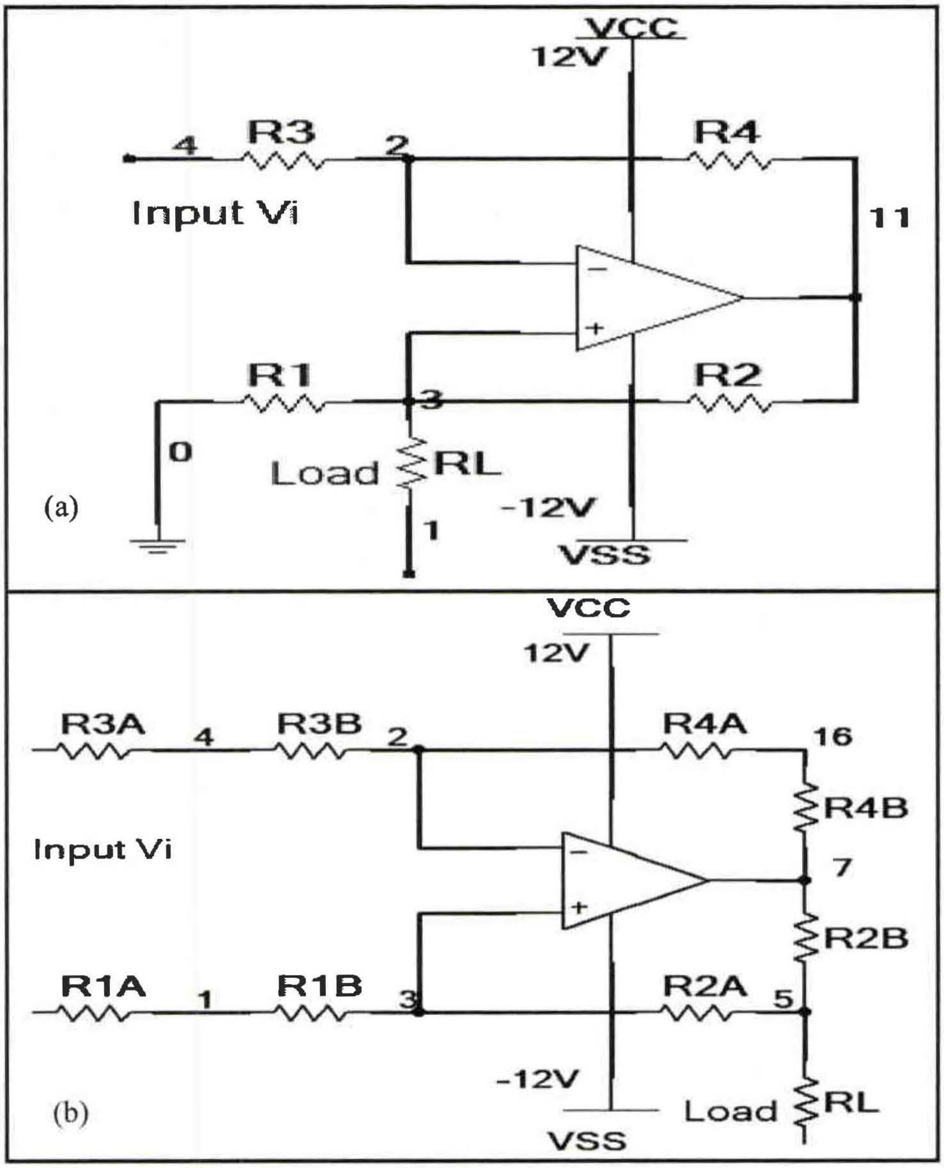

Figure 4.14 Howland current Source; (a) basic (b) Improved

The basic Howland current source can be unnecessarily wasteful of power as pointed out by Franco (Franco, 2002). This inefficient use of power can be avoided with the modification as shown in Figure 4.14(b), where the resistance R_2 is split into two R_{2A} and R_{2B}.

For differential current injection, the most important factor is to keep the balance between the two current sources connected in series with the load. Any imbalance in the parameters of the two Howland type VCCS's will result in a non-minimum value of the current injected through the load and a common mode signal.

Equations for output impedance R_0 current I_0 can be given by (see appendix B for derivation)

$$R_0 = \frac{R_{2B}\left(1+\frac{R_{2A}}{R_1}\right)}{\frac{R_2}{R_1}-\frac{R_4}{R_3}}$$

$$\text{For } \frac{R_4}{R_3} = \frac{R_2}{R_1} \quad \rightarrow R_0 \rightarrow infinity \qquad (9)$$

$$I_0 = \frac{R_2}{R_1 R_{2B}} V_1 \qquad (10)$$

The gain of the circuit determined by the ratio of the resistors $\frac{R_2}{R_1}$ and the output current by $\frac{1}{R_{2B}}V_1$. The output current I_0 of the Howland current source is controlled by the input voltage since the circuit gain and R_{2B} are kept constant.

Equation 9 shows that the output impedance approaches infinity if the ratios of both feedbacks are equal. However, equation 9 does not indicate how important it is to have precisely matched resistors. For example, if all 4 resistors were 10kΩ with a 1% tolerance, the error in the output impedance might be as much as 250kΩ. For some applications, it might be acceptable however, it is not acceptable for EIT, which requires an output current variation of 0.1% or better.

Another parameter relevant to the precision of the Howland current source is the CMRR of the operational amplifiers. Fortunately, an amplifier CMRR of 60dB would cause the output impedance to degrade only to 10MΩ, which is better for low impedance load (2KΩ). However, the CMRR of an operational amplifier is not always linear with reference to frequency, as the frequency increases the CMRR decreases (Franco, 2002) in case of EIT a constant CMMR is required over the entire frequency range.

This circuit can be use as a base structure for implementation of a differential constant current source. The improved Howland current source was used in the both versions of McMaster EIT system which will be describe in the next chapter of this thesis. For the remainder of this chapter, a brief review will be provided of how other groups have implemented current source in their EIT systems.

4.3 Literature review

Several groups have also developed EIT systems a very brief review of current sources will be given in the following section.

The Rensselaer group used the improved Howland circuit for their EIT current source and added a generalized impedance converter (GIC) in parallel to increase the output impedance and to cancel the capacitive effects. Reported simulated output impedance is in excess of 2GΩ for the frequency range from 100HZ to 1MHz. Their experimentally measured output impedance was 143MΩ at 1 KHz, 67MΩ at 20 KHz and 37MΩ at 100 KHz (Alexander S Ross, 2003).

The Kyung Hee University group did a similar implementation of the basic Howland current source. They placed a digital potentiometer at the inverting input to calibrate the output impedance at various frequencies and added a negative impedance converter (NIC) at the output to cancel out the capacitive effects of the load impedance. The voltage signal out from the signal generator was applied to the non-inverting input. The operating frequency range is selectable from 1 kHz to 1 MHz. They reported an output impedance of the current source greater than 64MΩ at DC however, the impedance degrade to 50 KΩ at 500 kHz (Jeong Whan Lee, 2003).

The basic Howland current source can be unnecessarily wasteful of power as pointed out by Franco (Franco, 2002). This inefficient use of power can be avoided with the modification as shown in Figure 4.14(b), where the resistance R_2 is split into two R_{2A} and R_{2B}.

	Casas *et al*		Modified Howland	
Frequency (Hz)	Z_{out} (Ω) PSPICE	Z_{out} (Ω) Measured	Z_{out} (Ω) PSPICE	Z_{out} (Ω) Measured
1k	3.0M	> 1.0M	610.0k	540.0k
10k	2.0M	> 1.0M	4.5M	750.0k
100k	288.0k	700.0k	409.0k	670.0k
300k	96.0k	400.0k	136.0k	330.0k
1M	29.0k	70.0k	41.0k	70.0k

Table 4.1 Comparison of output impedance for current mirror and modified Howland current source by load variation from 200Ω to 500Ω

The group at the University of Sheffield (Bertemes-Filho P, 2000), compared the performance of a mirror current source and enhanced Howland current source through simulation and experiments, the results are shown in table 4.1.

The output impedance degraded from 1MΩ to 70kΩ as the frequency is increased from 1 KHz to 1 MHz, the author suggest that the output impedance reduced due to the output resistance having a parallel output capacitance which reduces the output impedance at high frequency.

The topology of the supply-current sensing VCCS circuit is simple, no positive feedback arrangement exists and thus they are very stable (Wilson, 1981). Because of the operational amplifier, feedback arrangement they operate over a wide bandwidth and the circuit exhibits an excellent slew rate, but the current mirrors are slightly weak links in the designs i.e., it is very difficult to exactly match the gain for both current mirrors, and therefore determine the ultimate limitation on the accuracy (Lidgey(a), 1990; Toumazou, 1990). See section 4.2.3.4 for more details.

A constant current source, based on the current mirror technique is presented by (Leung, 1990). Practical measurements show changes in current with load between 500Ω and 5KΩ: 0.832 – 0.830mA at 10 KHz and 0.811 – 0.800mA at 100 KHz. The Leung system, which includes a constant current generator, realized by measuring the current and controlling the output voltage to constant current, suffers from the limitation of speed. A stable output current has to be generated after switching current carrying electrodes (Blad, 1991).

There are two commonly used approaches to implement a VCCS i.e., current mirror and Howland current source. As mentioned earlier, for current mirror implementation the characteristics of two current mirrors must be exactly matched otherwise a slight mismatch will not produce a constant and balanced current injection and there are no external component to precisely match/adjust the current mirror characteristics. Due to these reasons the current mirror circuit was not implemented in the second version of the McMaster current source..

The improved Howland current source is a better approach however, matching the resistor ratio is not easy. Constant current could be produced, by using resistors of higher tolerance like 0.01% or better and by resistance trimming (a technique use to match the resistance ratio). The gain of the operational amplifier reduces as the frequency increases this could be addressed by increasing the input voltage. The differential voltage application to the VCCS would reduce the problem associated with unbalance current injection.

This thesis is devoted to changes to the initial prototype of the McMaster EIT current source. These changes were implemented to address the know issue of the resistance ratio mismatch, current variation due changes in load and frequencies, reduction in gain, unbalance current injection. In the next chapter of this thesis, the first version of the McMaster EIT prototype system is described also the proposed modifications will be outlined.

Chapter 5

McMaster EIT system voltage control current sources

In this section of the thesis, the first prototype version of the voltage control current source (VCCS) its limitations, the solution to those limitations, and the implementation in the second version of the McMaster EIT system VCCS will be described.

5.1 McMaster EIT system VCCS version I

For the first prototype of the VCCS, the current source used a DSP, interfaced to a PC through a serial communication port. The DSP was interfaced to the 16bit DAC using parallel communication as shown in Figure 5.1. A

LabView program on the PC was used to send command to control the frequency and amplitude of the current via the DSP. The DSP was programmed to update the input of the DAC every 2μsec for analog conversion. The 16bit DAC was used to convert the digital data to the corresponding analog signal. The maximum amplitude of the output analog signal was ±10V. The analog signal was then passed through a low pass filter to remove the unwanted frequencies.

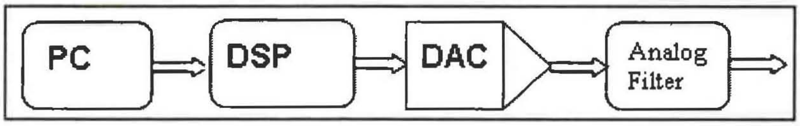

Figure 5.1. Block diagram of the McMaster EIT current source version I

The voltage output from this signal generator was applied to the inverting and non-inverting inputs of two power operational amplifiers in order to get two current signals, 180 degrees out of phase, for differential current injection. The power operational amplifiers were configured as an improved Howland VCCS as shown in Figure 5.2. The configuration of this type of improved Howland VCCS is called a single ended input current source, since the voltage is applied at one terminal of the operational amplifier and the other terminal is grounded.

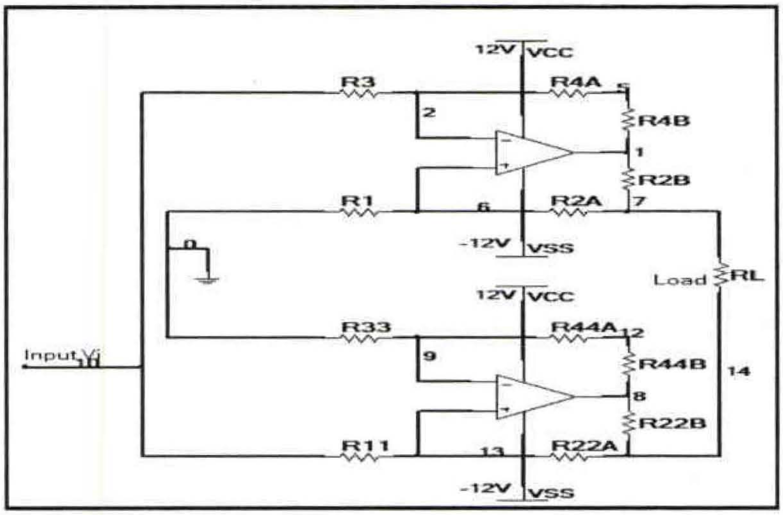

Figure 5.2 McMaster EIT voltage control current source version I

A power operational amplifier LM675 (http://www.national.com) was used as a voltage to current converter in an improved Howland circuit configuration with a gain of 1.1 as shown in Figure 5.2.

The output current of the improved Howland VCCS is controlled through the input voltage and it is given by the equation: $\boldsymbol{I_0} = \frac{R_2}{R_1 R_{2B}} \boldsymbol{V_i}$. Since the resistors ratio $\frac{R_2}{R_1 R_{2B}}$ is constant, only the input voltage $\boldsymbol{V_i}$ controls the output current. This improved Howland VCCS was able to inject currents up to 7mA over the preselected frequency range from 1 KHz to 125 KHz.

There were five disadvantages with this version VCCS. (1) The VCCS was not very stable. This instability will be exemplified in the tests on the initial prototype in chapter 6 of this thesis. The outcomes of these measurements indicates that this instability is probably due to the non-recommended gain setting of the operational amplifier that is the recommend gain is about 10, whereas the operational amplifier was operated with a gain of about 1.1 (http://www.national.com/ds/LM/LM675.pdf). National Instruments clearly indicate that this device is internally compensated for gains of 10 or more, and therefore "the LM675 is designed to be stable when operated at a closed-loop gain of 10 or greater". This flaw could be address by changing the gain of the power operational amplifier to 10. However, changing the gain would not solve the issues of the previous stage that is within the signal generator (chapter 3). (2) The injected current in the load was not balanced i.e., the negative current (current sink) was more than the positive current (current source). An unbalanced injected current would produce a non-nominal value of current within the object (under test) that would results in a common mode signal. Since the object under test would be floating, the measurements would be influence by this common mode signal in terms of elevated noise or shifted conductivity. (3) The output impedance was very low (constant current source must have a very high output impedance so, the output current remains constant under changes in load and frequency) due to resistor ratios those were not precisely matched and furthermore, due to this imprecise resistance matching. The accuracy of the current source was below the required accuracy by EIT that is, (4) a higher variations in the injected current due to changes in load at fixed frequencies and (5) a higher variations in the injected current due to changes in frequency at fixed loads.

Test performed on the initial prototype, which demonstrates these limitations are presented in chapter 6.

In the following section, the design of the new current source which overcomes these issues is presented.

5.2 Voltage control current source version II

To address the above-mentioned issues of Version I of the McMaster EIT VCCS, it was decided to test three different VCCS circuits to identify the circuit with the overall best performance. The three circuits selected are (1) the Current Pump, (2) the Improved Howland VCCS and (3) a Bipolar VCCS. These circuits were designed, then built on wire-board and printed circuit board (PCB)

The improvements proposed and implemented (chapter 3) in the signal generator second version of the McMaster EIT system are; (1) the frequency range is extended to cover the range from 1KHz to 1MHz instead of a maximum of 125 KHz. (2) The frequency resolution of the DDS in the signal generator circuit is 1Hz instead of preselected a few frequencies and (3) the issue of the DAC settling time was avoided by using a DDS.

The three VCCS circuits are described in the following sections.

5.2.1 Current pump voltage control current source (VCCS)

The current pump circuit was selected due to its high output impedance, accuracy and linearity over the operating range. The circuit is shown in Figure 5.3. The second operational amplifier (U1) in the feedback loop of the first operational amplifier (U) is used as a buffer and this should help to increase the circuit output impedance by more than a couple of mega ohms (Harrison, CURRENT SOURCES & VOLTAGE REFERENCES, 2005).

The differential voltage signals from a signal generator as described in chapter 3 (3.7.2) were applied to the inverting inputs of two operational amplifiers (UA i.e., UA/U1A) as shown in Figure 5.3. These operational amplifiers produced two current signals 180 degrees out of phase. Another two operational amplifiers (UB i.e., UB/U1B) were implemented as unity gain buffers. The voltage drop across the current sense resistor ($\boldsymbol{R_5}$ / $\boldsymbol{R_{5A}}$) was applied to the non-inverting terminal of the operational amplifier (UB). Since the input impedance of an operational amplifier is very high, no current will be shunted away by the operational amplifier. The output of these operational amplifiers was fed back to non-inverting input of the operational amplifiers (UA). The current sense resistor R_5 was placed between the operational amplifier output and the load. The output current ***(Io)*** depends on V_i the input voltage and it is given by:

$$I_O = \frac{R_2}{R_5 R_1} V_i \qquad (5.1)$$

The operational amplifiers (UA) are operating as difference amplifiers. For unity gain, the output voltage will be equal to the difference between the input voltage and the voltage drop across the current sense resistor (R_5).

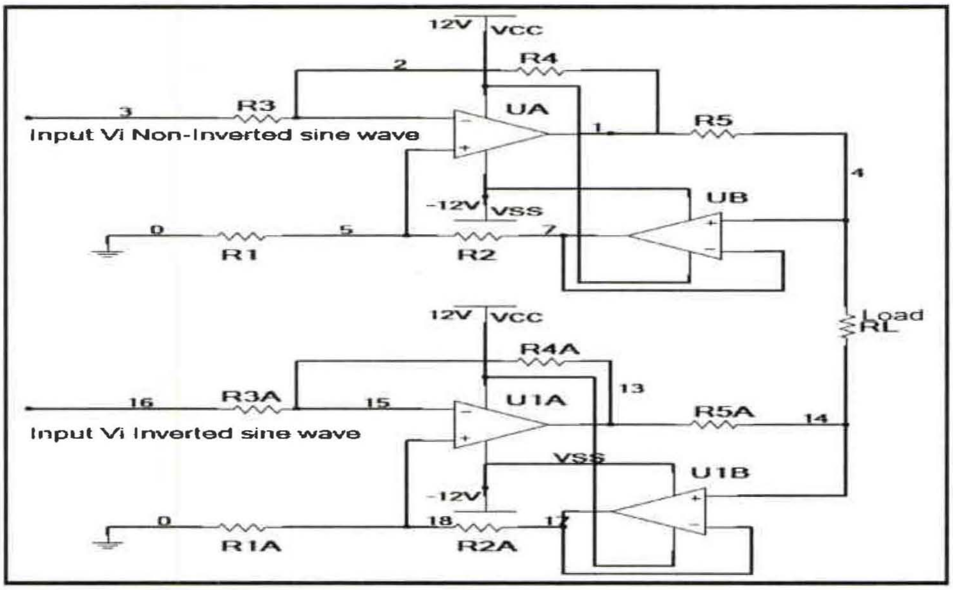

Figure 5.3 Current pump circuits diagram for floating load

It is very critical to match the resistance ratios ($\frac{R_4}{R_3} = \frac{R_2}{R_1}$). If this ratio is not matched then the output impedance will significantly degrade and the operational amplifier will no longer be a true difference amplifier and the output current will no longer be constant as well (Sergio, 2002). To minimize the resistors mismatching effects resistors having a 0.1% tolerance were used.

This circuit was implemented on a wire-o-board and configured for optimal performance. To obtain (1) greater stability and (2) to avoid unbalance current injection, dual operational amplifier IC (containing two operational amplifiers in a single integrated circuit) and manufacturer recommended gain settings were used. A dual operational amplifier IC provides better characteristics matching of both operational amplifiers as compared to using two, single operational amplifier packages. In this circuit two dual IC were used as shown in the Figure 5.3. The experimental tests performed on this circuit are outlined and results are presented in the next chapter of this thesis.

5.2.2 Improved Howland voltage control current source (VCCS)

The improved Howland VCCS circuit was selected due to its higher accuracy, lower drift and having the output current proportional to the input voltage. Two versions of an improved Howland VCCS circuits were built, i.e., single ended improved Howland VCCS as shown in the following Figure 5.4 and a differential ended improved Howland VCCS as shown in Figure 5.5.

In a single ended VCCS, the voltage signal is applied to one terminal of the operational amplifier and the other terminal is grounded.

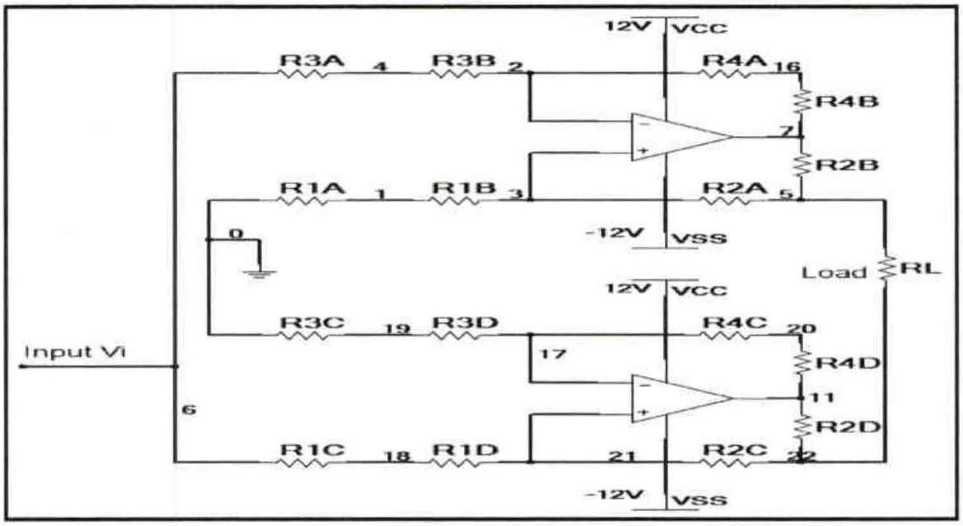

Figure 5.4 Improved Howland current source circuits diagram for single ended input

The output current signal is given by: $\boldsymbol{I_0} = \frac{R_2}{R_1R_3}\boldsymbol{V_i}$ [1] (5.2).

In a differential ended or double-ended VCCS the voltage signals are applied to both terminals of the operational amplifier. The output current signal is given by $\boldsymbol{I_0} = \frac{R_2}{R_1R_3}(\boldsymbol{V_{2i}}-\boldsymbol{V_{1i}})$ **OR** $\boldsymbol{I_0} = \frac{R_2}{R_1R_3}\boldsymbol{V_i}$ (5.3)

Where $\boldsymbol{V_i} = (\boldsymbol{V_{2i}}-\boldsymbol{V_{1i}})$

[1]Note:$R_{1A} + R_{1B} = R_1$, $R_{2A}+R_{2B} = R_2$, $R_{3A} + R_{3B} = R_{3B}$ and $R_{4A}+R_{4B}=R_4$
$R_{1C}+R_{1D}=R_1$, $R_{2C}+R_{2D} = R_2$, $R_{3C}+R_{3D}=R_3$ and $R_{4A}+R_{4B} = R_4$

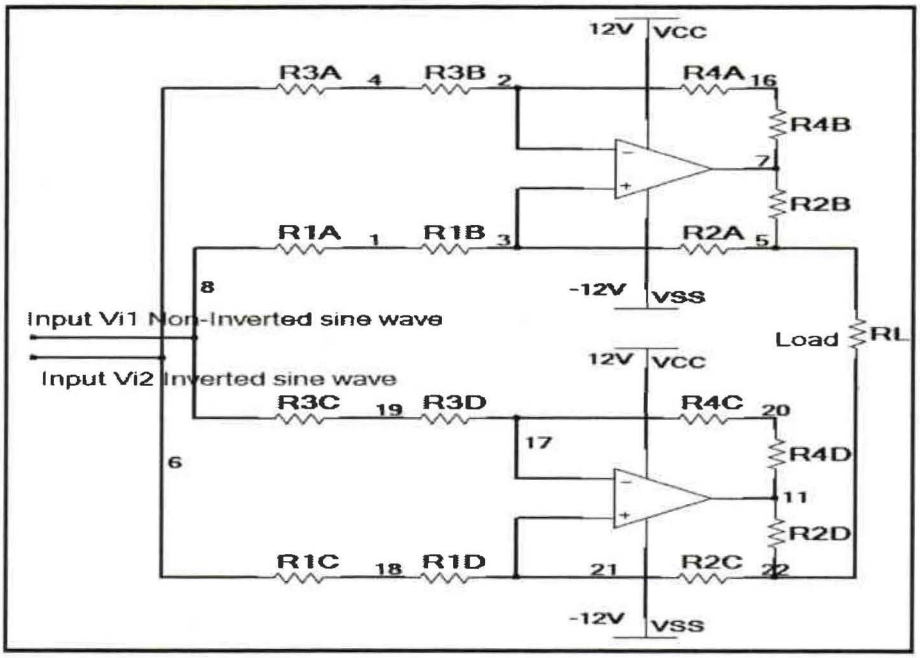

Figure 5.5 Improved Howland current source circuit diagram with differential input voltage

The gain of the operational amplifier in both above-mentioned circuits (improved Howland VCCS Figure 5.4 & 5.5) could be adjusted by the external resistors ratio $\frac{R_2}{R_1}$ or by changing the input voltage V_i.[2]

Adjusting the gain by changing the resistors ratio $(\frac{R_2}{R_1} = \frac{R_4}{R_3})$ is very difficult, since the ratios must be precisely matched and furthermore there are four ratios that have to be adjusted and precisely matched (two ratios from each operational amplifier).

[2] See Equation 5.2 and Equation 5.3

It is easier to just change the input voltage of the operational amplifier in order to change the output current, since the output current I_0 is proportional to the input voltage V_i keeping the resistors ratio $\frac{R_2}{R_1R_3}$ constant. The gain adjustment by this method i.e., increasing the input voltage whenever the gain degrades, gives the ability to keep electric current constant over a wide frequency range.

As indicated in chapter 4, EIT researchers have implemented basic and improved Howland VCCS circuits for their EIT systems (Alexander S Ross, 2003; Jeong Whan Lee, 2003). In the first version of the McMaster EIT system, an improved Howland VCCS circuit was implemented. In the second version of the system, two (as shown in Figures 5.4 and 5.5.) variations of the improved Howland VCCS circuits are implemented as well.

These two versions of improved Howland VCCS were built on the PCB, configured for optimal performance. As in the previous example, to obtain (1) greater stability and (2) to avoid unbalanced current injection, a dual IC of operation amplifier was used with manufacturer recommended gain settings, and resistors of 0.1% tolerance were used to increase the output impedance of the circuit. The experimental tests performed on this circuit are outlined and results are presented in the next chapter of this thesis.

5.2.3 Bi-Polar voltage control current source (VCCS)

This circuit is similar to the current pump circuit; a differential amplifier was used instead of conventional operational amplifier. The underlying architectures of both devices are very different.

The differential amplifier uses active feedback architecture. An obvious difference is the presence of two separate pairs of differential inputs as compared with conventional operational amplifiers that have a single pair. In the active feedback architecture, one of the two input pairs is driven by a differential input voltage signal while the other is used for feedback.

There are several advantages in the active feedback architecture over a conventional operational amplifier such as; excellent common-mode rejection; A higher common mode rejection ratio (CMRR) will ensure that the output signal (voltage/current) remains constant over a wide frequency range. That is in contrast to a conventional operational amplifier where the output signal (voltage/current) will degrade as the frequency is increased. Wide input common-mode range in the active feedback architecture, significantly minimizes the input noise transmission to the output. In addition, while an external feedback network establishes the gain response as in a conventional operational amplifier, its separate path makes it completely independent of the input signal. This eliminates any interaction between the feedback and input circuits, in conventional amplifiers that causes problems with CMRR and output current/voltage.

Due to these enhanced characteristics, a differential amplifier (AD8103) with extremely high common mode rejection ratio (CMRR), above 100dB @ 800 KHz and 70dB at 10 MHz was used in the third test circuit for the second version of the McMaster EIT system VCCS.

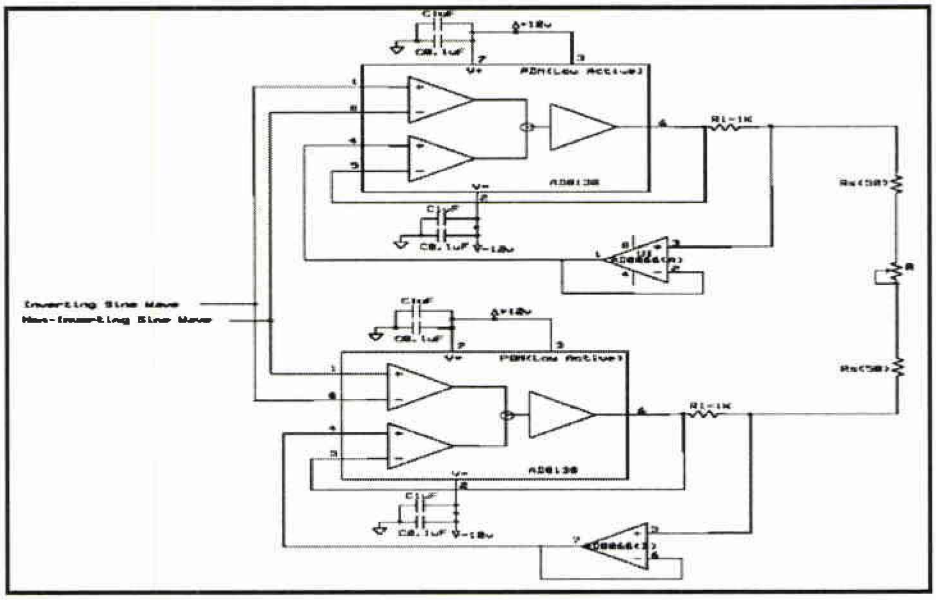

Figure 5.6 Bi-polar differential current pump circuit diagram.

The voltage signals (inverted and non-inverted) from the signal generator was applied to both inputs of the differential amplifier as shown in Figure 5.6. The differential amplifier converts the double-ended signal into a single-ended signal.

Another set of two conventional operational amplifiers are implemented as unity gain amplifiers which feedback the voltage drop across the current sense resistor R_I to the input of the differential amplifier. These current sense resistors R_I were placed between operational amplifiers output and the load. The output current I_O is controlled by the input voltage V_i and is given by

$$I_O = \frac{V_i}{R_1}. \qquad 5.4$$

The advantage of this design is that only two external components one passive (resistor) and another active (operational amplifier) are required for voltage to current conversion.

Matching these two resistors R_1(one for the upper section and another for the lower as shown in Figure 5.6) was much easier as compared to matching the resistor ratio ($\frac{R_2}{R_1} = \frac{R_4}{R_3}$) as in the improved Howland VCCS and the current pump circuits. As in the previous voltage control current source circuits, in this circuit for the two buffers amplifies a dual operational amplifier IC was used as well. The bipolar current source was built on wire-o-board, configured, tested and the experimental tests performed on this circuit are outlined and results are presented in the next chapter of this thesis.

Chapter 6

Testing methods and experimental results

In this chapter of the thesis, the following measurements were performed on two versions of the McMaster EIT system current source. (1) The stability, (2) the balance of the current injection, (3) the output impedance, and the variation in the output current due to both (4) prescribed changes in the impedance at a fixed frequency and (5) changes in the frequencies at a fixed load. The experimental circuit, procedure and results are described in the following sections.

6.1 Test circuit and experimental setup

The following test circuit was used to measure the various parameters of the two versions of the current source circuits.

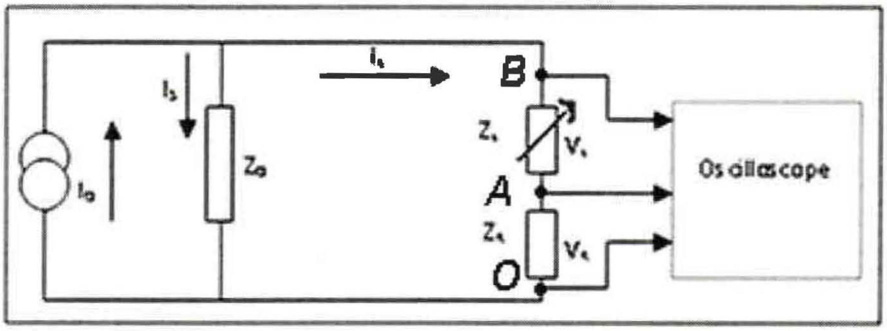

Figure 6.1 Test circuit to measure various parameters of the current source

For the first version of the McMaster EIT system current source, a digital oscilloscope[1] was used to measure the voltage drop across a fixed resistor Z_R of value 480Ω and a variable load resistor Z_L of value 0-700Ω.

For the second version of the McMaster EIT system current source, the same digital oscilloscope was used to measure the voltage drop across a fixed resistor Z_R of value 150Ω and a variable load resistor Z_L of value 0 - 2kΩ. The two different values fixed resistor Z_R of both versions will not effect, the

[1] Tektronix TDS 220 100MHz, dual channel, real-time oscilloscope

measured current. The value of Z_L was increased to observed the current variation at higher load.

Since these two resistors (Z_R, Z_L) are in series, the current through these resistors is equal in magnitude. The magnitude of the output (injected) current was calculated using Ohm's law by measuring the voltage drop across the fixed resistor Z_R.

Before testing each circuit performance the oscilloscope was calibrated using the built in calibration procedure. In order to avoid the loading effects of the oscilloscope, the input impedance of the oscilloscope probe was set to 10MΩ. To establish a common ground voltage between the oscilloscope and the circuit under test, the ground terminal of the oscilloscope was connected to the ground terminal of the circuit and power supply. Oscilloscope voltage and time scales were adjusted before each measurement to avoid any error due to voltage/time scale offset. The channel 1 of the oscilloscope was set to measure the voltage drop across Z_R (OA figure 6.1) and channel 2 was set to measure the voltage drop across the total load $Z = Z_R + Z_L$ (OB).

All circuits under test were calibrated before the experiment. The calibration consisted of: (1) DC offset adjustment, (2) gain adjustment of the 2nd stage operational amplifier. The DC offset was removed to ensure a balanced bipolar signal. The gain was adjusted in order to avoid any positive or negative saturation of the VCCS under maximum load.

Three sets of experimental measurements were conducted for both versions of the current source and the average of these measurements was used in the results. A diagram of the test circuit and oscilloscope is shown in Figure 6.1.

To calculate the output impedance and the output current variation of the current source circuits the following equations were used (see appendix D for derivation).

$$Z_o = \frac{V_{max} - V_{min}}{V_{min}/Z_{min} - V_{max}/Z_{max}} \quad (1)$$

$$I_{Lmin} = V_{min}/Z_{min} \quad (2)$$

$$I_{Lmax} = V_{max}/Z_{max} \quad (3)$$

6.2 Experimental methods:

To measure the various parameters of the current source circuits the following procedure was performed.

6.2.1 Stability of the circuits

In the first version of the McMaster EIT system current source, the stability was observed by measuring the fluctuation in the injected current through the fixed resistor Z_R. While the variable resistance Z_L was increased from 0Ω to 700Ω in steps of 50Ω, with a fixed frequency of 10 KHz. The measurements were repeated for frequencies 20 KHz, 25 KHz, 50 KHz and 62.5 KHz.

For the second version of the McMaster EIT system current source, the stability was observed by measuring the fluctuation in the injected current through the fixed resistor Z_R. While the variable resistance Z_L was increased from 0Ω to 2000Ω in steps of 50Ω, with a fixed frequency of 1 KHz. The measurements were repeated for frequencies from 1 KHz to 300 KHz in steps of 50 KHz.

6.2.2 Balance current injection test

The balanced nature of the current injection for the two versions of the McMaster EIT system current source circuits was observed. Instead of using fixed and variable resistances, as in Figure 6.1, two equal resistances with 0.1% tolerance were used. The voltage at both terminals with reference to the middle terminal A (AO and AB) was measured (see Figure 6.1). Two measurements were made. First, the resistance was increased from 50Ω to 500Ω, in steps of 50Ω, on both sides of terminal A using fixed frequencies (50 KHz and 100 KHz) and the injected current was measured. Second, the frequency was increased from 1 KHz to 100 KHz, at a fixed load of 500Ω, on both sides of terminal A and the injected current was measured.

6.2.3 Output impedance

To measure the output impedance, the following procedure was performed:

1. The frequency of the injected current was set to 62.5 KHz for the first version and in the second version the frequency was extended to 100KHz.
2. The variable resistance Z_L was set to 0.
3. The voltage across the resistors ($Z = Z_R + Z_L$) was measured.
4. The variable resistance Z_L was set to maximum, 700Ω for first version and for the second version the load was increased to2KΩ.
5. The voltage across the resistors ($Z = Z_R + Z_L$) was measured.

Equation 1 was the implemented to calculate the output impedance of the circuit under test.

6.2.4 Current vs load variations

To measure the variation in the output current, due to changes in the load at fixed frequencies the following procedure was followed:

1. The frequency of the injected current was set to 10 KHz for the first version and for the second version since our frequency interest range was higher therefore, 50KHz was selected.
2. The variable resistance Z_L was set to 0.
3. The voltage across the resistor Z_R was measured, Z_R was set to 480Ω for the first version and 150Ω for the second version. The different values of Z_R will not effect, the current measurements.
4. The variable resistance Z_L was set to ¼, ½, ¾ or maximum. The maximum Z_L was 700Ω for the first version and for the second version current dependence on load was measured at higher load of 2KΩ.
5. The voltage across the resistor Z_R was measured.
6. Steps 4 and 5 were repeated until Z_L reached the maximum value

Equations 2 and 3 were used to calculate the variation in the output current due to changes in the loads at a fixed frequency. To calculate the variation in the output current at different frequencies the above procedure was repeated (step 4-

6) after changing the frequency. The frequency upper limit for the first version was 62.5 KHz and for the second version the current dependence was measured at much higher frequency 300 KHz.

6.2.5 Current vs frequency variations

To measure the variation in the output current, due to changes in the frequency at a fixed load the following procedure was followed:

1. The frequency of the injected current was set to 10KHz for first version and for the second version frequency limit was lowered to 1KHz.
2. The variable resistance Z_L was set to maximum. Z_R was set to 480Ω for the first version and 150Ω for the second version. The maximum value of Z_L was 700Ω for the first version and 2KΩ for the second version. Different values of Z_R will not effect, the current measurements.
3. The voltage across the resistors ($Z=Z_R + Z_L$) was measured.
4. The frequency of the injected current was incremented (25 KHz, 50 KHz and 62.5 KHz for the first version and 50 KHz,100 KHz, 200KHz and 300 KHz for the second version).

5. Steps 2 through 5 were repeated until the frequency reached the maximum 62.5 KHz for the first version and extended frequency range dependence up to 300KHz for the second version

Equation 2 and 3 were used to calculate the variation in the output current due to changes in frequency at a fixed load.

6.3 Experimental results of the McMaster EIT system current source version I

The resultant magnitudes of the output (injected) current due to variable loads at fixed frequencies (10 KHz, 25 KHz, 50 KHz and 62.5 KHz) were measured. The results are shown in the following Figures 6.2, and 6.3.

It was observed that the circuit is not stable at lower values of load changes (below *600Ω* and frequencies higher than 62.5 KHz). The current source was not balanced.

The output impedance of the circuit was estimated to be ***8KΩ*** at 62.5 KHz, using equation 1.

Under the load fluctuations (***480Ω - 1180Ω***), the magnitude of the injected current is not constant and stable as shown in Figure 6.2 and 6.3. The magnitude of the injected current signal varies comparatively more at 10 KHz than at higher frequencies. The overall fluctuation in the magnitude of the injected current is approximately ***0.9mA***. The overall variation in the injected current is approximately ***0.86mA (12.5%)*** and ***0.65mA (10.55%)*** due to the same changes in the loads at frequencies 10 KHz and 62.5 KHz respectively. These output current magnitude slopes can be divided into three regions. In the first region where the load changes from ***480Ω*** to ***524Ω***, the output current increases as the load is increased for frequencies 20 KHz, 25 KHz and 50 KHz.

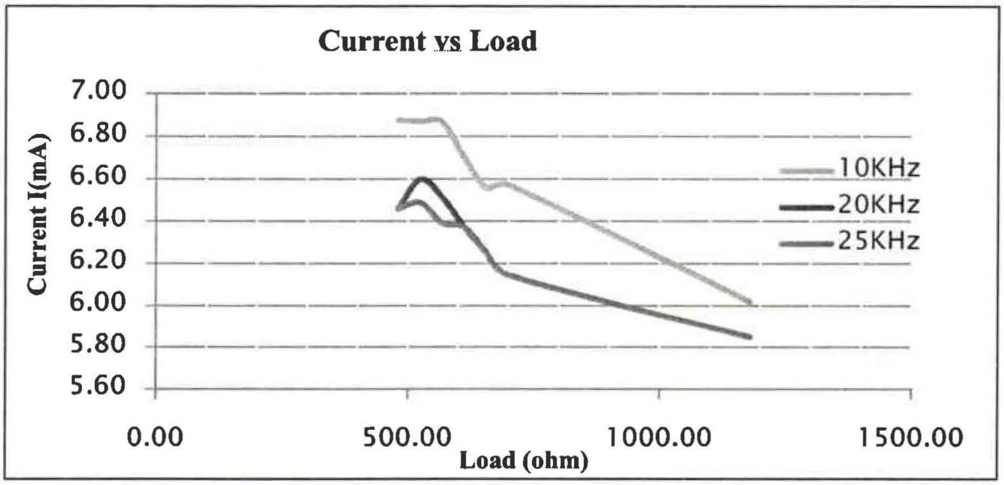

Figure 6.2 Current vs variable load at fixed frequencies (10KHz, 20KHz and 25KHz)

However, at 10KHz in the first region, the magnitude of the injected current remains approximately constant as compared to other frequencies. For the second region where the load changes from ***524Ω*** to ***568Ω*** the magnitude of the injected current drops more quickly than the third region where the load changes from ***568Ω*** to ***1180Ω*** of the current slope.

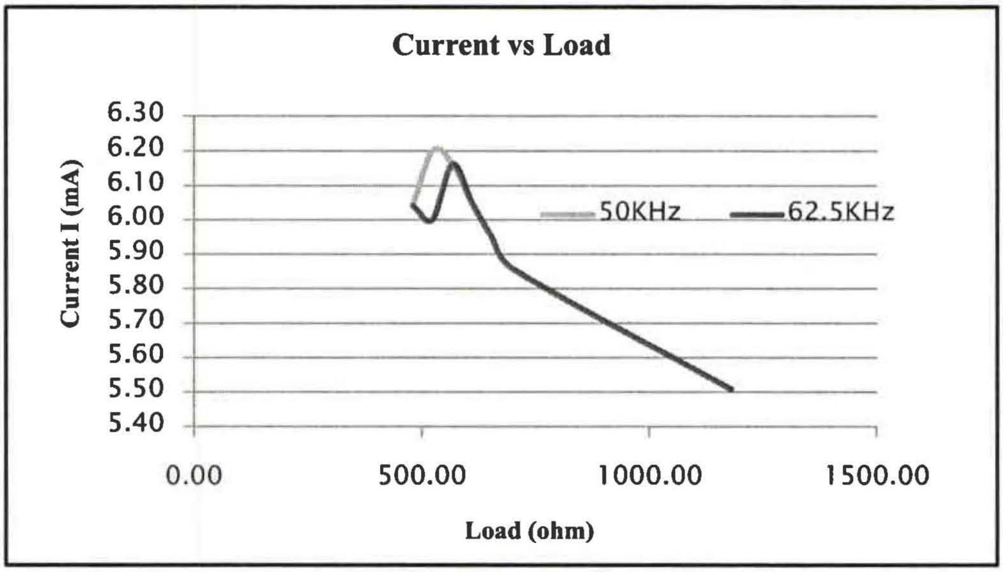

Figure 6.3 Current vs variable load at fixed frequencies (50KHz and 62.5KHz).

Figure 6.4 shows the variation in the magnitude of the injected current when frequency is increased keeping the load fixed ***(1180Ω)***. The magnitude of the injected current decreases, approximately ***0.51mA (8.47%)*** at the maximum fixed load ***1180Ω*** as the frequency is increased from 10 KHz to 62.5 KHz.

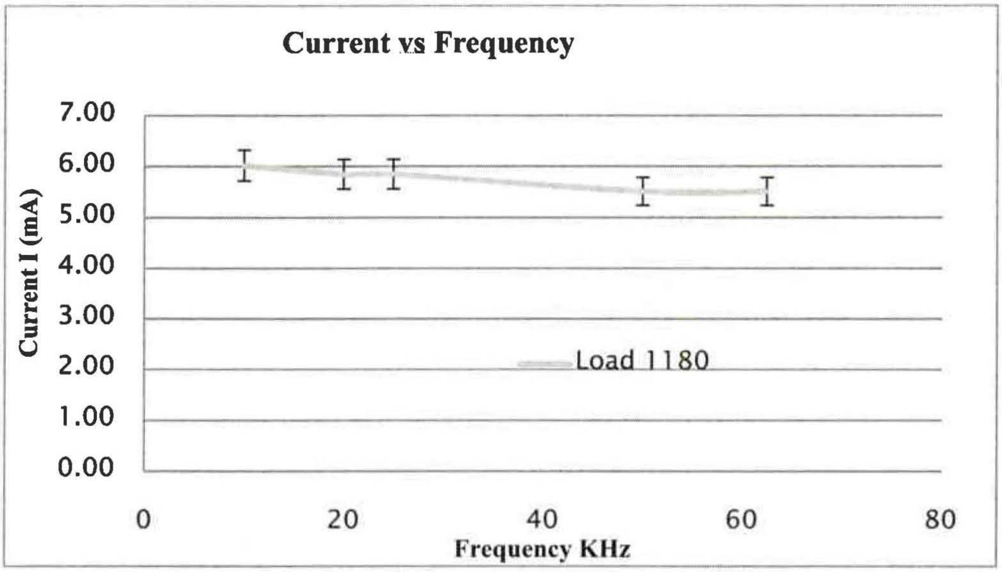

Figure 6.4 Current vs Frequency at fixed load (1180Ω).

6.4 Experimental results of the McMaster EIT system current source version II

For the second version of the McMaster EIT system current source, three different voltage control current sources (VCCS) circuits (Current pump, Howland and Bi-polar) were implemented on a printed circuit and a wire-board. These circuits were configured and the above-mentioned parameters were measured. The next sections of the thesis described the experimental results of these circuits.

6.4.1 Current pump VCCS results

It was observed that the circuit is stable, however the injected current was not balance. The output impedance of the current pump circuit was estimated using equation 1, to be ***7KΩ*** at 100 KHz.

The experimental results for the current pump circuit show the variation in the injected current due to changes in the load resistance ***(150Ω-2150Ω)*** at fixed frequencies as shown in Figure 6.5.

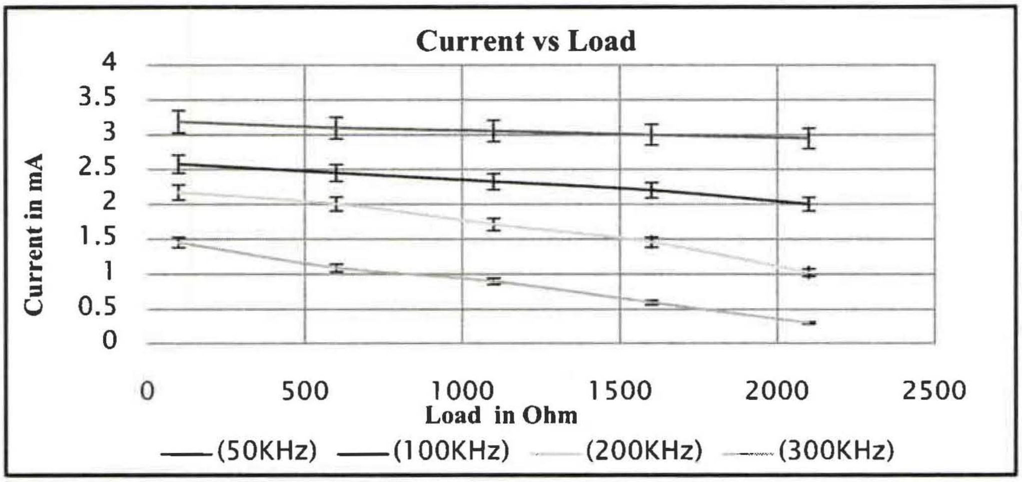

Figure 6.5 Current as a function of load at various fixed frequencies

These injected current were calculated at 50 KHz, 100 KHz 200 KHz and 300 KHz. The minimum variation in the injected current is approximately ***0.58mA (22.44%)*** at ***100 KHz*** and the maximum variation in the injected current is approximately ***1.15mA (79.35%)*** at ***300 KHz***. The variation in the injected current due to changes in loads is approximately the same for 50 KHz and 100 KHz frequencies. There is more variation in the injected current due to changes in load, at higher frequencies such as 200 KHz and 300 KHz.

The magnitude of the injected current decreases as the frequency increases as shown in Figure 6.6. The magnitude of injected current decreases more quickly for frequencies below 100KHz as compared to above 100 KHz. The magnitude of the injected current decreased approximately ***2.65mA (89.83%)*** at the maximum load (***2150Ω***) over the frequency range from 50 KHz-300 KHz.

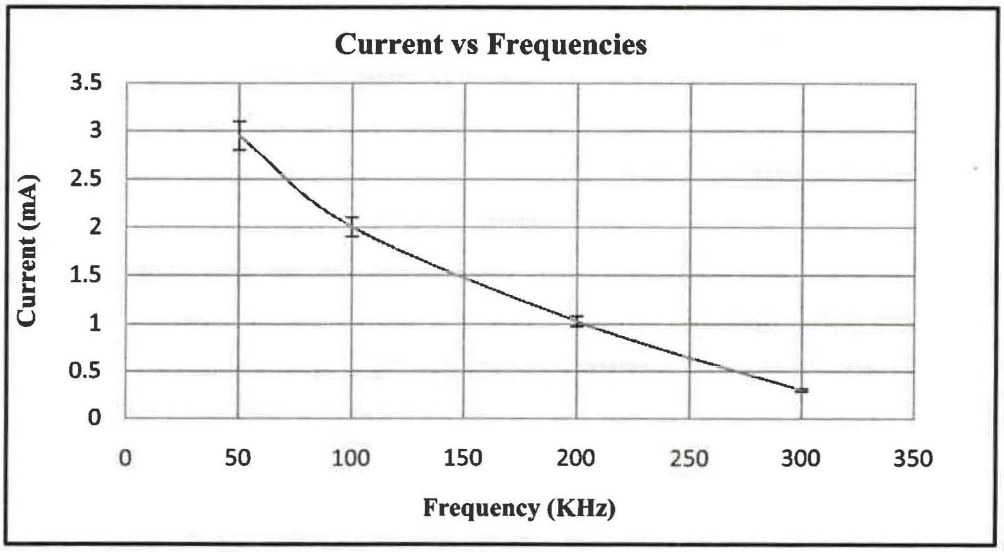

Figure 6.6 Current as a function of frequency at a fixed maximum load

6.4.2 Improved Howland VCCS results

Two versions, single-ended and double-ended injection of the improved Howland current source circuits were tested.

Both versions were stable. However only the double-ended current source was balanced. The output impedance of these improved Howland circuits was estimated to be ***256KΩ*** at 100 KHz, using equation 1.

Both circuits produced identical results for the output current variations.

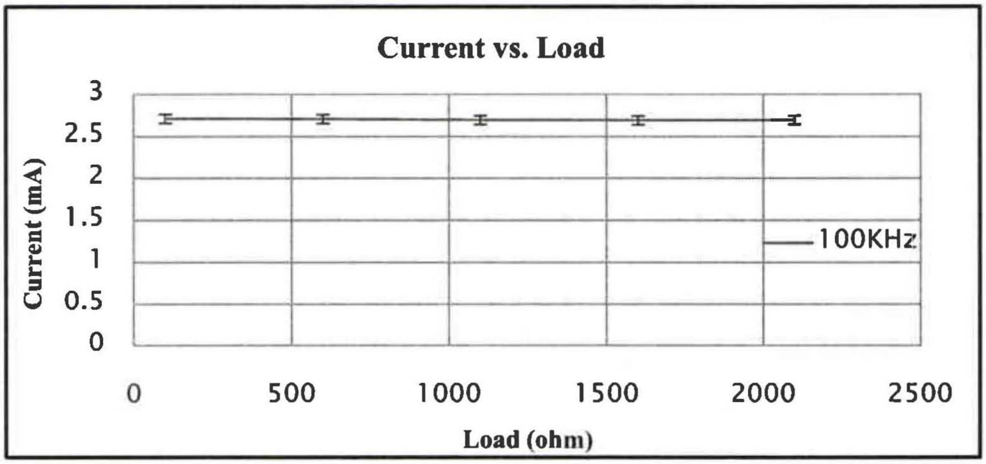

Figure 6.7 Current as a function of load at fixed frequency 100 KHz.

The experimental results for the improved Howland current source show the variation in the magnitude of the injected current due to changes in the load resistance (150Ω-2150Ω) at a fixed frequency of 100 KHz as shown in Figure 6.7.

The variation in the magnitude of the injected current due to changes in the loads (150Ω-2150Ω) was estimated to be approximately about ***0.021mA (0.77%)*** at 100 KHz.

As shown in Figure 6.8, the magnitude of the injected current for a fixed maximum load of ***2150Ω*** changes approximately ***1.74mA (55%)*** for frequency range from 1 KHz to 300 KHz as shown in Figure 6.8.

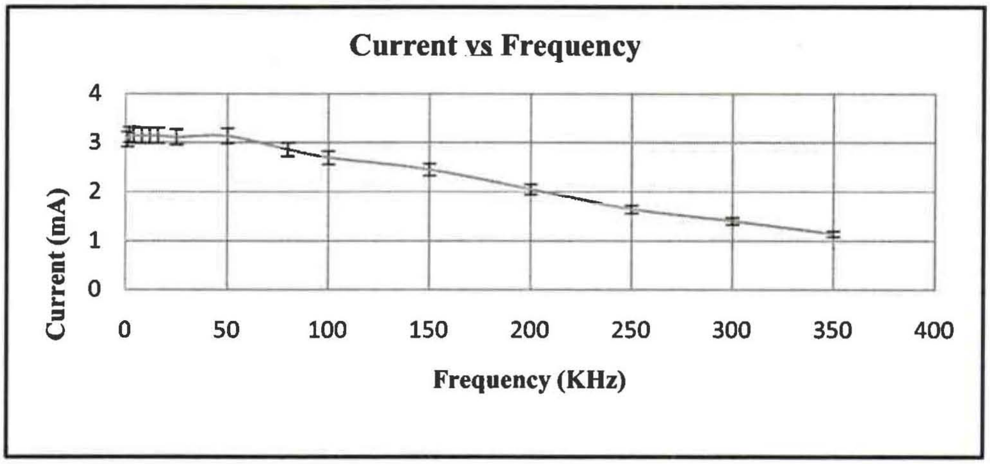

Figure 6.8 Current as a function of frequency at a fixed maximum load

6.4.3 Bi-Polar VCCS results

The experimental results for Bi-Polar voltage control current source are shown in the following figures 6.9 and 6.10.

The voltage control current source (bi-polar) circuit was stable however not balanced. The output impedance of this circuit was estimated to be ***25KΩ*** at 100 KHz, using equation 1.

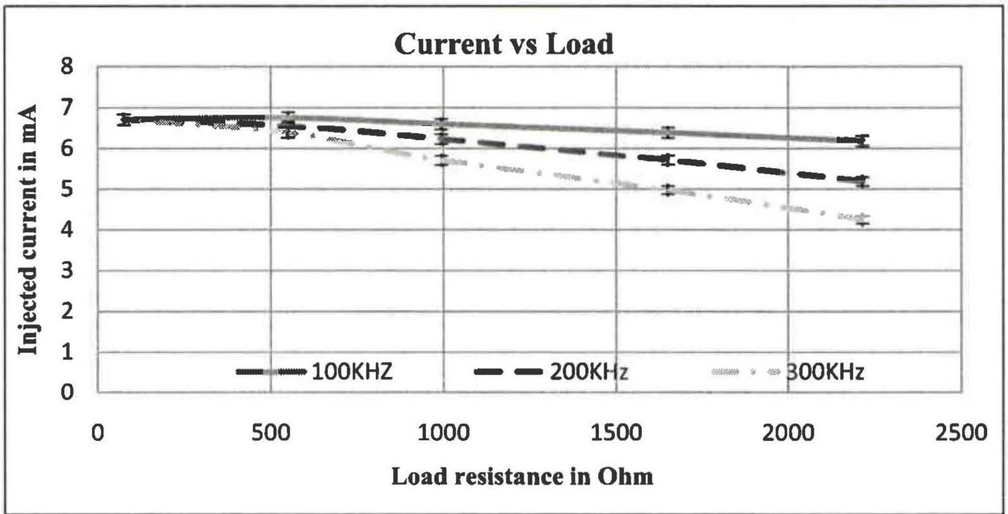

Figure 6.9 Current as a function of load at fixed frequencies

Figure 6.9 shows the variations in the magnitude of the injected current due to changes in the load resistance (150Ω-2150Ω). These outputs current were measured at 100 KHz, 200 KHz and 300 KHz frequencies. As the frequency was increased, the variation in the output current due to changes in load was increased as well. The variations in the output current are approximately 0.6mA at 100 KHz, 1.4mA at 200 KHz and 2.4mA at 300 KHz. The variation in the output current is a minimum approximately ***0.42mA (6.35%)*** at 100 KHz and maximum approximately 1.78mA (26.35%) at 300 KHz due to changes in loads.

Figure 6.10 shows the variation in the magnitude of the injected current due to changes in the frequency at fixed maximum load. The magnitude of the injected current for fixed load (***2150Ω***) changes approximately ***2.57mA (37%)*** for frequency range from 1 KHz to 300 KHz.

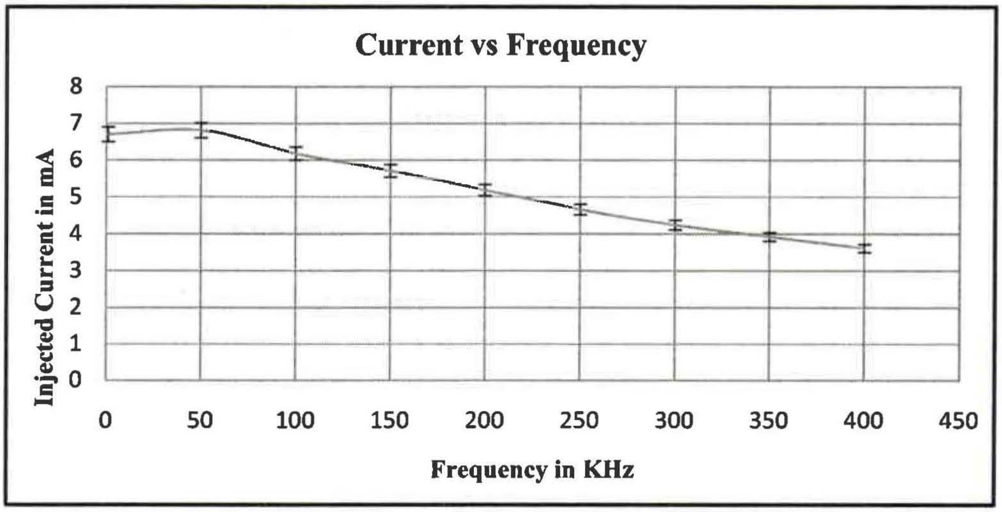

Figure 6.10 Current as a function of frequency at fixed maximum load

6.5 Discussion

In this thesis, both the previous and the new versions of the McMaster EIT system current source circuits, configuration, testing procedure and experimental performance are described.

In the second version of the signal generator, a different approach was adopted to avoid issues associated with the first version i.e., limited resolution, small set of frequency generation, lookup table and DAC settling time. A DDS was selected for the signal generator.

To overcome the issues of stability and the balanced nature of the current injection, a voltage controlled current source (VCCS) was implemented. This will further improve the output impedance and output current variation due to changes in loads and frequencies. Three different versions of VCCS circuits, including the first version the improved Howland assembled configured and tested in the second version.

The performance of the improved Howland current source circuit with differential input voltage outperforms the first version and other two current source circuits in the second version of the McMaster current source.

The following table summarise the results:

Current Source / Parameters	Stability	Balanced	I_L (mA) (Due to load)	I_L (mA) (Due to Frequency)	Output Impedance Z_0
Imp. Howland (first version)	*No*	*No*	*10.55%* *480Ω - 1180Ω* *@62.5 KHz*	*8.47%* *10KHz to 62.5KHz* *@1180Ω*	*8KΩ* *@62.5KHz*
Imp. Howland (second version)	***Yes***	***Yes***	***0.77%*** ***150Ω-2150Ω*** ***@100KHz***	*55%* *1KHz to 300KHz* *@2150Ω*	***256KΩ*** ***@100 KHz***
Bi-Polar (second version)	*Yes*	*No*	*6.35%* *150Ω-2150Ω* *@100KHz*	*37%* *1KHz to 300KHz* *@ 2150Ω*	*25KΩ* *@ 100 KHz*
Current Pump (second version)	*Yes*	*No*	*22.44%* *150Ω-2150Ω* *@100KHz*	*89.83%* *50KHz-300 KHz* *@2150Ω*	*7KΩ* *@ 100 KHz*

Table 6.1 Current source parameters (Stability, Balance, Output Impedance, and Current Variations)

The operational amplifier should be operated in the manufacturer recommended stable gain region since these components are optimized for that; otherwise, there would be variations in the stability of the operational amplifier as observed in the first version.

Another factor with the VCCS was observed, namely that the current injected into an object was not balanced in all circuits except for the improved Howland current (source second) version.

The current was injected more in the negative phase as compared to the positive phase therefore the center point of the injected current within the object was shifted towards negative, rather than the origin, as required by the EIT system. This issue was solved by applying a differential voltage to the improve Howland current source instead of single-ended voltage application.

The output impedance of the second version was improved from ***8KΩ*** to ***256KΩ*** by using resistors of 0.1% tolerance were used. Higher precision components could further improve the output impedance.

Two types of variations in the magnitude of the injected current were observed; the variation due to changes in loads while the frequency was fixed and the variation due changes in frequencies while the load was fixed. These variations in the magnitude of the injected currents were to some extent due to the incorporated components, resistors precision and operational amplifier characteristics.

The variation in the magnitude of the injected current due to changes in the load at fixed frequency was reduced over 13 fold i.e., from 10.55% to 0.77%. However; the variation in the injected current is still higher since, 0.10% of variation in the output current is required for 10-bit precision measurement and this could be achieve by automatic gain adjustment in the 2nd stage of the operational amplifier.

The gain of the operational amplifier drops as the frequency is increased; an operational amplifier with very high CMRR (over 100dB) over frequency of interest could minimize the gain reduction issue.

The above-mentioned current source circuits are voltage control current sources (VCCS) meaning that the output current is control through the input voltage. Both types of variations (due to loads and frequencies) in the injected current could be minimized further by precisely adjusting the input voltage of the VCCS.

Beside these factors, there are other factors to consider as observed in the first version such as; connecting shielded coaxial cables; these should be grounded or opposite signal should be injected to minimize the stray capacitance (tri-axial cables perhaps). The lengths of different electrode wires or copper tracks on the PCB should be equal, otherwise different impedance might be offered.

There are several advantages with the new current source (Howland differential) as compared to the first version;

1. The current source was more stable.
2. The current injection is now balanced.

3. Increased output impedance 256K instead of 8K
4. The frequency range was increased from 1 Hz to 1 MHz instead of 1 KHz to 125 KHz. The second version of the current source was only tested over frequency range from 1 KHz to 300 KHz due to the gain degradation of the operational amplifier. The reduction in the gain at higher frequencies could be readjusted by increasing the input voltage however; in this experiment, the input voltage was kept constant for all circuits to avoid any discrepancies in the input voltage and the resultant output current.
5. Increased frequency resolution 1Hz is available instead of limited preselected frequencies
6. Reduced output current variation due to loads i.e., 0.77% @100 KHz (2150 ***Ω***) instead of 10.55% @62.5KHz (1180***Ω***).

In the next chapter of the thesis, the conclusions and future goals will be described.

Chapter 7

Conclusion and future goals

This chapter of the thesis lists the improvements made and highlights future recommendations for the current source. For the McMaster EIT current source version II the following features were implemented.

The human interface for McMaster EIT system current source version II is now through DIP switches. Using these DIP switches a predefined set of frequencies (1KHz- 1MHz) and shapes (Sine, Triangular and Square wave) can be selected (see Appendix C).

The voltage output signal from the DDS has a DC offset. In order to remove this DC offset and to translate it to a bi-polar signal as required, the DC offset is removed through the use of an operational amplifier using a potentiometer[1].

The magnitude of the output voltage from the DDS was 650 mV uni-polar. It was translated into a bi-polar signal of ±325 mV (peak-to-peak) and a gain (amplification) of about 30 was required to translate into ±10 V (peak-to-peak). The amplitude was amplified in two stages using operational amplifiers. The first stage amplification was fixed and it was implemented within the DC offset stage, the second stage amplification was made variable (to control the injected current magnitude) and it was implemented using a potentiometer in the feedback path of the operational amplifier[2].

The output after the variable gain stage was a single-ended signal. In order to translate into double-ended signals, two unity gain operational amplifiers (one

[1] See chapter 3 Signal Generator Version II (V.2) of McMaster EIT System Figure 3.8(a)
[2] See chapter 3 Signal Generator Version II (V.2) of McMaster EIT System Figure 3.8(b)

inverting, one non-inverting as shown in Figure 3.9 chapter 3), were implemented to translate the voltage signal 180 degrees out of phase.

It was observed that the magnitude of the injected current degrades with increasing frequency. It was readjusted using the second stage gain potentiometer, to maintain a constant current magnitude.

For maximum flexibility and future designs considerations, the three different voltage control current source circuits discussed in this thesis (chapter 5.2), were all fully implemented on the printed circuit board and wire-board. However, the second version Howland circuit performance was better than the other circuits including the first version.

For the second version of the McMaster EIT system signal generator (ch 3), the improvements implemented (separate from the signal generator improvements above) are; (1) the frequency range is extended to cover the range from 1KHz to 1MHz instead of 1KHz to 125 KHz, (2) the frequency resolution of the DDS in the signal generator circuit is 1Hz instead of a few preselected frequencies and (3) the issue of the DAC settling time was avoided by using a DDS.

The following five parameters measurements were performed on both versions of EIT system voltage control current source (VCCS). (1) The stability, (2) the balance of the current injection, (3) the output impedance, and the variation in the output current due to both (4) prescribed changes in the impedance at a fixed frequency and (5) changes in the frequencies at a fixed load. The experimental circuit, procedure and results are described in the following sections.

All the circuits in second version were stable; the first version was not stable due to DA settling time and gain settings design flaw.

The injected current was balanced only for Howland current in the source second version. Under balanced current injection, the center point of the injected current within the object conductivity will not shift.

The output impedance of the second version current source circuits was 25KΩ (bi-polar), 256KΩ (Howland) and 7KΩ (current pump) at 100 KHz as compared to first version 8KΩ at 62.5 KHz. The output impedance for second version (Howland circuit) was much higher than the other circuits.

For EIT current source, it is required to have very high output impedance (at least few mega Ohm). The second version was unable to achieve, a very high output impedance, due to the mismatch in the components, temperature and capacitive effects of the circuit. However, the output impedance could be further increased by incorporating a generalized impedance converter (GIC). A GIC contains two operational amplifiers and five passive elements that is, four resistors and a capacitor. This type of GIC will synthesize an inductance, and in an ideal compensation scheme, the effects of the capacitance are completely cancelled. This prevents reduction in the output impedance due to stray capacitance. (Analog Devices). The GIC was not implemented in either version of the McMaster EIT system current sources.

The maximum variation in the output current was 6.35% (bi-polar), 22.44% (current pump) and 0.77% (Howland) due to variation in load (150Ω - 2150Ω) at a fixed frequency (100 KHz). This is in comparison to the first version, which was 10.55% due changes in load (480Ω -1180Ω) at a fixed frequency (62.5 KHz).

Clearly, in the second version (Howland circuit) the variation in the output current is reduced by approximately 12 times with respect to the first prototype version, despite the fact, that the load changes from 150Ω- 2150Ω at fixed frequency 100 KHz instead of 148Ω -1180Ω at frequency 62.5 KHz for the first version.

The maximum variation of the output current due to changes in frequency range from 1 KHz to 300 KHz was about 37% (bi-polar), 55% (Howland) and 89.83% (current pump) at a fixed maximum load 2150Ω for this second version of the McMaster EIT current source. This compares to the first version of the current source that was about 8.47% due changes in frequency range from 1 KHz to 62.5 KHz at maximum load 1180Ω.

The first version (Howland circuit) current variations due to changes in frequency (1 KHz to 62.5 KHz) at fixed maximum load (1180Ω) are better than the other circuits. However, in the first version, the frequency range under test was 1KHz to 62.5KHz whereas for the second version the it was much higher up to 300 KHz. Also, the maximum load at the time of testing for the first version was 1180Ω and for the second version, it was 2150Ω.

The variation in the output current (8.47%) for the first version could be much higher, if the frequency range was increased to 300 KHz at a fixed load (2150Ω). The first version however became very unstable for frequencies above

62.5 KHz, and therefore it was not possible to test it reliably. Furthermore, the voltage control current source was implemented using operational amplifiers and their output gain (output current) degrades, as the frequency is increased (ch 5).

The performance parameters: stability, balanced current injection, high output impedance, and low output current variations due to changes in load, of the improved Howland voltage control current source out-perform the other voltage control current source circuits. The variation in the injected current, due to changes in frequencies at fixed maximum load could be further adjusted by increasing the input voltage (ch 5).

After review of these experimental results, it is evident that there are some practical limitations such as; matching the resistance ratios, operational amplifier characteristics, noise due to elevated temperature (components used in the circuit will behave minutely different), while components are in operation and stray capacitive effects. These practical limitations prevent the current source in achieving a high accuracy over changes in the loads and frequencies.

The second version of Howland voltage control current source circuit performance was better than the other voltage control current source circuits. In Howland circuit, all resistances were quoted to a tolerance 0.1%, a dual IC for operational amplifiers, and to further minimize the stray capacitive effects, all components used were surface mount miniature versions. However, there were still variations (0.77%) in the output current, due to changes in loads at fixed frequency of 100 KHz.

There is an alternative way to inject a constant current of lesser variations (better precision 0.01%) and to be able to have a less accurate (about 1%) current source with the addition a very precise known value (±0.001% tolerance) resistor in series with the load. Measure the voltage drop across this series resistor with a differential amplifier that has a very high CMRR (about 100dB) over all frequencies of interest. Monitor and keep the voltage drop precisely constant across this resistor by readjusting the input voltage to the VCCS, over output current changes (0.1% or better) due to loads and frequencies.

The voltage drop across i.e., current through the series resistor, can be adjusted by changing the input applied voltage to the voltage control current source. The applied voltage is coming from an operational amplifier and it could be adjusted by adjusting the gain of this operational amplifier. The manual gain adjustment was implemented in the second version (ch 5).

Based upon this experimental experience, a number of improvements and enhancements could be implemented in this system, but were not performed in the interest of time. The major suggestions are outlined here.

1. Human interface through a PC instead of DIP switches.

   1.1 PC software could allow the user to select any single frequency from frequency range of 0Hz to 1MHz with increment of 1Hz. No hardware changes are required, but provide greater flexibility to user with no loss in speed.

2. Automatic adjustment of the DC offset instead of manual. This will speed up the calibration process by eliminating the time consuming calibration process, i.e., measure and adjust the DC offset each time the current source is used.
3. Automatic gain adjustment of the output current i.e., to inject a constant magnitude of current under both, load and frequencies changes. Currently the gain is adjustment is manual.
4. Use single IC instead of two unity gain buffer operational amplifiers ICs for single-ended signal to double-ended signals translation. To avoid the unbalanced current injection in a floating load, due to any mismatch in the operational characteristics of these two separate units.

5. The output impedance of the VCCS could be further improved by implementing a generalized impedance converter (GIC). The GIC will cancel the effects of the capacitance and this will prevents reduction in the output impedance due to stray capacitance.
6. Current source should be operated through a battery power not through a socket power for patient safety and noise propagation from power line to the current source and furthermore PC and current source circuit should be isolated i.e., both systems should have their own power.

To implement the above modifications, the following hardware changes are required. Note that both PC software and microcontroller software modifications would be required as well.

1. Serial interface between PC and microcontroller
2. Digital potentiometer instead of manual DC offset potentiometer (stage 1[3]).

   2.1 DC offset detection circuit i.e., feeding back the voltage polarity information to the microcontroller and the microcontroller control a digital potentiometer for DC offset adjustment.

3. Digital potentiometer instead of manual gain potentiometer (stage 2[3])

[3] See chapter 4 for stage 1 description

3.1 Circuit for voltage drop detection across current sense resistor

3.2 A fast analog to digital converter to digitize the detected voltage drop

3.3 Interfacing ADC to microcontroller where the magnitude of the injected current can be calculated

3.4 Interfacing microcontroller to a digital potentiometer for injected current magnitude adjustment

4. Single-ended to double-ended operational amplifier interfacing between stage two and voltage control current source.
5. A generalized impedance converter (GIC) circuit added in parallel to current source and before load under test.
6. Battery operated power supply with DC outputs 0V,+5V, ±12V, which will operate the microcontroller, current source and voltage measurement circuit.

6.1 The serial interface between PC and microcontroller should be optically isolated.

Appendix A:

The current pump voltage control current source

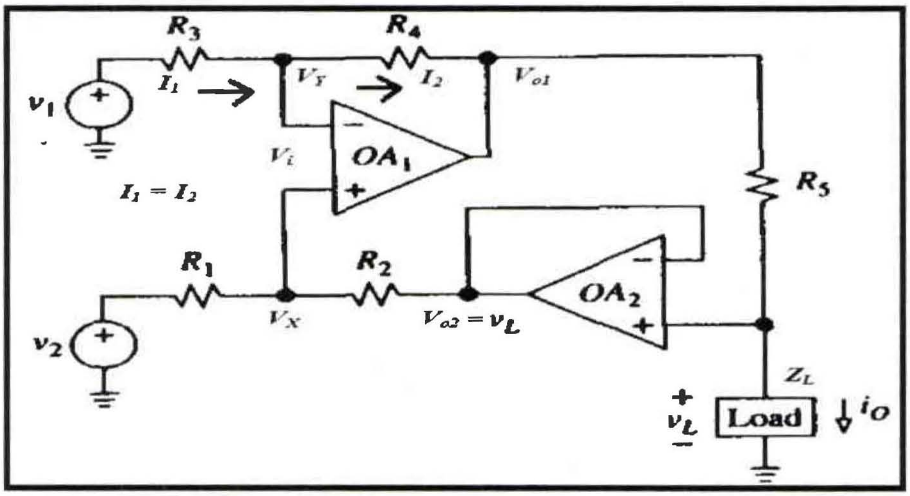

Figure A.1 Current pump circuit

The output of the operational amplifiers OA_1 is V_{O1} and OA_2 is V_{O2} is shown in the Figure A.1 The output $V_{O2} = V_L$ due to the unity gain of the operational amplifier OA_2. Since the open loop gain of the operational amplifier is infinite therefore $V_X = V_Y$.

$$I_1 = \frac{V_1 - V_Y}{R_3} = I_2$$

$$V_X = \frac{R_2V_2 + R_1V_L}{(R_1 + R_2)}$$

$$V_{O1} = V_Y - I_2R_4$$

$$V_{O1} = V_Y - \frac{V_1 - V_Y}{R_3}R_4$$

$$V_{O1} = \frac{(R_3 + R_4)}{R_3}V_Y - \frac{R_4}{R_3}V_1$$

$$V_{O1} = \frac{(R_3 + R_4)}{R_3}\frac{R_2V_2 + R_1V_L}{(R_1 + R_2)} - \frac{R_4}{R_3}V_1$$

$$V_{O1} = -\frac{R_4}{R_3}V_1 + \frac{\left(1 + \frac{R_4}{R_3}\right)}{\left(1 + \frac{R_1}{R_2}\right)}V_2 + \frac{\left(1 + \frac{R_4}{R_3}\right)}{\left(1 + \frac{R_2}{R_1}\right)}V_L$$

The load current is given by

$$I_O = \frac{V_{O1} - V_L}{R_5}$$

$$I_O = \frac{1}{R_5}(V_{O1} - V_L)$$

$$I_O = \frac{1}{R_5}\left\{-\frac{R_4}{R_3}V_1 + \frac{\left(1 + \frac{R_4}{R_3}\right)}{\left(1 + \frac{R_1}{R_2}\right)}V_2 + \frac{\left(1 + \frac{R_4}{R_3}\right)}{\left(1 + \frac{R_2}{R_1}\right)}V_L - V_L\right\}$$

Assume

$$A_1 = \frac{R_4}{R_5 R_3} \qquad A_2 = \frac{1}{R_5}\frac{\left(1+\frac{R_4}{R_3}\right)}{\left(1+\frac{R_1}{R_2}\right)}$$

$$\frac{1}{R_O} = \frac{1}{R_5}\left(1 - \frac{\left(1+\frac{R_4}{R_3}\right)}{\left(1+\frac{R_2}{R_1}\right)}\right)$$

$$\frac{1}{R_O} = \frac{1}{\left(1+\frac{R_2}{R_1}\right)R_5}\left(\left(1+\frac{R_2}{R_1}\right) - \left(1+\frac{R_4}{R_3}\right)\right)$$

$$\frac{1}{R_O} = \frac{1}{\left(1+\frac{R_2}{R_1}\right)R_5}\left(\frac{R_2}{R_1} - \frac{R_4}{R_3}\right)$$

Therefore $\boxed{I_O = A_2V_2 - A_1V_1 - \frac{1}{R_O}V_L}$

Appendix B:

Voltage control current source using improved Howland current source

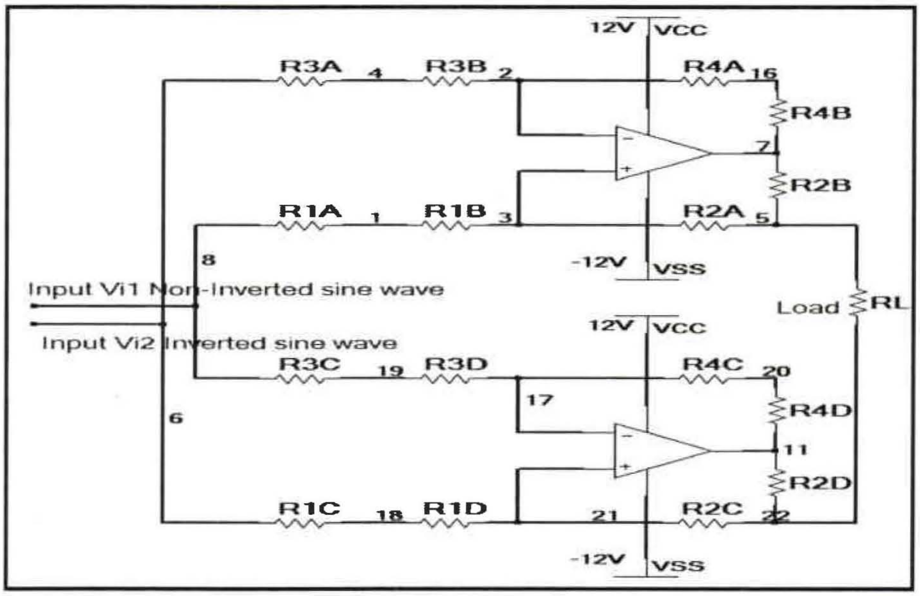

Figure B.1 Improved Howland Current Source Circuit

Equations for output impedance and source/sink current can be derived as follows:

$$V_0 = \left(1 + \frac{R_4}{R_3}\right) V_p \qquad (5)$$

$$V_p = \frac{R_1}{R_1 + R_{2A}} V_L + \frac{R_{2A}}{R_1 + R_{2A}} V_1 \qquad (6)$$

$$I_0 = \frac{V_1 - V_L}{R_1 + R_{2A}} + \frac{V_0 - V_L}{R_{2B}}$$

$$I_0 = \frac{V_1}{R_1 + R_{2A}} - \frac{V_L}{R_1 + R_{2A}} + \frac{V_0}{R_{2B}} - \frac{V_L}{R_{2B}} \quad (7)$$

Substituting the value of V_p from equation 6 into equation 5

$$V_0 = \left(1 + \frac{R_4}{R_3}\right)\left[\frac{R_1}{R_1 + R_{2A}} V_L + \frac{R_{2A}}{R_1 + R_{2A}} V_1\right]$$

$$V_0 = \left(\frac{R_3 + R_4}{R_3}\right)\left(\frac{R_1}{R_1 + R_{2A}}\right) V_L + \left(\frac{R_3 + R_4}{R_3}\right)\left(\frac{R_{2A}}{R_1 + R_{2A}}\right) V_1 \quad (8)$$

Substituting the value of V_0 from equation 8 into equation 7

$$I_0 = \frac{V_1}{R_1 + R_{2A}} - \frac{V_L}{R_1 + R_{2A}} - \frac{V_L}{R_{2B}} + \frac{1}{R_{2B}}\left[\left(\frac{R_3 + R_4}{R_3}\right)\left(\frac{R_1}{R_1 + R_{2A}}\right) V_L + \left(\frac{R_3 + R_4}{R_3}\right)\left(\frac{R_{2A}}{R_1 + R_{2A}}\right) V_1\right]$$

After simplification

$$I_0 = \frac{V_1}{R} - \frac{V_L}{R_0}$$

$$R_0 = \frac{R_3 R_{2B}(R_1 + R_{2A})}{R_3 R_2 - R_1 R_4}$$

$$R_0 = \frac{R_{2B}\left(1 + \frac{R_{2A}}{R_1}\right)}{\frac{R_2}{R_1} - \frac{R_4}{R_3}}$$

For $\frac{R_4}{R_3} = \frac{R_2}{R_1} \quad \rightarrow R_0 \rightarrow infinity$ (9)

$R = \frac{R_3 R_{2B}}{R_4}$ Or $R = \frac{R_1 R_{2B}}{R_2}$

Since $\frac{R_4}{R_3} = \frac{R_2}{R_1}$

Therefore $\boxed{I_0 = \frac{R_2}{R_1 R_{2B}} V_1}$

Appendix C:

DIP switch settings for waveform shape and frequency selection

The following table list the DIP switch setting for waveform shape selection **0= Low, 1 = High**

DIP Switch Position Binary		**Waveform Shape Selection**
D7	**D6**	
0	**0**	**Sine Waveform**
0	**1**	**NC**
1	**0**	**Triangulate Waveform**
1	**1**	**Square Waveform**

Table C.1 DIP switch position for waveform shape selection

The following table list the DIP switch setting for Frequency selection

DIP Switch (Binary)						Hex	Selected Frequency (KHz)
D5	D4	D3	D2	D1	D0		
0	0	0	0	0	0	0	1
0	0	0	0	0	1	1	2
0	0	0	0	1	0	2	4
0	0	0	0	1	1	3	8
0	0	0	1	0	0	4	12
0	0	0	1	0	1	5	16
0	0	0	1	1	0	6	20
0	0	0	1	1	1	7	25
0	0	1	0	0	0	8	30
0	0	1	0	0	1	9	35

DIP Switch (Binary)						Hex	Selected Frequency
D5	D4	D3	D2	D1	D0		
0	0	1	0	1	0	A	40
0	0	1	0	1	1	B	45
0	0	1	1	0	0	C	50
0	0	1	1	0	1	D	60
0	0	1	1	1	0	E	70
0	0	1	1	1	1	F	80
0	1	0	0	0	0	10	90
0	1	0	0	0	1	11	100
0	1	0	0	1	0	12	125
0	1	0	0	1	1	13	150
0	1	0	1	0	0	14	175
0	1	0	1	0	1	15	200
0	1	0	1	1	0	16	225
0	1	0	1	1	1	17	250
0	1	1	0	0	0	18	275
0	1	1	0	0	1	19	300
0	1	1	0	1	0	1A	325
0	1	1	0	1	1	1B	350
0	1	1	1	0	0	1C	375
0	1	1	1	0	1	1D	400
0	1	1	1	1	0	1E	425
0	1	1	1	1	1	1F	450
1	0	0	0	0	0	20	475
1	0	0	0	0	1	21	500
1	0	0	0	1	0	22	525
1	0	0	0	1	1	23	550
1	0	0	1	0	0	24	575
1	0	0	1	0	1	25	600
1	0	0	1	1	0	26	625
1	0	0	1	1	1	27	650
1	0	1	0	0	0	28	675
1	0	1	0	0	1	29	700
1	0	1	0	1	0	2A	725
1	0	1	0	1	1	2B	750

DIP Switch (Binary)						Hex	Selected Frequency
D5	D4	D3	D2	D1	D0		
1	0	1	1	0	0	2C	775
1	0	1	1	0	1	2D	800
1	0	1	1	1	0	2E	825
1	0	1	1	1	1	2F	850
1	1	0	0	0	0	30	875
1	1	0	0	0	1	31	900
1	1	0	0	1	0	32	925
1	1	0	0	1	1	33	950
1	1	0	1	0	0	34	975
1	1	0	1	0	1	35	1024
1	1	0	1	1	0	36	1024
1	1	0	1	1	1	37	1024
1	1	1	0	0	0	38	1024
1	1	1	0	0	1	39	1024
1	1	1	0	1	0	3A	1024
1	1	1	0	1	1	3B	1024
1	1	1	1	0	0	3C	1024
1	1	1	1	0	1	3D	1024

Table C.2 DIP switch position for frequency selection

Appendix D:

Output impedance calculation

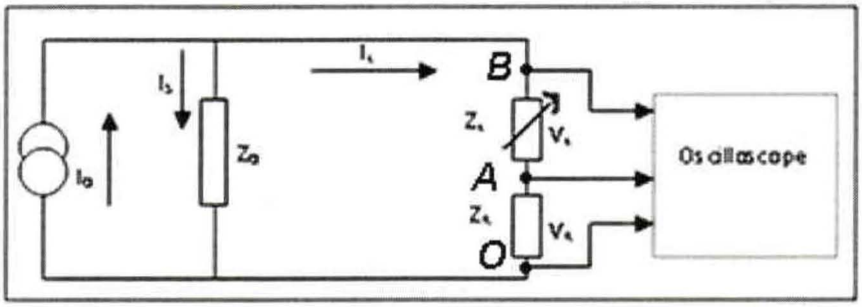

Figure D.1. Output impedance, current variations measurement circuit

To calculate the output impedance of the current source circuits the following equation was used (see appendix Impedance Equation for derivation).

Where I_O is the output current from the current source, I_s is the shunt away current by the internal output resistance Z_O and I_L is the current provided to the load ($Z_R + Z_L$). Z_R and Z_L are two series resistors and the voltages across them are V_R and V_L respectively, the resistor Z_L is a variable resistor, this combined impedance ($Z_R + Z_L$) is connected in parallel to the internal resistor Z_O as shown in the Figure D.1.

The current provided by the current source is given by $I_O = I_s + I_L$. The output impedance can be calculated by measuring the voltages V_R and V_L for minimum ($Zmin = Z_R\ Z_L=0$) and maximum ($Zmax = (Z_R + Z_L)$) load conditions.

For minimum load condition the equation $I_O = I_s + I_L$ can be written as $I_O = I_{smin} + I_{Lmin}$ and for maximum impedance: $I_O = I_{smax} + I_{Lmax}$. By combining these two equations and solving for output impedance Z_o. Since the current source is constant therefore I_O remains constant under minimum and maximum load. $I_{Smin} + I_{Lmin} = I_{Smax} + I_{Lmax}$

$$I_{Smax} - I_{Smin} = I_{Lmin} - I_{Lmax}$$

$$\frac{V_{max}}{Z_o} - \frac{V_{min}}{Z_o} = I_{Lmin} - I_{Lmax} \text{ and } Z_o = \frac{V_{max}-V_{min}}{I_{Lmin}-I_{Lmax}}$$

$$Z_o = \frac{V_{max}-V_{min}}{V_{min}/Z_{min} - V_{max}/Z_{max}} \qquad (1)$$

$$I_{Lmin} = V_{min}/Z_{min} \qquad (2)$$

$$I_{Lmax} = V_{max}/Z_{max} \qquad (3)$$

BIBLIOGRAPHY

Alexander S Ross, S. G. (2003). Current source design for electrical impedance tomography. *Physiol. Meas* , 509-516.

Analog Devices AD9833. (n.d.). Programmable Waveform Generator AD9833.

Andy Adler, W. R. (2006). Uses and abuses of EIDORS: as extensible software base for EIT. *Physl. Meas* , S25-S42.

Avis N J and Barber D C (1995). Incorporating a priori information into the Sheffield filtered backprojection algorithm. *Physiol. Meas* , A11-A112.

Baek1, H.-M. (2008 September 1). Choline as a Biomarker for Cell Proliferation: Do the Results from Proton MR Spectroscopy Show Difference between HER2/neu Positive and Negative Breast Cancers? *Int J Cancer* , 1219–1221.

Baker L.E, Coulter T. W and Bourland J. D. (1973). Simple versatile instrument for measuring impedance changes accompanying physiological events. *Med. Biol. Eng* , 221-229.

Bertemes-Filho P, B. H. (2000). A comparison of modified Howland circuits as current generators with current mirror type circuits. *Physiol. Meas.* , 1–6.

Bertero M, B. P. (1998). *Introduction to Inverse Problems in Imaging.* London: IOP .

Blad B, Bertenstam L, Persson BR, Holmer NG. (1991). A non invasive imaging system, for temperature monitoring. *Acta Radiol.* , 85-87.

Boone K G, H. D. (1996). Current approaches to analogue insturmetation design electrical impedance tomography. *Physiol. Meas.* , 229-247.

Boone K, Barber D, Brown B. (1997). Review: Imaging with electricity: Report of the European Concerted Action on Impedance Tomography. *J Med. Eng Tech* , 201-232.

Borsic, A. (2002). Regularisation methods for imaging from electrical measurements, Ph D. dissertation. *Oxford Brookes University.*

Brown B. H and Seagar A D. (1987). The sheffield data collection system. *Clinical phy and physio, meas* , 91-97.

Morand Piert, Maria Burian (2007). Positron detection for the intraoperative localisation of cancer deposits. *Eur J Nucl Med Mol Imaging* , 1534–1544.

Brekelmans CT, Seynaeve C, Bartels CC (2001). Effectiveness of Breast cancer surveillance in BRCA 1/2 gene mutation carriers and women with high familial risk. . *J Clin Oncol* , 924–930.

Canadian Cancer Statistics (2009).

Cheng K S, David Isaacson, Newell J. C and David G. Gisser. (1989). Electrode models for electric current computed tomography. *IEEE Trans. Biomed. Eng* , 918-924.

Chris Guy. (2005). An Introduction to The Principles of Medical Imaging. London: *Imperial College Press London.*

Kuhl CK, Scharding S, Leutner CC (2005). Mammography, breast ultrasound, and magnetic resonance imaging for surveillance of women at high familial risk for breast cancer. . *J Clin Oncol* , 8469-8476.

Kenneth S. Cole. (1940). Permeability and impermeability of cell membranes for ions. *Quant. Biol.* , 110-122.

Barber C. C, Brown B. H and Freeston I.L. (1983). Imaging spatial distributions of resistivity using applied potential tomography. *Electronic Letter* , 933-935.

Dale L Bailey, D. W. (2005). *Positron Emission Tomography Basic Sciences.* London: *Springer-Verlag London Limited*.

Denyer C W. Lidgey, F.J, Zhu Q.S. (1994). A high output impedance current source. *Physio. Meas.* , 79-82.

Elmore G.Joann, K. A. (2005). Screening for Breast Cancer. *JAMA* , 1245-1256.

Eva Murphy, C. S. (2004). Retrieved from Analog Device: *http://www.analog.comlibrary/analogdialogue/archives/38-08/dds.html*

Francesco Sardanelli, Franca Podo. (2007). Breast MR imaging in women at high-risk of breast cancer. Is something changing in early breast cancer detection? . *Eur Radiol* , 873–887.

FRICKE, H and Morse S. (1926). The electric capacity of tumors of the breast. *J. Cancer Res* , 340-376.

Geselowitz, B. D. (1971). An Application of Electrtocardiographic Lead Theory to Impedance Plethysmography. *IEEE Trans. Biomed. Eng* , 38-41.

Goharian, M. (2007). A Trust Region Method for EIT Application for Human Brain. *IFMBE Proceedings 17* , 400–403.

Goldberg, B.-G. (1999). Digital Frequency Synthesis Demystified. *LLH Technology Publishing.*

Grebennikov, A. (2007). RF and Microwave Transistor Oscillator Design. Chippenham, Wiltshire: *John Wiley & Sons Ltd.*

Landis K. Griffeth (2005). Use of PET/CT scanning in cancer patients:technical and practical considerations.*Proc (Bayl University Medical center).* 321-330

Halter, R. (2004). Design and implementation of a high frequency electrical impedance tomography system. *Physiol. Meas.* , 379–390.

Harrison, L. T. (2005). CURRENT SOURCES & VOLTAGE REFERENCES. Copyright © 2005, *Elsevier Inc.*

Heinz W. Engl, M. H. (2000). Regularization of Inverse Problems. Netherlands: *Kluwer Academic publishers*.

Higham, N. J. (1996). Accuracy and stability of numerical algorithms. Philadelphia: *Siam.*

Holder, D. S. (2005). Electrical Impedance Tomography. *UK: Istitute of Physics Publishing* Bristol and Philadelphia.

Houssami, N. (2003). Sydney Breast Imaging Accuracy Study. *AJR* , 935-940.

Howland. (1964). Impedance & admittance transformations using operational amplifiers. *Lightning Empiricist* .

Hua P, W. J. (1987). Effect of the measurement method on noise handling and image quality of EIT imaging. *Ninth Int. Conf. IEEE Eng. In Med. And Biol. Society*, (pp. 1429-1430). (1987)

Ian K. Komenaka, Beth-Ann Ditkoff. (2004). The development of interval breast malignancies in patients with BRCA mutations. Cancer 2004; 100:. *Cancer* , 2-79-2083:.

Isaacson, D. (1986). Distinguishability of conductivities by electric current computed tomography. *IEEE Trans Med. Imaging* , 92-95.

Jacques Jossinet. (1998). The impedivity of freshly excised human breast tissue. *Physiol Meas* , 61-75.

Jacques Jossinet, Michel. Schmitt. (1999). A Review of Parameters for the Bioelectrical Characterization of Breast Tissue. *INSERM* U281, 69424 Lyon Cedex 03,, France: Institut National de la Sante et de la Recherche Medicale,.

Jane Wang, K.-J. C. (2007). Efficacy of Mammographic Evaluation ofBreast Cancer in Women Less Than 40 Years of Age: Experience from a Single Medical Center in Taiwan. *J Formos Med Assoc* , 736-747.

Jane Wang, T. T.-F. (2000). The evaluation of false negative mammography from malignant and benign breast lesions. *Journal of Clinical Imaging 24 (2000) 96 103* , 96- 103.

Jegatheesan, A. (2008). *EIT SYSTEM DEVELOPMENT & MULTIVARITE IMAGE IMPROVEMENT(Thesis).*

Jeong Whan Lee, T. I. (2003). Precision constant current source for electrical impedance tomography. *IEEE EMBS*, (pp. 1066-1069). Cancun, Mexico.

Joann G., E. (1998). TEN-YEAR RISK OF FALSE POSITIVE SCREENING MAMMOGRAMS AND CLINICAL BREAST EXAMINATIONS. *The New England J of Medicine* , 1089-1096.

Jacques Jossinet (2008). Elementary electrodynamics. *Technology and Health care , 465-474.*

Boone K, Barber D and Brown B. (1997). Review: Imaging with Electricity: Report of the European Concerted Action on Impedance tomography. *J Med. Eng Tech* , 201-232.

Kari Hemminki, C. G. (2002). Morphology types of breast cancer in family members and multiple primary tumors: is morphology genetically determined? *Breast Cancer Res* .

Leung. (1990). A wide band current source for electrical impedance tomography. CAEIT EEC, (pp. 144-149). Copenhagen.

Liberman, L. (2004). Breast cancer screening with MRI - What are the data for patients at high risk. *The New England Journal of Medicine* , 497-500.

Lidgey(a). (1990). Development in current driver circuitry. *Electrical Impedance Tomography*, (pp. 183-189). Copenhagen.

Lidgey(b). (1990). Developments in current driver circuitry. *CAEIT EEC Workshop*, (pp. 1-20). Copenhagen.

Liu, N. (2003). A Multichannel Synthesizer and Voltmeter for Electrical Impedance Tomography. *Proceedings of the 25' Annual lnternational Conference of the IEEE EMBS.* Cancun, Mexico .

Mieke Kriege, Cecile T.M. Brekelmans. (2004). Efficacy of MRI and ammography for breast-cancer screening in women with a familial or genetic predisposition. . *New Engl J Med* , 427-437.

Malich, A. (2007). The impact of lesion vascularisation on tumours detection by electrical impedance scanning at 200 Hz. *Biomedical Imaging and Intervention Journal* .

Malmivuo, J. (1995). Bioelectromagnetism, Principles and Applications of bioelectric and biomagnetic fields. *Oxford Univeristy Press (http://www.ijbem.org).*

McKenna, R. (1994). The abnormal mammogram radiographic findings, diagnositc options, pathology, and stage of cncer diagnosis. *Cancer* , 244-255.

Mieke Kriege, C. T. (2004). Efficacy of MRI and mammography for breast cancer screening in women with a fmilil or genetic predisposition. *N Engl J Med* , 427-437.

Tikhonov A. N. (1963). Solution of incorrectly formulated problems and the reqularization method. *Soviet Math* , 501-504. (http://www.ps.uci.edu)

Natterer, F. (1982). The Mathematics of Computerized Tomography. *Wiley.*

Newell. (1988). An electric current tomography . *IEEE Trans. Biomed. Eng , 828-833.*

Ng, E.Y.K. (2007). Numerical modelling of biopotential field for detection of breast tumour. *Computers in Biology and Medicine* , 1121 – 1132.

Oh1, Tong. In, Woo Eung Je and Holder David. (2007). Multi-frequency EIT system with radially symmetric architecture: KHU Mark1. *Physiol. Meas.* , S183–S196.

Oliveira, Luis. B Jorge R. (2008). Analysis and design of quadrature oscillators. *Springer.*

Bertemes-Filho P, Brown B. H and Wilson A J. (2000). A comparison of modified Howland circuits as current generators with current mirror type circuits. *Physiol. Meas* .

Kauppinen P, Hyttinen J. Mamivuo J. (2005). Sensitivity Distribution Visualizations of Impedance Tomography Measurement Strategies. International *Journal of Bioelectromagnetism* , 1-9

Hua P, Webster J. G and Tompkins W J. (1988). A regularised electrical impedance tomography reconstruction algorithm. *Clin. Phys. Physiol. Meas* , 137-141.

Morucci J P, Marshilli P. M. (1994). A direct sensitivity matrix approach for fast reconstruction in electrical impedance tomography. *Physiol. Meas* , A107-A114.

Paula 3. Gordon, M. a. (1995). Malignant Breast Masses Detected Only by ultrasound. *Cancer* .

Pavel Crystal, S. D. (2003). Using Sonography to Screen Women with Mammographically Dense Breasts . *American Roentgen Ray Society* , 177–182.

Phillips, D. L. (1962). A Technique for the Numerical Solution of Certain Integral Equations of the First Kind. *J. Assoc. Comput. Mach* , 84-97.

Polydoried N, L. W. (2002). A Matlab toolkit for three-dimensional electrical impedance tomography: a contribution to the electrical impedance and diffuse optical reconstructin software project. *Meas. SCi. Techniol* , 1871-1883.

Gadd R, Record P and Rolfe P. (1992). Electrical impedance tomography. A sensitivity region reconstruction algorithm using adjacent drive current injection strategy. *Clin. Phys. Physiol. Meas* , 101-105.

Rafiei-Naeini. (2007). Low-noise measurement for electrical impedance tomography. *ICEBI 2007, IFMBE proceedings 17* (pp. 324-327). Berlin: Springerlink.

Rafiei-Naeini, M. H. (2008). Low-noise current excitation sub-system for medical EIT. *Physiol. Meas.* , S173–S184.

Richard Aster, B. B. (2005). Parameter Estimation and Inverse Problems. San Diego: *Elsevier Academic Press.*

Rob Morrison presentation http://www.cerpa.unsw.edu.au/resources/presentations /An Overview of Tomography Work at the JKMRC_Rob Morrison.pdf

Ruddon, R. W. (2007). *Cancer Biology.* Oxford University Press, Inc.

Kramer S, Schulz-Wendtland R, Hagedorn K. (1998). MRI and its Role in the diagnosis of multicentric breast cancer. *Anticancer res* , 2163-2164.

Sergio, F. (2002). Design with operational amplifiers and analog integrated circuits. *McGraw-Hill.*

Skidmore. (1987). Errors in four electrode impedance plethysmography. *Clin. Phys. Physio. Meas.* , 99-102.

Tarantola, A. (2004). *Inverse Problem Theory. Siam (http://www.ipgp.fr/~tarantola/Files/Professional/SIAM/index.html).*

Tomo Osaka, T. I. (2007). Diagnostic mammography and ultrasonography for palpable and nonpalpable breast cancer in women. *Breast Cancer* , 255-259.

Toumazou. (1990). Extending voltage mode op amps to current mode performance., (pp. 116-130).

Tzu-Jen Kao, J. N. (2006). Radiolucent electrode array for combined EIT and mammography. *IFMBE Proceedings* (pp. 3893-3896). Seoul, Korea: Springer Berlin Heidelberg.

Kolehmainen V, Vauhkonen M. Karjalainen P A. (1997). Asseement of erros in static electrical impedance tomography with adjacent and trigonometric current patters. *Physiol. Meas* , 189-303.

Vallabhajosula, S. (2009). Molecular Imaging Radiopharmaceuticals for PET and SPECT. Berlin Heidelberg: *Springer.*

Vogel, C. R. (2002). Computational Methods for inverse problems. Philadelphia: *Siam.*

Vogelius, R. V. (1987). Relaxation of a Variational Method for Impedance Computed Tomography. *Comm. Pure Appl. Math* , 745-777.

Malmivuo Jakko and Plonsey Robert.Webster. (1990). Electrical impedance tomography. *Oxford university pres.*

Wexler, A. (1988). Electrical Impedance Imaging in Two and Three Dimensions. *Clin. Phys. Physiol. Meas* , 29-33.

Wexler, A. (1985). Impedance-Computed Tomography algorithm ans system. *Applied Optics* , 3985-3992.

Widlar R. J. (1965). Some Circuit Design Techniques for Linear Integrated Circuits. *IEEE Transctions on Circuit Theory*, 586-590.

William R. Hendee. (2002). *Medical Imaging Physics.* New York: Wiley-Liss A John Siley & Sons, Inc., Publication.

Wilson. (1981, December). Current mirros, amplifiers and dumpers. pp. 47-50.

Wilson, G. R. (1968). A Monolithic Junction FET–n-p-n Operational Amplifier. *IEEE Joutnal of Solid-State Circuits*, 341–348.

XILINX FPGA CA SanJose, P. L. (n.d.). Xilinx Programmable Logic (FPGA). San Jose, CA. Retrieved from http://www.xilinx.com/technology/logic/index.htm.

Zou Y, Guo Z. (2003). A review of electrical impedance techniques for breast cancer. *Medical Engineering & Physics* , 79-90.